8-2015

Prophylactic Cranial Irradiation Reduces the Incidence of Brain Metastasis in a Mouse Model of Metastatic Breast Cancer

Daniel L. Smith

PROPHYLACTIC CRANIAL IRRADIATION REDUCES THE INCIDENCE OF BRAIN METASTASIS IN A MOUSE MODEL OF METASTATIC BREAST CANCER

by

Daniel Smith, B.S.

APPROVED:

Wendy Woodward, M.D., Ph.D.
Supervisory Professor

Sunil Krishnan, M.D.

Osama Mawlawi, Ph.D.

James Bankson, Ph.D.

Sendurai Mani, Ph.D.

APPROVED:

Dean, The University of Texas
Graduate School of Biomedical Sciences at Houston

PROPHYLACTIC CRANIAL IRRADIATION REDUCES THE INCIDENCE OF BRAIN METASTASIS IN A MOUSE MODEL OF METASTATIC BREAST CANCER

A

DISSERTATION

Presented to the Faculty of
The University of Texas
Health Science Center at Houston
and
The University of Texas
M.D. Anderson Cancer Center
Graduate School of Biomedical Sciences
in Partial Fulfillment

of the Requirements

for the degree of

DOCTOR OF PHILOSOPHY

by
Daniel Smith, B.S.
Houston, Texas

August, 2015

ACKNOWLEDGEMENTS

First and foremost, I would like to thank my advisor, Dr. Wendy Woodward. Without her continued support, guidance, and above all else her patience, I would not be in the position I am today. I appreciate her contribution of ideas, time, and funding that enabled my experience as a graduate student to be productive and stimulating. The freedom she gave me allowed me to discover in which niche I could be the most effective, and I certainly could not have asked for a better advisor.

Thanks to Dr. Bisrat Debeb and Dr. Lara Lacerda for all of the scientific input, and for really being my co-second advisors. Their presence and enthusiasm made graduate school enjoyable at times, and their leadership kept me on the right track.

I would like to thank my mentor, Dr. Kendra Woods, for her support during tough times in my pursuit of a Ph.D. I am also thankful that she did not let me forget that what we do is about the patients, and that she opened my vision to the possibilities outside of academia.

The members of Dr. Woodward's lab contributed immensely to my scientific growth at MD Anderson. I would especially like to thank Richard Larson and Travis Solley for always being prepared to help with my experiments and for the large amount of time they saved me. Also, this work would not have been possible without the help of Jessica Li, Dr. Parmesh Diagaradjane, Adam Wolfe, and Dr. Wei Xu.

I would like to thank Dr. David Yang for introducing me to radiochemistry and for his continued professional support and advice. Among his group, I would particularly like to thank Dr. Fanlin "Emi" Kong.

Thanks to Dr. Ed Jackson, who supported my interest in trying to bridge medical physics and cancer biology; Dr. Firas Mourtada and Dr. Sims-Mourtada, who noticed my aptitude for

molecular imaging before even I did; and Dr. Howard Thames, who provided valuable feedback on my computational modeling project.

It would not have been possible to complete this and other work without the support of several other people, including Charlie Kingsley and Jorge DeLacerda in the Small Animal Imaging Facility and numerous members of the Inflammatory Breast Cancer program.

I would also like to recognize my other (super)advisory committee members – Dr. James Bankson, Dr. Osama Mawlawi, Dr. Sunil Krishnan, and Dr. Sendurai Mani – for their invaluable time and scientific input to my thesis work.

Last, I am especially thankful for my family members and friends, who supported and encouraged me throughout my studies, and for which my mere expression of thanks does not suffice.

This study was funded in part from the following sources: The National Institutes of Health RO1CA138239-01, the State of Texas Grant for Rare and Aggressive Cancers, and the Morgan Welch IBC Clinic and Research Program. I also received a fellowship from the Center for Stem Cell and Developmental Biology at the University of Texas M.D. Anderson Cancer Center.

PROPHYLACTIC CRANIAL IRRADIATION REDUCES THE INCIDENCE OF BRAIN METASTASIS IN A MOUSE MODEL OF METASTATIC BREAST CANCER

Daniel Smith

Advisory Professor: Wendy Woodward, M.D., Ph.D.

Prophylactic cranial irradiation (PCI) is a preventative whole-brain irradiation technique used to reduce the incidence of brain metastasis and improve overall survival in select patients with small cell lung cancer and acute lymphoblastic leukemia. A population of breast cancer patients – stage IV, HER2+ or triple-negative – has emerged as having a high risk of developing brain metastases. Because only 10-20% of breast cancer patients diagnosed with brain metastases survive longer than one year, in this high-risk population the benefit of PCI – potential for reduced incidence of brain metastasis and improved overall survival – may outweigh the risks – radiation toxicity. The objective of this thesis was to determine if a PCI dose could reduce the incidence of brain metastasis.

A mouse model of metastatic, HER2+ inflammatory breast cancer was used to evaluate the effect of 4-Gy whole-brain irradiation on the incidence of brain metastasis. Mice were irradiated at different time points and were sacrificed at either four or eight weeks after cell injection. The principal endpoints of incidence of brain metastasis, the number of brain metastases per mouse, and the metastatic burden were all significantly decreased in the PCI arm, but unaffected when the whole-brain irradiation was delayed.

To expand on the experimental findings, a computational model of subclinical breast cancer dose-response was developed. After optimization, the model was validated by conducting a limiting dilution assay. By adjusting the model inputs of radiation dose and time of irradiation, a time course of the incidence of brain metastasis and related endpoints was

mapped. The model predicts that delaying treatment introduces a dose threshold below which the incidence is unchanged, a finding that is consistent with the experimental data.

This work highlights the importance of the timing of radiation therapy as it relates to the treatment of subclinical disease, specifically breast cancer micrometastases in the brain. The principal findings have the potential to impact how breast cancer patients at high risk of developing brain metastases are managed in the clinic, and PCI clinical trials in these patients could be considered.

TABLE OF CONTENTS

LIST OF FIGURES

Figure

LIST OF TABLES

Table

ABBREVIATIONS

Abbreviation	*Full Description*
^{13}C	Carbon-13
^{131}I	Iodine-131
AI	Aromatase Inhibitors
ALL	Acute Lymphoblastic Leukemia
BBB	Blood Brain Barrier
BMFS	Brain Metastasis Free Survival
BMT	Autologous Bone Marrow Transplantation
CNS	Central Nervous System
CSCs	Cancer Stem Cells
CSF	Cerebrospinal Fluid
CT	Computed Tomography
DSBs	Double Strand Breaks
EGFR	Epidermal Growth Factor Receptor
EMT	Epithelial-Mesenchymal Transition
ER	Estrogen Receptor
GFP	Green Fluorescent Protein
Gy	Gray
HER2	Human Epidermal Growth Factor Receptor 2
IBC	Inflammatory Breast Cancer
IMRT	Intensity-Modulated Radiation Therapy
IR	Ionizing Radiation
IV	Intravenous

LABC	Locally Advanced Breast Cancer
mBC	Metastatic Breast Cancer
MET	Mesenchymal-Epithelial Transition
miR	Micro RNA
MRI	Magnetic Resonance Imaging
NCF	Neurocognitive Function
NSCLC	Non-Small Cell Lung Cancer
OS	Overall Survival
PCI	Prophylactic Cranial Irradiation
PET	Positron Emission Tomography
PFS	Progression-Free Survival
PR	Progesterone Receptor
RFS	Relapse-Free Survival
SCLC	Small Cell Lung Cancer
SERMs	Selective Estrogen Receptor Modulators
SSBs	Single Strand Breaks
SRS	Stereotactic Radiosurgery
STAT3	Signal Transducer and Activator of Transcription 3
TGFβ	Transforming Growth Factor Beta
TNBC	Triple-Negative Breast Cancer
TNM	Tumor Node Metastasis Staging System
VEGF	Vascular Endothelial Growth Factor
WBRT	Whole-Brain Radiation Therapy

CHAPTER 1: INTRODUCTION

SECTION I. BREAST CANCER

Breast cancer is the most common malignancy and the second leading cause of cancer death among females in the United States, who have an approximately 12% lifetime risk of developing the disease. It was estimated that 232,340 new cases of invasive breast cancer were diagnosed in the United States in 2013, with 39,620 fatalities [1]. According to the National Cancer Institute, the five-year survival rate for breast cancer patients ranges from 99% for localized disease to approximately 24% for advanced disease at the time of diagnosis [2].

A. Molecular Subtypes

Breast cancer is increasingly considered a group of diseases distinguished by molecular or receptor subtypes, clinical behaviors, and treatment response. Breast cancers are commonly stratified into receptor subtypes based on the presence or absence of the estrogen receptors (ER), progesterone receptors (PR), and human epidermal growth factor receptor 2 (HER2) [3]. For the purposes of this report, I will group breast cancers into three unique subtypes: luminal, HER2-enriched, and basal-like.

The majority of breast cancers are of the *luminal* subtype, which are estrogen receptor-positive (ER+) and/or progesterone receptor-positive (PR+). Patients with luminal breast cancers tend to have a better prognosis than other breast cancer patients, due in large part to the slow-growing, less aggressive nature of these tumors. The luminal subtype is further subdivided into luminal A and luminal B: luminal B breast cancers are HER2-enriched and these patients have a worse prognosis than luminal A breast cancer patients. In patients with luminal A breast cancers, expression of the hormone receptors ER and/or PR is predictive of a favorable response to hormonal therapies such as tamoxifen.

Approximately 15-20% percent of breast tumors overexpress human epidermal growth factor receptor 2, but do not express the hormone receptors, ER and PR [3]. *HER2-enriched* (HER2+) breast cancers tend to grow faster and spread more aggressively than luminal tumors and, consequently, these patients have worse short-term prognosis. In recent years, targeted therapies for HER2+ breast cancers, such as trastuzumab and lapatinib, have improved the overall prognosis for these patients.

Ten to twenty percent of breast cancers patients have *basal-like* breast cancer, and most of these are referred to as triple-negative breast cancer, as they are ER-, PR-, and HER2. Like HER2+ breast cancers, these tumors are normally very aggressive and the patients have poor prognosis; moreover, due to the triple-negative status, there is a dearth of treatment options. For simplicity, *I will refer to this subset of breast cancers as triple-negative breast cancer throughout the report*.

B. Inflammatory Breast Cancer

Inflammatory breast cancer (IBC) – a variant of locally advanced breast cancer (LABC) – accounts for approximately 2.5% of all breast cancer cases. It is characterized by aggressive behavior, rapid progression, breast enlargement, *peau d'orange* appearance, erythema, skin thickening, and dermal lymphatic invasion. Due in part to its rarity, IBC is commonly misdiagnosed as mastitis or generalized dermatitis [4]. Currently, IBC is primarily a clinical diagnosis, according to the American Joint Committee on Cancer (AJCC) staging manual [5], as no gene or molecular signatures have been identified that clearly distinguish IBC from other breast cancers [6, 7].

IBC may possess any combination of the hormone receptors and HER2, but they most often fall into the HER+ or triple-negative breast cancer clusters. In fact, HER2 has been reported to be overexpressed with greater frequency in IBC (36-60%) compared to non-IBC [8].

Subtype	Expression Profile	Prevalence	Common Treatments	Prognosis
Luminal A	ER+, PR+, HER2+	25-35%	Hormonal therapy	Good
Luminal B	ER+, PR+, HER2-	20-25%	Chemotherapy	Poor
HER2-enriched	ER-, PR-, HER2+	15-20%	Trastuzumab, Lapatinib	Poor
Basal-like/Triple-negative	ER-, PR-, HER2-	10-20%	EGFR inhibitors	Poor
(+): overexpressed		(-): low or undetectable		

Adapted from these publications:

1) Carey L, *et al* . *Journal of the American Medical Association* 2006, 295(21): 2492-2502.

2) Perou C, et al. *Nature* 2000, 406: 747-52.

Table 1: Major Molecular Subtypes in Breast Cancer. The principal subytpes in breast cancer are the luminal tumors, charaterized by their expression of the hormone (estrogen and progesterone) receptors; HER2-enriched, breast cancers that overexpress human epidermal growth factor receptor 2, but do not express hormone receptors at high levels; and basal or triple-negative breast cancer, which overexpresses neither the hormone receptors nor HER2. Patients with luminal tumors fare well compared to patients with the more aggressive HER2 and triple-negative breast cancers.

Patients with IBC have a worse prognosis – a 35-40% five-year survival – than other LABC patients because of the high incidence of distant metastasis (roughly 70%) [9] and because of a higher incidence of recurrence after multidisciplinary treatment [10]. Similarly, the median survival for IBC patients is 2.9 years compared to 6.4 years for LABC patients [11].

C. Breast Cancer Treatment Options

Treatment options for patients with breast cancer include surgery, radiation therapy, and systemic therapies such as chemotherapy, hormone therapy, and/or targeted therapy. Most patients with breast cancer will undergo surgery (either breast-conserving surgery or mastectomy [entire breast removal]), both to remove the cancer from the breast tissue and also to determine the stage of the disease. Surgery to remove the cancerous tissue from the breast is normally accompanied by removal of axillary lymph nodes (or a sentinel lymph node biopsy [12]) to help determine the spread of disease beyond the breast and to inform the course of subsequent therapy. Surgery is typically combined with other treatments.

HIGHLIGHTS

- Breast cancers are grouped in molecular subtypes: luminal, HER2-enriched (HER2+), and triple-negative (estrogen and progesterone receptor-negative, HER-)
- Patients with HER2-enriched and triple-negative breast cancers (TNBC) have the worst prognosis
- Inflammatory breast cancer is an aggressive form of breast cancer distinguished by its rapid progression and appearance; most cases fall into the HER2-enriched or TNBC subtypes
- Most breast cancer patients will be treated with surgery and radiation therapy, while systemic therapy is the primary treatment option for patients with metastatic breast cancer
- The monoclonal antibody trastuzumab is a common systemic agent that targets the HER2 protein and reduces recurrence in HER2-enriched breast cancer patients
- Five-year survival rates range from 99% for localized disease to 25% for advanced disease

Radiation therapy, either external-beam radiation therapy or brachytherapy, is used as an anti-cancer treatment in the majority of breast cancer patients. Radiation therapy has several applications in breast cancer patients, including shrinking previously inoperable tumors prior to surgery, destroying cancer cells in the breast after a potentially curative surgery, or as a palliative in patients with advanced disease.

Radiation therapy is given after breast-conserving surgery to reduce the risk of recurrence by 50% and the risk of breast cancer death by approximately 20% [13]. These patients who receive the combined breast-conserving surgery plus radiation regimen have the same expected long-term survival as patients who undergo a mastectomy [14].

Systemic therapies, administered orally or intravenously, affect all parts of the body and can be given to breast cancer patients either before surgery – neoadjuvant therapy – or after the surgery – known as adjuvant therapy. Neoadjuvant systemic therapies are often used, like radiation, to shrink the tumor enough to enable its surgical removal or to allow for less extensive surgery. Adjuvant therapies are primarily used to kill residual tumors cells or cells that have migrated to other parts of the body. For women with metastatic breast cancer, systemic therapy is generally the principal treatment as the patients may not benefit from surgery or radiation.

The most common systemic treatment is chemotherapy, a class of agents that are designed to target rapidly dividing cancer cells. However, chemotherapy has very well-known side effects because rapid cell division is not a characteristic unique to cancer cells. Chemotherapy drugs – alkylating agents, antimetabolites, anti-microtubule agents, topoisomerase inhibitors, and anthracyclines – prevent mitosis by damaging DNA and inhibiting the cell division process. In most cases, drug combinations are more effective than monotherapies in the treatment of breast cancer [15]. Triple-negative and HER2+ breast cancers tend to be more sensitive to chemotherapy than their luminal counterparts [16].

Hormone therapy, a different class of systemic agents, is often given to breast cancer patients whose tumors are ER+ or PR+. Estrogen receptor and progesterone receptor transmit the signals from the steroid hormones estrogen and progesterone, respectively, promoting the growth of luminal breast cancers. There are three major hormonal therapies: selective estrogen receptor modulators (SERM), ovarian ablation, and aromatase inhibitors (AI). SERM, such as tamoxifen and raloxifene, prevent estrogen from binding to the estrogen receptor, and it has

been shown that they reduce the rate of breast cancer recurrence and mortality [17]. Ovarian ablation involves either surgical removal of the ovaries – the major source of estrogen prior to menopause – or with drugs known as luteinizing hormone-releasing hormone analogs [1]. Finally, AI such as letrozole and anastrozole act against aromatase, the enzyme that synthesizes estrogen, and demonstrate a clear benefit in postmenopausal women [18].

Therapies targeted at HER2 – the protein that is important in the development and progression of HER2+ breast cancers – have improved the prognosis for patients with this breast cancer subtype. Most notably, the humanized monoclonal antibody trastuzumab directly targets the HER2 protein, and it has been shown that combining trastuzumab with chemotherapy reduces the risk of recurrence by 52% and death by 33%, compared to chemotherapy alone [19]. Trastuzumab was approved by the U.S. Food and Drug Administration in 2006 for all HER2+ breast cancers. Other systemic treatments have also exhibited benefit for HER2+ breast cancer patients, such as pertuzumab and lapatinib.

Most patients with inflammatory breast cancer present with locoregional disease, and there is a high probability of residual disease if surgery is used upfront. It is recommended that IBC patients first receive a primary systemic regimen consisting of an anthracycline and a taxane, with the goal of shrinking the tumor to allow for mastectomy and axillary lymph node dissection [20]. Similar to non-IBC patients, the addition of trastuzumab to systemic chemotherapy is associated with higher pathologic complete response in HER2+ inflammatory breast cancer patients [21], and it is recommended that all women with ER- or PR-positive inflammatory breast cancer receive either tamoxifen or an aromatase inhibitor [20]. All IBC patients who undergo a mastectomy are recommended to receive radiation therapy. Finally, IBC patients with metastatic disease should undergo systemic therapy first and then local therapy (radiation and/or surgery) for palliative purposes [4].

While multimodality therapies have improved the prognosis for breast cancer patients, there is a need for novel therapeutic approaches to improve the outcomes of patients whose cancer metastasizes to the lungs, liver, bone, and, most relevant to this investigation, to the brain.

SECTION II. BRAIN METASTASIS

Cancer metastasis is the process by which malignant cells spread from the primary tumor to unconnected organs. Despite major advances in diagnosis, surgical techniques, and local and systemic treatments, most deaths due to cancer result from the progression of metastases that are resistant to conventional therapies [22]. Metastasis is the primary clinical challenge due to its unpredictability and the adverse impact it has on cancer patients, and therefore the development of improved therapies for metastasis is one of the primary goals of cancer research.

A. The Biology of Metastasis

Metastases arise from a selected subpopulation within the biologically heterogeneous primary tumor [23]. Because of the many steps required to form metastases, fully metastatic cells are rare clones in the tumor; less than 0.01% of the cancer cells entering the circulation in animal models develop into metastases [24, 25].

The metastatic cascade consists of a series of sequential and interrelated steps, beginning when tumor cells invade the host stroma, which contains thin-walled venules and lymphatic channels [26]. This is possible only after the tumor cells undergo the epithelial-mesenchymal transition (EMT), through which they shed many of their epithelial phenotypes and acquire the transcriptional program characteristic of mesenchymal cells. The EMT process affects not only the shape and motility of tumor cells, but also leads to major alterations in their gene expression

profiles: Most notably, expression of E-cadherin, a protein that enables epithelial cells to adhere to one another, is repressed [27].

After the tumor cells have moved into the lumina of blood and lymphatic vessels (known as intravasation), they detach from the extracellular matrix in the host tissue and can circulate in both the hematologic and lymphatic vasculature as aggregates. The rare cells that are able to survive the actively hostile environment of the circulation then arrest in distal capillary beds [28].

To form metastases, cancer cells must escape from the vasculature and penetrate into the surrounding tissue – a process known as extravasation – and they are able to do so via multiple mechanisms [26]. Tumor cells could either migrate *between* adjacent endothelial cells across intercellular junctions or *through* an endothelial cell that lines the vessel lumen [29]; for example, certain cancer cells secrete acid that stimulates endothelial cell retraction [30], while others can proliferate and form a mass within the lumen that exerts enough pressure on the vessel well to cause a rupture [31].

Last, the tumor cells proliferate within the newly-accessed organ parenchyma and establish their own vasculature supply, resulting in a metastatic focus [28].

The outcome of the metastatic process is in large part determined by complex interactions between metastatic cells and the host tissue [26]. Within the metastatic cascade, studies indicate that the rate-limiting step is the initiation of cell growth in the secondary organ, or colonization [32]: some tumors cells remain dormant in secondary organs [33], while in other tumors the absence of angiogenesis places a ceiling on tumor growth [34]. In general, the quantity of micrometastases in the body greatly outnumbers those that will grow large enough for clinical detection. These micrometastases could be widely disseminated throughout the tissues of a cancer patient and, because of their potential to form life-threatening masses,

targeting them before they become full-fledged metastases may in certain cases be an effective strategy.

Over a century ago, Stephen Paget suggested that metastasis is not a random process; rather, some tumor cells (the "seed") are specialized to grow preferentially in certain organs (the "soil"), and that metastasis was possible only when the "seed" grew in the appropriate "soil", analogous to the dispersal of plant seeds [35]. In the past half century, studies have demonstrated that the microenvironment plays a crucial role in regulating metastatic growth, supporting the "seed and soil" hypothesis [36]. Others have declared that the principal factor that dictates metastatic spread is the anatomy of the hematologic and lymphatic drainage from the primary tumor site [27]. While these hypotheses are not mutually exclusive, there is consensus that certain primary tumor types demonstrate an organ-specific pattern of dissemination, and the brain is one of the most common sites for the development of treatment-resistant metastases.

B. Brain Metastasis

Central nervous system (CNS) metastases account for the majority of malignant brain tumors, with an estimated annual incidence of 150,000-170,000 cases [37]. In the course of their disease, approximately 8-10% of adults with cancer will develop symptomatic brain metastases [38, 39] and, in up to half of these patients, the cause of death can be attributed to progression of brain metastasis [40]. Most brain metastases arise from the lung (40-50%), from melanoma (5-20%), or from the breast (15-25%) [38, 39]. Brain metastases tend to occur late in the course of a patient's cancer, when the primary tumor has already spread extensively to other organs; when the primary tumor was successfully treated, brain metastases may actually be the result of secondary metastasis [37]. Metastatic brain tumors are expected to become more prevalent, as more effective treatments of systemic disease lead to longer patient survival after primary

cancer diagnosis. In addition, the frequency of diagnosis is also likely to increase due to improvements in advanced imaging modalities and earlier detection [41].

Cognitive decline has been observed in almost two-thirds of patients with brain metastases [42, 43]. These lesions are often specified by symptoms, including headaches, seizures, loss of motor or sensory function, cranial neuropathy (abnormal function of a cranial nerve), and cognitive impairment – and validated with advanced imaging modalities, where lesions of a few millimeters in size are detectable [44].

HIGHLIGHTS

- Metastasis is an inefficient, multi-step process that involves tumor cells accessing the systemic circulation, exiting the circulation at distant sites, and colonizing the new host organ
- Brain metastases account for most malignant brain tumors
- Ten percent of cancer patients will develop symptomatic brain metastases during their disease, most of which arise from the lung, the breast, or from melanoma
- Cognitive decline is observed in two-thirds of patients with brain metastases
- Autopsy reports have identified micrometastases in the brain below the threshold for clinical detection, and brain metastases have formed several years after the cure of the primary cancer in some patients, suggesting a dormant cancer cell population
- Treating this undetectable dormant cell population as a prophylactic is an attractive strategy to reduce the incidence of brain metastases
- Astrocytes and microglia in the brain may promote the colonization step of metastasis

In the metastatic process, tumor cells that arrest in brain capillaries must extravasate into the brain parenchyma to form a clinically detectable metastatic focus; however, the cells may begin to proliferate while still in the capillary bed [45]. Eighty percent of brain metastases are detected in the cerebral hemispheres, 15% in the cerebellum, and 5% in the brainstem, closely mirroring the tissue volume and blood flow in the brain [37]. There is evidence that endothelial cells lining the brain vasculature actually promote metastatic cell growth and invasion [46, 47]. The blood-brain barrier (BBB) – the permeability barrier that separates the systemic circulation from extracellular fluid in the brain – does not inhibit tumor cell extravasation, although it does have major implications for systemic therapies [37].

If the "soil" is not fertile, tumor cells that leave the brain vasculature and enter the parenchyma may not grow, but instead die or remain dormant for years [24]; one label-retention study found that for every overt metastasis formed in the mouse brain, three disseminated tumor cells remained dormant [48]. Also, there is evidence of brain metastases developing in patients several years after the cure of the primary cancer: surgery and chemotherapy may have eradicated all extracranial disease, with the BBB protecting dormant tumor cells in the brain, providing a substantial pool of cancer cells to potentially lead to further metastases. This is one of the proposed reasons prophylactic whole-brain radiation therapy treatments have been successful in small-cell lung cancer patients [49], to be discussed in depth later.

After infiltration into the brain parenchyma, the tumor cells encounter several host cells, most notably the microglia and astrocytes, and a microenvironment that is conducive to tumor growth and treatment resistance. In experimental systems, activation of both microglia – glial cells that are the principal macrophages in the brain – and astrocytes – brain cells that form a physical and metabolic support system for nerves – has been well-documented [50-52]. Additional studies have suggested that microglia can enhance the invasion and colonization of disseminated tumor cells [53], and that astrocytes may both protect brain metastases from toxicity induced by chemotherapy [54, 55] and promote tumor cell proliferation.

Tumor growth is highly dependent on the establishment of an adequate blood supply, and tumors are able to recruit blood vessels through a variety of mechanisms. During the colonization process, vascular changes in the brain lead to lower vessel density as well as more dilated and tortuous vasculature compared to the normal brain [56]. The production of vascular endothelial growth factor (VEGF) seems to be necessary, but not sufficient, for cancer cells to proliferate in the brain [57]; however, anti-angiogenic therapies have shown mixed results in preclinical studies. Other prominent genetic alterations play a role in brain metastases, many of which may be specific to primary cancers, such as those of the breast.

C. Brain Metastasis in Breast Cancer Patients

Breast cancer is the second most common cause of brain metastasis, after lung cancer. Brain metastases are diagnosed roughly three years after the initial diagnosis of breast cancer [58] and, in most cases, after the appearance of systemic metastases in the bone, lung, and/or liver [59]. The prognosis is poor for all breast cancer patients who develop brain metastases, with reported median survival after brain metastasis diagnosis of 3.7, 9, and 15 months for triple-negative, HER2+, and luminal subtypes, respectively [60-62]. Historically, the one-year survival is less than 20%. Notably, due to improvements in systemic therapy, control of extracranial disease may no longer be the limiting factor in survival among breast cancer patients with brain metastases [63].

The risk of brain metastases is low – approximately 5% – when considering the entire breast cancer patient population; however, 10-16% of patients with stage IV breast cancer develop metastases [64, 65], while many brain lesions are asymptomatic and go unidentified until autopsy in 20-40% of advanced stage patients [66]. Broken down further, it is estimated that 25-35% of HER2+ stage IV breast cancer patients and 40-45% of TNBC stage IV patients will develop brain metastases [67, 68]. Because these stage IV, HER2+ and TNBC patients not only have the highest risk of developing brain metastases but also of succumbing to them, prevention is an attractive option. Risk factors and prevention of breast cancer brain metastasis will be explored thoroughly in Section III.

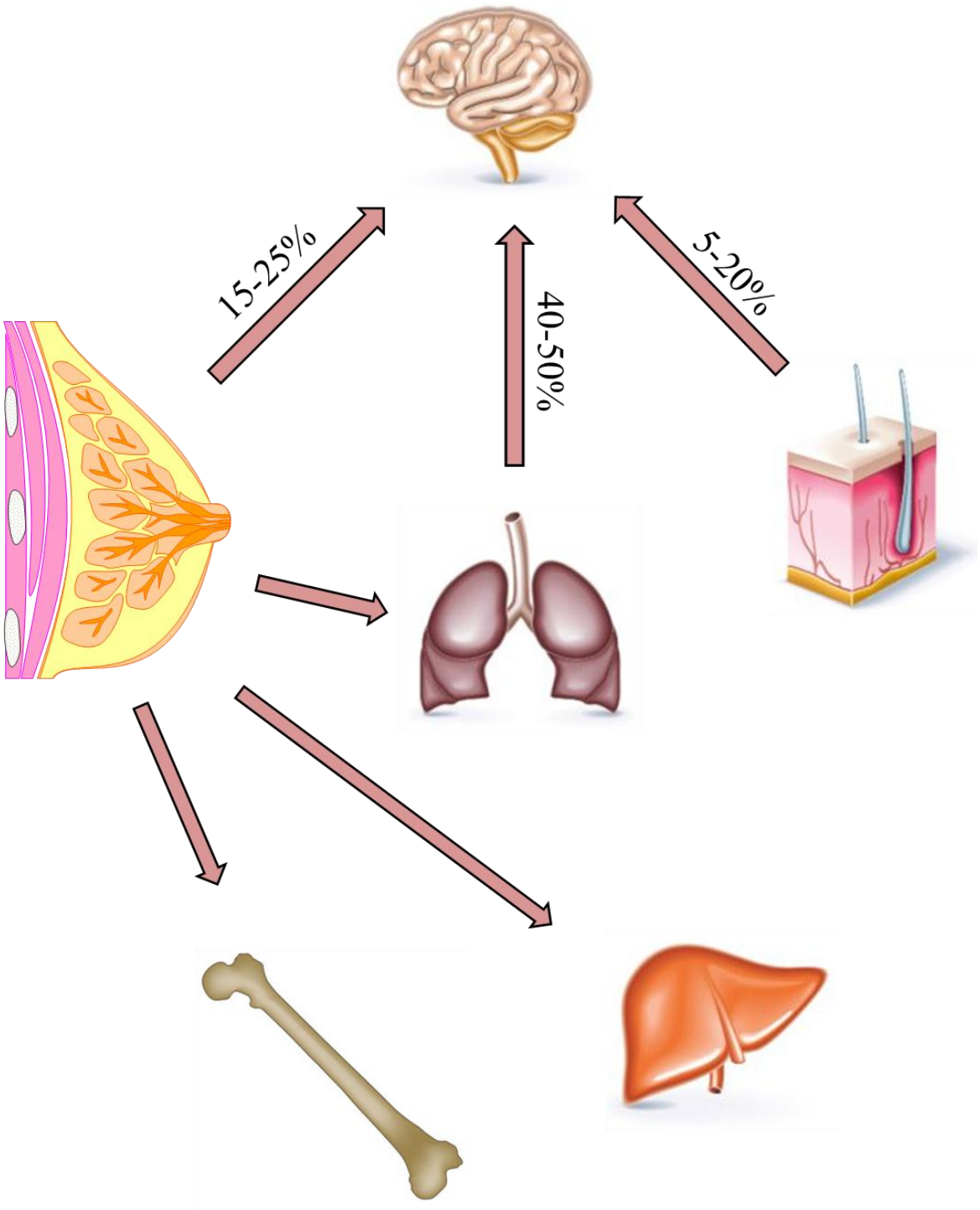

Figure 1: Metastatic Spread from Breast and to Brain. The principal organs to which the breast metastasizes are the lungs, the liver, bone, and the brain. Typically, breast cancer brain metastasis will occur after the primary breast cancer has spread to other organs throughout the body. The most common tumors that metastasize to the brain are lung cancer (40-50%), breast cancer (15-25%), and melanoma (5-20%). Interestingly, secondary metastases have been observed in the brain, notably from primary breast tumors via lung metastases.

Several genetic alterations are involved in the formation of brain metastases originating from breast cancer [41, 69], most of which are beyond the scope of this review. However, HER2, the member of the epidermal growth factor receptor superfamily, is critical in the understanding of the present study. In mouse preclinical experiments, one group found that overexpression of HER2 had no effect on the number of micrometastases in a brain-seeking clone of a human breast cancer cell line, but it increased the number of large brain metastases three-fold [70]. This suggests that HER2 promoted the colonization step of brain metastasis in this breast cancer cell line, rather than driving the initial stages of the metastatic cascade [44], and that therapies targeted at HER2 may inhibit the progression of already-present brain metastases.

HIGHLIGHTS

- Brain metastases originating from breast cancer tend to occur late, after metastasis to the bone, lungs, and/or liver
- Median survival from time of brain metastasis diagnosis for HER2+ and TNBC patients is on the order of months
- Risk of brain metastasis is highest in stage IV breast cancer patients, at 25-35% for HER2+ and 40-45% for TNBC
- These high-risk patients are candidates for therapies focused on prevention of brain metastasis formation
- HER2 may promote the final colonization step of brain metastasis
- Our group developed a mouse model of HER2+ and TNBC breast cancer that can reliably recapitulate the latter steps of the metastatic process in the brain

Animal model systems that recapitulate many aspects of brain metastases are crucial in our understanding of basic biology, and also for the preclinical evaluation of novel therapeutic strategies. As mentioned above, one group created a brain-seeking clone from the MDA-MB-231 breast cancer cell line. A different group found that a variant of a TNBC cell line spontaneously metastasizes to the brain in 42% of mice [69]. More recently, our group developed mouse models of breast cancer that reliably metastasize to the brain [71]. In this model, tail-vein injection of both a HER2+ and a triple-negative breast cancer cell line led to a high rate (~67%) of brain metastases in SCID/Beige mice; the cells, labeled with green fluorescent protein (GFP), could be easily identified after brain resection by fluorescent stereomicroscopy. Furthermore, the utility of the model was

validated when genetic knockdown of a specific microRNA led to almost complete inhibition of the formation of brain metastases. This robust model could provide an effective platform to advance not only the field of brain metastasis research but also treatments directed at breast cancer brain metastases.

Cell Line	*Vector*	*Subtype*	*Lung Mets*	*Brain Mets*
SUM149	Empty	**Triple-negative IBC**	7/9	**6/9**
MDA-IBC3	Empty	**HER2+ IBC**	3/15	**10/15**
MDA-231	miR-141 OE	Triple-negative	10/10	5/9
SUM159	miR-141 OE	Triple-negative	7/12	1/10

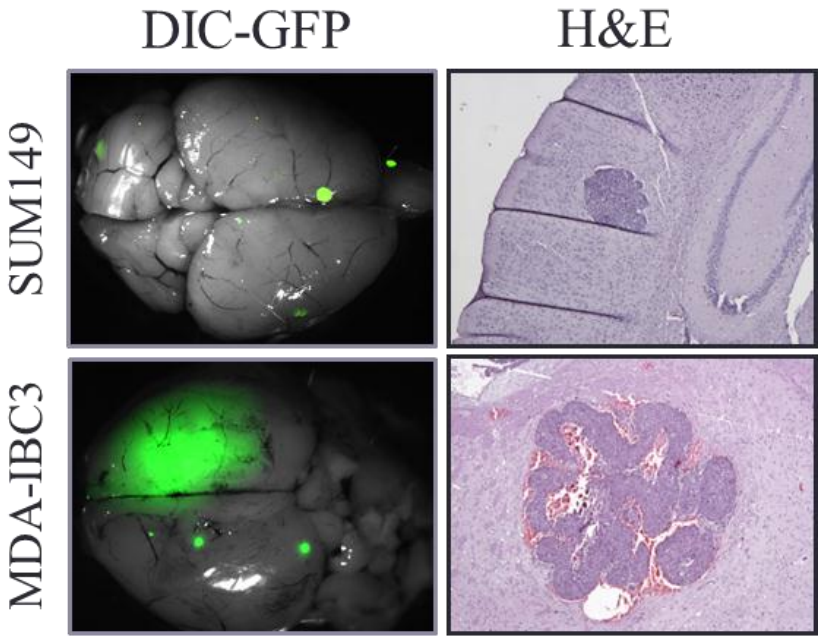

Figure 2: Mouse Model of Inflammatory Breast Cancer. Our group has developed a mouse model of metastatic breast cancer, where injection of 500k green fluorescent protein-labeled breast cancer cells results in approximately 67% incidence in untreated SCID/Beige mice in the SUM149 and MDA-IBC3 cell lines. In cell lines with low baseline miR-141 and high E-cadherin, overexpression of miR-141 can lead to the same incidence (MDA-231). In this thesis, the MDA-IBC3 line was used.

While there is an opportunity to vastly improve the outcomes of breast cancer patients who develop brain metastases, current treatments have demonstrated a measurable, albeit small, benefit.

D. Brain Metastasis Treatment Options

For patients with brain metastases, many factors dictate the direction of therapy: performance status, expected prognosis, number, location, and size of brain metastases, presence of symptoms, suitability for surgical resection, and availability of options to control extracranial disease. Several groups have formulated guidelines for managing these patients, including the National Comprehensive Cancer Network (NCCN) and the American Society for Radiation Oncology. Treatment options include surgical resection, whole-brain radiation therapy (WBRT), and stereotactic radiosurgery (SRS). WBRT consists of a series of low-dose treatments to the entire brain, while SRS is used as an alternative to surgical resection to irradiate a single brain metastasis. No systemic therapies have been approved to specifically treat brain metastases from solitary tumors in the United States, although data is available from clinical trials [72].

Patients with a single metastatic brain lesion are assessed for their suitability for surgical resection and SRS. Two studies demonstrated an advantage to using surgical resection followed by WBRT compared to WBRT alone, with an increase in overall survival from 15 to 40 weeks [40, 73]. The addition of SRS to WBRT versus WBRT alone has produced mixed results [74, 75]. However, these patients are rare, as it has been well-documented that solitary brain metastases are uncommon [64-66].

Patients who present with limited brain metastases generally receive SRS, combined SRS and WBRT, or WBRT [76]. Two studies found no differences in overall survival with the addition to WBRT to SRS, compared to SRS alone [77, 78]. Surgery has a limited role in patients with more than one brain metastasis. Both surgical resection and SRS are ineffective in patients with multiple brain metastatic lesions, where WBRT is the principal treatment [76]. In patients with poor performance status, best supportive care is also an option [72].

There is little data to support specific treatment strategies in patients with recurrent or progressive brain metastases. The NCCN guidelines recommend that patients with stable systemic disease should be considered for surgery, re-irradiation, or chemotherapy; patients with systemic disease progression should be considered for best supportive care or re-irradiation.

HIGHLIGHTS

- In most cases, surgery is limited to treating patients with only one detectable brain metastasis
- Stereotactic radiosurgery, which irradiates single metastatic sites, is used in patients with limited brain metastases
- Whole-brain radiation therapy is the principal treatment in patients with extensive brain metastases
- Systemic agents are largely ineffective in treating brain lesions, as many do not penetrate the blood-brain barrier
- As the success of systemic agents in treating extracranial disease improves patient survival, an increasing number of cancer patients are presenting with and succumbing to brain metastases
- Trastuzumab treatment was found to increase the relative risk of developing brain metastases by over 50% in a meta-analysis
- Brain treatment-related toxicity is difficult to evaluate

Chemotherapy use in the treatment of brain metastases has been limited, as many patients have undergone several rounds of chemotherapy prior to the development of brain metastases and also because of the exclusion of patients with brain metastases from clinical trials [41]; the data that does exist is discouraging. One of the major impediments to systemic agents effectively treating brain metastases is the blood-brain barrier (BBB).

The BBB is formed by endothelial cells lining the cerebral vasculature, and separates the cerebrospinal fluid (CSF) from the systemic circulation. Tight junctions between the endothelial cells create a physical barrier, forcing molecules to pass through cells rather than around them. The endothelial cells express large amounts of active transporters, which pump certain substances out of the cells and back into the systemic circulation, away from the brain parenchyma. The molecules that are able to pass from the blood into the brain tend to be small and lipophilic, unrecognized by the efflux pumps [79]; however, most standard chemotherapy agents are substrates of these pumps and do not cross into the CSF [80, 81]. When lesions in the brain grow beyond a 1-2 mm diameter, the BBB becomes structurally compromised [82],

increasing BBB permeability and permitting chemotherapeutic agents to enter the CSF. Unfortunately, the lack of success in treating brain metastases indicates that if the BBB is compromised near a lesion, there is insufficient accumulation of chemotherapy agents in the brain to effect a response.

Trastuzumab, the monoclonal antibody that is used as a systemic agent in patients with HER2+ breast cancers, does not cross the BBB. A meta-analysis of clinical trials using trastuzumab to treat breast cancer patients revealed a relative risk of brain metastasis of 1.57 [83]. This could be due to improvements in systemic control with trastuzumab, prolonging patient survival and increasing the timeframe through which brain metastases can become symptomatic. In addition, it has been proposed that trastuzumab alters the underlying biology of invasive breast cancer cells in such a way as to preferentially drive them towards the brain.

Lapatinib, an inhibitor of both EGFR and HER2, is indicated for use with the anti-metabolite capecitabine for the treatment of patients with advanced or metastatic HER2+ breast cancers who have received a prior systemic therapy [72]. Lapatinib can reach therapeutic levels in brain metastases, although it does not cross the intact BBB [84]. A trial comparing the combination of lapatinib and capecitabine versus WBRT alone is in the planning stages; several trials of other HER2-targeting inhibitors for the treatment of breast cancer brain metastases are in progress [72].

Evaluating toxicity from therapies directed at brain metastases is difficult, as morbidity due to the treatment must be differentiated from the morbidity due to the brain lesion(s). Nevertheless, it is critical to understand the potential neurocognitive decline that patients could exhibit after the course of treatment, especially if the intracranial metastases respond to therapy, prolonging patient survival. Neurological toxicity associated with whole-brain radiation therapy will be discussed in detail in the following section.

Major improvements in local and systemic therapies are increasing patient survival times and, as a result, more patients are presenting and then succumbing to brain metastases. Despite the use of surgical resection, radiation therapy, and systemic therapies in breast cancer patients with brain metastases, outcomes remain extremely poor. Novel strategies to treat brain metastases include enhancing therapeutic delivery to the brain, the development of radiosensitizers, or the implementation of preventative agents. The use of whole-brain irradiation (WBI) as a preventative strategy, known as prophylactic cranial irradiation, has improved overall survival in non-small cell lung cancer and acute lymphoblastic leukemia patients who are at high risk of developing brain metastases – whether or not the same strategy could be used effectively for high-risk breast cancer patients remains unresolved.

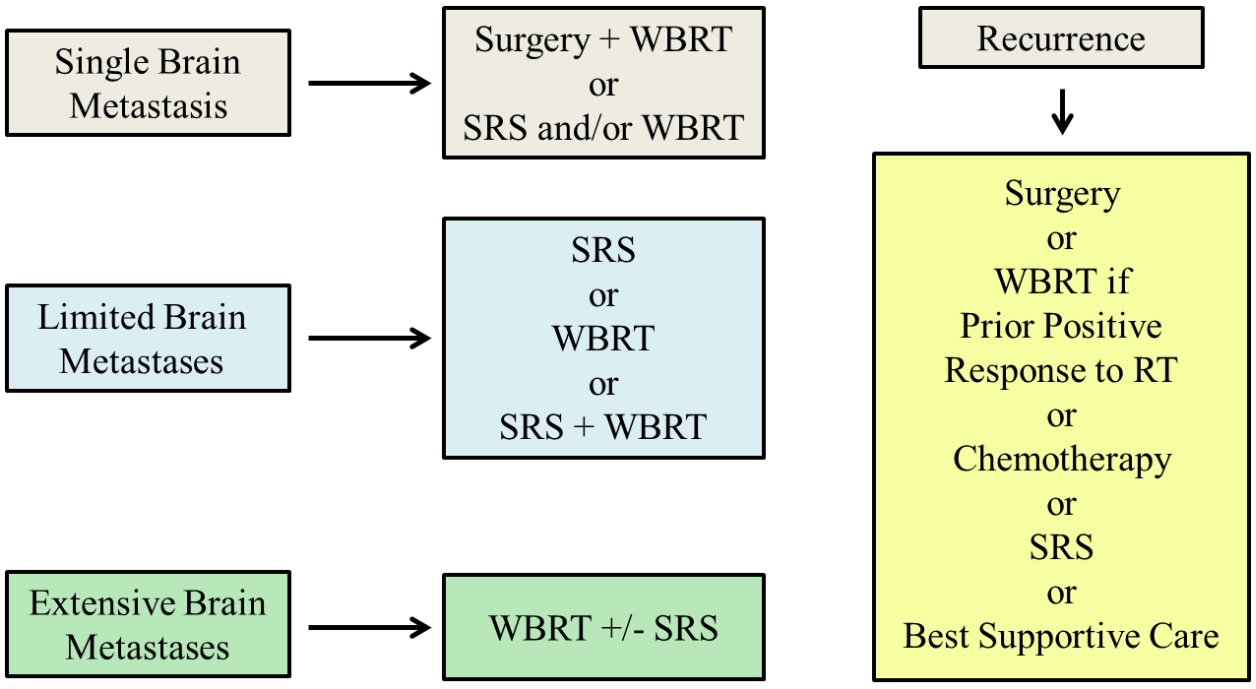

Figure 3: Treatment guidelines for patients with brain metastases. Common treatments for patients with brain metastasis include surgery, SRS, WBRT, and chemotherapy.

SECTION III. PROPHYLACTIC CRANIAL IRRADIATION

The risk of brain metastasis is high when considering the advanced stages of certain primary cancers, such as small-cell lung cancer, acute lymphoblastic leukemia, and breast cancer. Even with major advances in multimodal therapy, the patients who are diagnosed with brain metastasis have very short survival times, usually less than one year from the time of diagnosis. As mentioned in the preceding section, novel strategies to treat brain metastases are being explored, but improvements in the treatment of brain metastases continue to be marginal.

The presence of non-symptomatic, undiagnosed micrometastases in the brain of many advanced stage cancer patients was also noted above. This pool of lesions below the threshold for clinical detection presents both a problem – the dormant cells could become activated at any point, even years after the primary tumor has been cured, leading to overt brain metastases that have major adverse consequences for the patient – and an opportunity – it may be possible to use therapeutics to treat the micrometastases or to alter the brain microenvironment in such a way as to reduce or altogether inhibit the future develop of brain metastases. In addition, prophylactics may minimize neurocognitive impact in patients, whereas typical therapies for brain metastases are each associated with side effects that adversely impact quality of life.

To be successful, prevention strategies in general require several factors, including a high incidence rate of the event to be prevented, efficacy and durability, and acceptable levels of morbidity [85]. The most promising preventative approach in patients with advanced disease, known as prophylactic cranial irradiation (PCI), utilizes whole-brain irradiation (WBI) in patients who are at high risk of developing brain metastases. This technique has been used successfully to improve intracranial control and survival for patients with small-cell lung cancer and children with acute lymphoblastic leukemia, and there is rising interest to explore the potential for PCI in high-risk breast cancer patients.

A. Acute Lymphoblastic Leukemia

Acute lymphoblastic leukemia (ALL) refers to a group of lymphoid disorders characterized by the overproduction of cancerous, immature white blood cells, known as lymphoblasts, in the blood, bone marrow, and other organs. ALL is most common in children around the ages of 4-5 years, with a peak incidence of five per 100,000 [86]. Prior to the adoption of prophylactic techniques in children with ALL, the brain accounted for roughly 75% of recurrences [87]; with modern treatments, only 5-10% of children with ALL relapse in the brain [88].

Due to the high rate of relapse in the brain, PCI was introduced over four decades ago as a prevention strategy in children with ALL who were at high risk for brain relapse. In the initial studies using PCI (24 Gy), relapse was observed in the brain in 4% of children who underwent PCI compared to 67% of children in the non-irradiated control group [89]. PCI is currently used in less than 20% of children with ALL, and overall five-year survival rates for all child ALL patients are above 85% [90].

When PCI is used in children with ALL, it is most often combined with either systemic or intrathecal (direct delivery to brain, rather than through systemic circulation) chemotherapy. Due to the intrinsic radiosensitivity of leukemic cells and improvements in chemotherapy regimens, the PCI doses administered to children were lowered to 12-18 Gy, in ten fractions.

Because these patients are children and the long-term survival rates are high, treatment-related late effects are a major concern. The use of PCI in childhood ALL has been steadily reduced since the late 1970s, as it can cause neurocognitive impairment and increased incidence of second cancers twenty years after the initial diagnosis of ALL [91]. Furthermore, two recent studies have shown that by intensifying systemic and intrathecal chemotherapy, PCI can be omitted without compromising overall survival [92, 93].

B. Small Cell Lung Cancer

Small cell lung cancer (SCLC) accounts for roughly 15% of all lung cancers, and is characterized by its rapid doubling time and early development of widespread metastases. Although SCLC responds initially to radiation and chemotherapy, most patients die from recurrent disease, with five-year survival rates ranging from 30% for patients with local disease to 2% for patients with advanced disease [94].

Brain metastasis is common in patients with SCLC: 15% of patients present with brain metastases at the time of diagnosis, and approximately half of patients in complete remission after treatment for limited disease SCLC will relapse in the brain, causing serious impairment of patient survival and quality of life [95]. For patients treated for SCLC, median survival after brain relapse is six months [96].

PCI was introduced in the early 1980s to reduce the incidence of brain metastasis in patients with both limited and extensive disease SCLC [96]. A meta-analysis, based on SCLC patients (85% limited disease, 15% extensive disease) in complete remission that were included in seven randomized phase III studies, reported a decrease from 59% to 33% in the cumulative incidence of brain metastasis three years after PCI; this corresponded to an overall survival increase from 15.3% to 20.4% in patients who received PCI [49]. In the same analysis, the authors noted a significant trend towards decreased incidence of brain metastasis with both higher radiation dose and earlier administration of PCI after the start of SCLC treatment. For patients with limited disease SCLC who respond to first-line treatments, 25 Gy in ten fractions is recommended for PCI [96].

Similarly, PCI is also standard treatment for all patients with extensive disease SCLC. In a randomized phase III trial comparing PCI (20-30 Gy) versus observation, PCI significantly reduced the cumulative incidence of brain metastasis at one year from 40.4% to 14.6%, with an associated increase in one-year overall survival from 13.3% to 27.1% [97].

HIGHLIGHTS

- Patients with certain primary cancers, in advanced stage, are at high risk of developing brain metastases
- Even with advances in multimodality therapy, the prognosis of patients with brain metastases is very poor
- In experimental studies and in autopsy reports from deceased cancer patients, micrometastases below the threshold for clinical detection have been identified, suggesting a dormant tumor cell population that had yet to be activated and cause a detectable metastasis
- Prevention strategies require a high incidence rate of the event to be prevented (high risk of brain metastasis), efficacy and durability of the treatment (prevention of metastasis to extend patient survival), and acceptable levels of morbidity (minimal cognitive impairment)
- Prophylactic cranial irradiation uses whole-brain radiation therapy as a preventative measure in patients at high risk of developing brain metastases
- This technique has been used for decades in children with acute lymphoblastic leukemia and adults with small cell lung cancer to reduce the incidence of brain metastases and to significantly improve overall survival in these high-risk patients

Although toxicity from PCI is much less of a concern in patients with SCLC compared to children with ALL, there are efforts to identify patients at high risk of developing brain metastases. For example, one group reported that response to chemotherapy and weight loss of less than 5 kg at presentation were independent predictors of future brain metastasis [98].

C. Non-Small Cell Lung Cancer

Non-small cell lung cancer (NSCLC) accounts for the other 85% of lung cancers, and is the leading cause of cancer-related deaths for both men and women in the United States with five-year survival rates ranging from 1-50% [99]. The incidence of brain metastasis in NSCLC patients ranges from 13-54% and half of these patients will die from brain metastasis progression [96]. The addition of chemotherapy to the treatment of patients with locally advanced NSCLC has substantially improved the prognosis of patients in the past fifteen years; however, the longer resulting survival times combined with the ineffectiveness of chemotherapy agents in the brain have actually led to increased risk among NSCLC patients of developing brain metastases [100].

	ALL	SCLC		NSCLC
	Children	Limited Disease	Extensive Disease	Stage III-IV
Incidence of Brain Metastasis	Observed: 67% PCI: 4%	Observed: 40% PCI: 33%	Observed: 59% PCI: 15%	Observed: 22-55% PCI: 4-13%
Overall Survival	Significant Benefit to PCI	Significant Benefit to PCI	Significant Benefit to PCI	No Benefit from PCI
Indications	Poor response to chemo Overt CNS disease	All patients after CR to chemotherapy	Following chemotherapy	Undetermined
Dose	12-18 Gy (1.8-Gy fxs)	8 Gy/1 fx to 40 Gy/20 fxs	20 Gy/5 fxs to 30 Gy/10 fxs	30 Gy/15 fxs

ALL: Acute lymphoblastic leukemia; SCLC: Small cell lung cancer; NSCLC: Non-small cell lung cancer

PCI: Prohylactic cranial irradiation; CR: complete response; Gy: Gray; fx: fraction

Adapted from these publications:

1) Bovi JA and White J. *Current Oncol Rep* 2012, 14:55-62.
2) Aur R, Hustu H, and Verzosa M. *Blood* 1973, 42(3): 349-357.
3) Pui C, *et al*. *Blood* 2012, 120(6): 1165-1174.
4) Pui C, *et al*. *New England Journal of Medicine* 2003, 349(7): 640-649.
5) Auperin A, *et al*. *New England Journal of Medicine* 1999, 341(7): 476-484.
6) Slotman B *et al*. *New England Journal of Medicine* 2007, 357(7): 664-672.
7) Paumier A, Cuenca X, and Le Pechoux C. *Cancer Treatment Reviews* 2011, 37(4): 261-265.
8) Gore EM, Bae K, and Wong S. *J Clin Oncol* 2009, 27(15 S).

Table 2: Clinical Data for Prophylactic Cranial Irradiation in SCLC and ALL Patients. PCI reduces the incidence of brain metastasis in patients with ALL, SCLC, and NSCLC, althought improvements in overall survival have only been observed in ALL and SCLC patients.

Several groups have addressed this trend by investigating the use of PCI in patients with locally advanced NSCLC. In five of six randomized studies, the NSCLC patients who received PCI had significantly lower incidence of brain metastasis than patients in the control arm (usually by more than 50%); the sixth study found a trend in the same direction. However, no benefit in overall survival was detected in any of these reports, likely due to low sample sizes and high systemic failure rates [101-106]. Currently, PCI is not considered standard of care for patients with locally advanced NSCLC; nevertheless, due to the improved intracranial disease control despite the lack of improvement in overall survival, the role of PCI in NSCLC continues to be investigated.

D. Breast Cancer

Brain metastases lead to compromised survival and a poor quality of life in breast cancer patients and, therefore, the use of prophylactic cranial irradiation in breast cancer patients at high risk of developing brain metastases has garnered increased interest in recent years. Moreover, with an aging population and improvements in extracranial disease control with trastuzumab and other systemic agents, the number of breast cancer patients who are diagnosed and succumb to brain metastases will continue to rise.

As mentioned in the preceding section, there is considerable evidence that patients with advanced stage, HER2+ or triple-negative breast cancers have a propensity for developing brain metastases. This differs vastly from the entire breast cancer patient population, which has an estimated 5% risk of developing brain metastasis during the course of their disease. Further, the incidence of brain metastasis is too low in early-stage breast cancer for prevention to be a reasonable option, as the patients would be subject to unnecessary toxicity. Conversely, the high-risk cohort which already has extracranial metastases has an incidence of brain metastasis that is high enough (25-45%) to consider PCI.

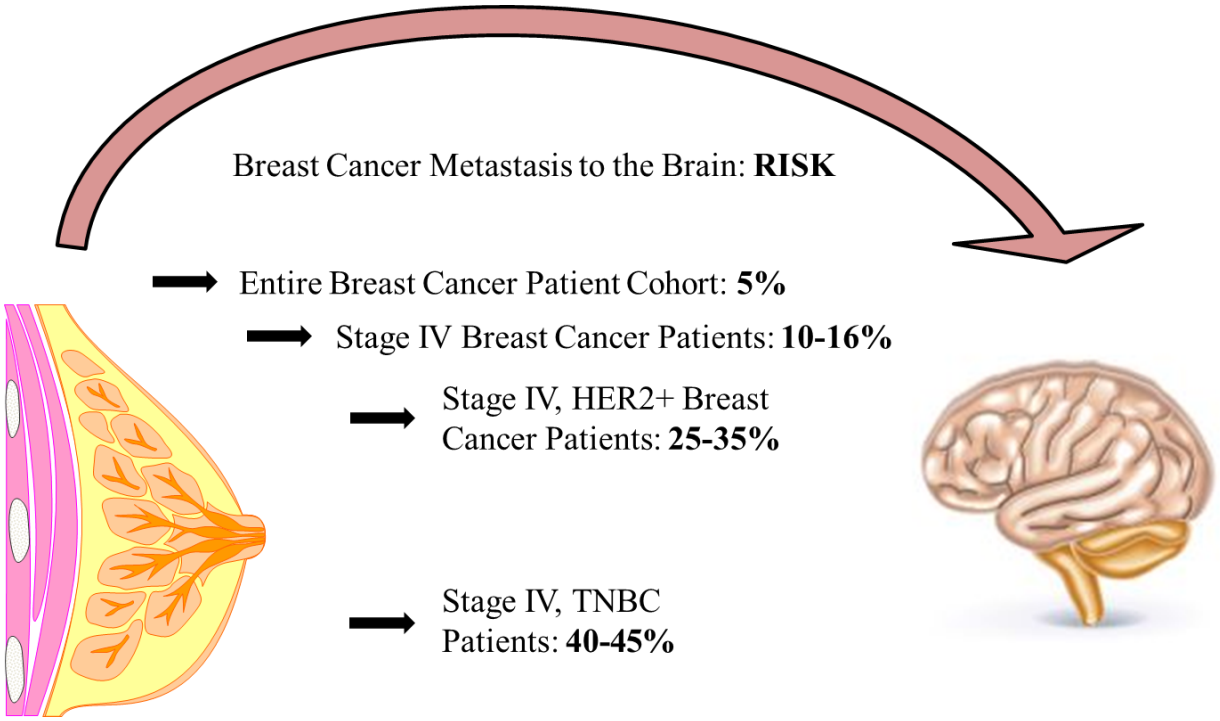

Figure 4: Stratification of Breast Cancer Patients at Risk of Brain Metastasis. Specific breast cancer patient cohorts are at increased risk of developing brain metastases, broken down by disease stage, molecular subtype, and other factors. The patients at the highest risk of developing brain metastases are within the stage IV, HER2+ or TNBC subtype cohorts.

Other variables besides molecular subtype are reported to have an association with risk of brain metastasis in breast cancer patients, including age and histologic grade; however, taken individually these factors are qualitative. To quantify the risk of brain metastasis for *individual* breast cancer patients, rather than the risk of an entire patient cohort, Ibrahim and colleagues constructed a nomogram by combining clinical and pathologic variables using a multivariate model [107]. In the patient set used to develop the nomogram, the area under the receiver operating characteristic curve (AUC) was 0.68, while the AUC was 0.74 in the validation set. The factors independently associated with higher probability of brain metastasis were younger age, higher histologic grade, triple-negative and HER2+ status, shorter delay between breast cancer diagnosis and first metastasis, and more than one non-brain metastatic site. Based on the nomogram, the range of probabilities for an individual non-brain metastatic breast cancer patient

to develop brain metastasis is approximately 5-50%. The same group is constructing a similar nomogram for inflammatory breast cancer patients.

HIGHLIGHTS

- There is a breast cancer patient cohort – Stage IV, TNBC or HER2+ -- that has a high enough risk of developing brain metastasis to consider prevention strategies such as PCI
- Recent efforts have attempted to quantify the risk that individual patients have of developing brain metastasis, which would enable selection of individual patients for clinical trials with PCI
- In one study, ten breast cancer patients in complete remission received PCI: two patients had central nervous system failures and three survived long enough to exhibit severe cognitive decline
- In a separate study, WBRT reduced the cerebral deaths threefold in a breast cancer population with occult (detected by MRI but asymptomatic) brain metastases, although there was no improvement in overall survival
- The brain is a late-responding tissue to irradiation, and is one of the least radiosensitive organs
- Common toxicities observed in WBRT patients and in SCLC PCI patients are quality of life factors (hair loss & fatigue) and neurocognitive decline (memory loss)

The clinical utility of this nomogram is to further define the breast cancer patients with the highest risk of developing brain metastases, and who were most likely to benefit from a preventative strategy such as PCI. For example, if selecting only the patients with a greater than 25% probability of developing brain metastasis, only 30% of the population (of non-brain metastatic breast cancer patients) would be treated, but roughly 80% of the subsequent brain metastases would potentially be prevented [107]. An optimal percentage of high-risk breast cancer patients could be selected for clinical trials evaluating the efficacy of PCI.

No large-scale studies evaluating the use of PCI in breast cancer patients have been conducted; however, we can draw insight from smaller studies. In one investigation, stage IIIB/IV breast cancer patients who responded to anthracycline-based induction chemotherapy underwent autologous marrow transplantation, after which the ten patients in continued remission were referred for PCI [108]. In those ten patients treated with PCI, there were two central nervous system failures (20% incidence post-PCI), but no comparisons could be drawn with the non-PCI group because of inherent bias in the study design.

In a separate study, Niwinska et al. [109] compared the efficacy of WBRT to treat HER2+ breast cancer patients with symptomatic (overt) versus non-symptomatic (occult) brain metastases. There was a threefold decrease in the number of cerebral deaths when patients with occult brain metastases were treated with WBRT as compared to the symptomatic patients; however, overall survival was not affected. They concluded that an early onset of WBRT can reduce the occurrence of severe neurologic complications and can have a major impact on quality of life. Nonetheless, the study had significant limitations, including a relatively small sample size and a large rate of extracranial failure. With improvements in the treatment of extracranial disease with systemic agents, a threefold decrease in cerebral deaths would likely translate to improvements in overall survival. Further, this study looked at HER2+ breast cancer patients with occult brain metastases that were treated with WBRT; prophylactic cranial irradiation would be administered to high-risk patients *before* the onset of (a)symptomatic brain metastases or to prevent intracranial relapse.

Finally, a recent study out of the UK looked at the effect of PCI in HER2+ breast cancer patients with locally advanced or metastatic disease as the first relapse [Canney]. The recruitment target was 390 patients to randomize into the PCI or non-PCI arm; unfortunately, only 51 patients were enrolled, mostly due to the reluctance of physicians to approach patients recently diagnosed with metastatic disease about the possibility of PCI. While the incidence was decreased in the PCI group – 30 Gy in ten fractions – from 32% to 21%, this was not significant. It is important to note that there was no additional toxicity associated with the PCI.

The prevention of brain metastases with PCI could substantially improve the survival and quality of advanced stage breast cancer patients. Additional investigations are needed to precisely define the breast cancer patients that would most benefit from PCI, ideal timing of delivery, dose and fractionation schedule, and systemic agents to be administered concurrently to PCI.

E. Neuropsychological Problems

The importance of identifying the breast cancer patients most likely to develop brain metastases stems in large part from the potential toxicity associated with WBRT. Any intervention must weigh the benefits against the potential morbidity, and only patients with high enough risk of developing brain metastases would be considered for PCI in the event that the technique is adopted clinically.

It is generally accepted that DNA damage occurs in the minutes to hours following irradiation; cell death in the days following irradiation; early effects (toxicity) are caused by the death of a large number of cells in rapidly proliferating tissues, occur within days to weeks after irradiation, and is generally repaired rapidly because of the proliferation rate; and late effects (toxicity) manifest in slowly proliferating tissues, in the months to years following irradiation, and is never completely repaired. The principal cells in the brain are either non-proliferating or slowly proliferating, and consequently it is a late-responding tissue. Furthermore, the brain is considered one of the least radiosensitive organs [110]. Nevertheless, there are common adverse effects observed in patients treated with PCI or WBRT that need to be mentioned.

In the case of PCI in SCLC, patients are likely to present some neurocognitive abnormalities at baseline, but the whole-brain irradiation can lead to further decline in many of the treated patients [111]. First, quality of life is adversely affected by PCI, but the impact seems to be limited to fatigue and hair loss. A different study found that 75% of PCI patients had neurologic complaints such as difficulty with walking or balance and memory loss. Another sixty-five percent had abnormal neuropsychologic testing, generally due to memory or IQ impairment; however, no baseline information was collected so the effect of PCI is not definitive [112]. The same study also found that higher radiation fraction sizes or concurrent chemotherapy was associated with greater abnormalities. A separate study identified increasing age as a risk for neurocognitive decline [113], which indicates that not only do we have to

consider patient selection for PCI from the vantage point of benefit but also from risk (toxicity). In conclusion, it seems that the major adverse events from PCI are likely to be a decrease in the quality of life (fatigue and hair loss) and neurocognitive decline (most notably, memory).

In the small breast cancer PCI study mentioned in the previous section, Huang and colleagues found that of the ten breast cancer patients who received PCI, three lived long enough to exhibit signs of neurocognitive decline [108]. The prescription was 36 Gy in 20 fractions – higher than is typical for SCLC patients – and the neurocognitive decline was noted at 9 months, 4 years, and 5 years post-PCI in the three patients. Unfortunately, no control groups were included in the study, and due to the small sample size no strong conclusions could be drawn.

SECTION IV. SCOPE OF DISSERTATION

Breast cancer patients whose tumors metastasize to the brain have extremely poor prognosis, and treatment options are severely limited due to the poor penetration of the blood-brain barrier by systemic agents. From both animal studies and autopsy reports, it is evident that there is a large population of micrometastases – below the threshold for clinical detection but with the potential to form overt, life-threatening metastases – in many advanced stage cancer patients. In acute lymphoblastic leukemia and small cell lung cancer patients at high risk of developing brain metastases, this population of micrometastases has been effectively targeted, with prophylactic cranial irradiation, in an attempt to slow the incidence of overt brain metastases and improve patient survival. Patients with stage IV, HER2+ or triple-negative breast cancer are at high risk of developing brain metastases; whether prophylactic cranial irradiation can benefit these patients is a gap in knowledge that needs to be addressed. The central hypothesis of this dissertation is:

Prophylactic cranial irradiation will reduce the incidence of brain metastasis by 50% in a mouse model of metastatic, HER2+ inflammatory breast cancer

Three specific aims will be addressed in the present work:

Specific Aim 1: Show that a dose of 4 Gy will reduce the incidence of brain metastasis only when administered as a prophylactic

- Examine if irradiation prior to cell injection primes the brain for metastasis
- Determine if there is an association between the incidence of brain and lung metastasis

Specific Aim 2: Develop a computational model of radiation dose-response for subclinical breast cancer based on the metastatic HER2+ mouse model

- Recapitulate the experimental non-irradiated mice data by optimizing input parameters
- Validate the model assumptions and inputs by performing a limiting dilution assay

Specific Aim 3: Demonstrate that 4 Gy prophylactic cranial irradiation in the computational model reduces the incidence of brain metastasis by 50%

- Investigate if the experimental incidence can be realized by the assumptions used to develop the model
- Demonstrate that delaying treatment introduces a dose threshold below which no reduction in the incidence is observed

By examining the use of PCI in a mouse model of metastatic HER2+ inflammatory breast cancer, we will move closer to understanding the utility of using PCI in breast cancer patients who are at high risk of developing brain metastases.

CHAPTER 2: PROPHYLACTIC CRANIAL IRRADIATION REDUCES BREAST CANCER BRAIN METASTASIS IN MICE

SECTION I. INTRODUCTION

We elected to investigate the utility of whole-brain irradiation to prevent brain metastases – a technique known as prophylactic cranial irradiation (PCI) – in a mouse model surrogate of breast cancer patients at high risk of developing brain metastasis. As mentioned in the introduction, clinicians are now able to identify a subset of breast cancer patients who have a risk of developing brain metastasis upwards of 30%. Because the outcomes of breast cancer patients with brain metastasis are abysmal, even with the use of multimodality therapies, prevention strategies are attractive. PCI has been used in children with acute lymphoblastic leukemia and adults with small cell lung cancer to both reduce the incidence of brain metastasis and to improve overall survival, and there is interest in running clinical trials with high-risk breast cancer patients in order to evaluate the efficacy of PCI. My work, described in the present chapter, addresses the question of whether micrometastatic breast cancer in the brain is treatable with a PCI dose, and if any observed effect is durable.

This chapter represents the principal line of inquiry for my thesis, for which the hypothesis is that **prophylactic cranial irradiation will reduce the incidence of brain metastasis by 50% in mouse model of metastatic, HER2+ inflammatory breast cancer**. The specific aim that will be addressed in this chapter is to *show that a dose of 4 Gy will reduce the incidence of brain metastasis only when administered as a prophylactic*. There are two sub-aims: 1) examine if irradiation prior to cell injection primes the brain for metastasis, and 2) determine if there is an association between the incidence of brain and lung metastasis.

In SCLC patients who are diagnosed with brain metastases and treated with WBRT, the total dose is usually 30 Gy; in the case of SCLC PCI, the total dose is 25 Gy (i.e. the WBRT and

PCI doses are very similar). Therefore, the aim for this experiment was to identify if there is a dose that would be *effective for PCI but not for WBRT*.

In order to investigate my hypothesis, I utilized the mouse model that was recently developed in our lab [71]. In this model, two-thirds of untreated mice developed brain metastases, in two separate inflammatory breast cancer cell lines, when SCID/Beige mice were tail-vein injected with five hundred thousand cells. Eight weeks after injection, the mice were sacrificed and we were able to observe the green fluorescent protein-labeled metastases under a stereomicroscope. In the past, metastasis has been a difficult process to study due to the death of experimental systems; this model allows us to examine therapies which may be effective in mitigating the adverse effects caused by brain metastases, and forms the backbone of this chapter.

A second major limitation which would have hindered this study in the recent past is the lack of precision of small-animal radiation research. Fortunately, several platforms have been developed in the past decade that permits the delivery of x-rays to a specified area with excellent precision and accuracy. One such platform is the X-RAD C225x, developed by medical physicists at the University of Toronto [114]. Here, I exploit this increased translational potential of small animal radiation research in order to investigate how PCI affects the incidence of brain metastasis in mice.

For the experiment in this chapter, I sacrifice half of the mice at four weeks after tail-vein injection of breast cancer cells, and the other half at eight weeks post-injection. The rationale for having two endpoints is to understand the time dynamics of any differences observed between the treatment groups. Specifically, if PCI decreases the incidence of brain metastasis four weeks after cell injection, would the effect persist at the eight-week endpoint? If so, then it is likely that PCI has a durable effect in decreasing the incidence of brain metastasis;

if not, then it would seem that PCI merely delays the incidence of brain metastasis, rather than preventing it outright.

In this study, there are four different time points at which the mice are treated with WBI (and one untreated control), and all groups are treated in the exact same manner. The major focus of this thesis is PCI, which is the group of mice irradiated five days after tail-vein injection of breast cancer cells. The three other irradiated groups serve as controls:

1. One group of mice receives WBI two days before cell injection; the question this addresses is if a mechanism other than radiation-induced cell death or senescence is responsible for any observed decrease in the incidence of brain metastasis. Only if the PCI displays decreased incidence of brain metastasis compared to both the control *and* this group could I conclude that the mechanism is primarily due to cell death of induced senescence. Previous work has demonstrated that irradiation of the mammary gland causes unirradiated, non-transformed cells to form tumors in the mammary gland at a significantly higher rate than would be observed in the unirradiated mammary gland [115].
2. One group of mice receives WBI three weeks after cell injection; many single cells should have grown into small masses by this point, so I am effectively comparing a *therapeutic* against a *prophylactic*, as the only difference between the groups is the day of irradiation. Inclusion of this time point would specify that any observed effect that PCI has on the incidence of brain metastasis is due to the timing of the irradiation (i.e. prophylactic), rather than due to a dose high enough to eradicate overt or occult metastases.
3. One group of mice receives WBI six weeks after cell injection; the rationale is the same as for the mice treated with WBI three weeks after cell injection.

The last aspects of the experiment I will rationalize are the conditions for the WBI. If PCI was used clinically in breast cancer patients, it would be administered in several fractions at a total dose of approximately 25 Gy. Here, I am irradiating each mouse with a single fraction of 4 Gy. The reasoning behind the single fraction, as opposed to two or more fractions, is to simplify the experiment: Because over sixty mice are being irradiated, each additional fraction adds significant time and cost and, perhaps more importantly, introduces the problem of between-fraction time variability. Further, the scientific benefit of utilizing multiple fractions, rather than one, in this experimental system is dubious. I use a dose of 4 Gy as this is comparable to other treatment doses used for the mouse brain. Last, I am irradiating the brains with two lateral opposed fields, at 2 Gy each. The purpose of this is to administer the dose to the entire brain as uniformly as possible, and is the same setup used clinically.

Based on information in the literature as well as from previous work done in our lab with the mouse model of breast cancer brain metastasis, I expected to see the following results:

1. Reduced incidence of brain metastasis in mice that were treated with PCI compared to control; similarly, reduced brain metastasis tumor burden in PCI-treated mice (number and area of brain metastases)
2. No differences in the incidence of lung metastases between the different groups
3. Approximately 67% of non-treated mice develop brain metastases [71]
4. Approximately 20% of mice develop lung metastases [71]
5. Because breast cancer brain metastasis can be a secondary metastasis that arrives in the brain via the lungs, mice with lung metastases will have a greater incidence of brain metastasis than mice without lung metastases
6. Mice with brain metastases will display symptoms of disease through weight loss

SECTION II. METHODOLOGY

A. Cell culture

MDA-IBC3, a HER2+ inflammatory breast cancer cell line, was generated in our lab and has been described previously [116]. MDA-IBC3 was cultured in Ham's F-12 media supplemented with 10% fetal bovine serum (FBS), 1 μg/mL hydrocortisone, 5 μg/mL insulin, and 1% antibiotic-antimycotic. This cell line was maintained in humidified conditions with 5% CO_2 at 37°C. MDA-IBC3 cells were passaged approximately every four days prior to injecting the cells into mice.

MDA-IBC3 was previously transfected [71] with a plasmid that encodes for green fluorescent protein (GFP). Briefly, the plasmid was purchased from Systems Biosciences and was packaged with pRSV-Rev, pMDLg-pRRE, and pCMV-VSVG in 293T cells. MDA-IBC3 was then transduced via lentivirus as we described previously [116].

B. Mouse Strain

Three- to five-week-old female immunocompromised SCID/Beige mice (Harlan, USA) were housed and used in accordance with the institutional guidelines of the University of Texas M.D. Anderson Cancer Center under the Institutional Animal Care and Use Committee approved protocol (ACUF 07-08-07213). M.D. Anderson Cancer Center's animal care and use program has been fully accredited by the Association for the Assessment and Accreditation of Laboratory Animal Care International (AAALAC). Mice were monitored regularly and were weighed weekly.

C. Intravenous Tail-Vein Injection

MDA-IBC3 cells were prepared for injection by trypsinizing all cells and then neutralizing with culture media. The cells were washed twice with PBS before counting and placed in sterile 1.5-mL Eppendorf tubes at a concentration of 2.5 x 10^6 cells/mL PBS. Cells were kept on ice until ready for injection.

Five hundred thousand MDA-IBC3 cells in 200 µL PBS were injected via tail vein with 27-gauge needles into each 6- to 8-week-old mouse.

D. Irradiation

Mice received WBI at different time points with respect to tail-vein injection of cells (see Figure 5). Twenty-three mice were used as non-irradiated controls; twenty were irradiated two days prior to cells injection; twenty were irradiated five days after injection, the prophylactic cranial irradiation group; seventeen were irradiated three weeks after irradiation, and eight were irradiated six weeks after injection.

To perform the WBI, mice were placed in an inhalation anesthesia induction chamber (isoflurane: 5% induction, <3% maintenance). Once anesthetized, each mouse was transferred to the imaging and treatment stage in the X-RAD 225 Cx small-animal irradiator (PRECISION X-RAY, North Branford, CT, USA), which includes a nose cone through which anesthesia was maintained with isoflurane. Once on the imaging and treatment stage, a scout cone-beam computed tomography image – with a 2.0-mm aluminum filter – was run for each mouse at 40 kVp and 2.50 mA in order to manually set the isocenter.

The same treatment plan, developed with the PilotXRAD 1.10.4 software, was used for all mice that were irradiated. Each mouse received a single fraction of 4 Gy for the whole-brain irradiation, with two 2-Gy lateral opposing fields. The treatment field (Figure 6) was defined by a 15-mm diameter (at isocenter) copper collimator, and a 0.3-mm copper filter was used. The

treatment was performed at 225 kVp and 13.0 mA, at a rate of approximately 320 cGy per minute (36-38 seconds for each field).

E. Fluorescent Microscopy

Mice were euthanized at either four or eight weeks after injection (Figure 5), and the lungs and brain were collected in 10% formalin. All organs were evaluated for metastatic colonization by assessing GFP levels with the Nikon AZ100 fluorescent stereomicroscope at 20X magnification (Tokyo, Japan). The primary endpoint was the presence or absence of metastasis (binary) in each organ. This was evaluated visually with the Nikon NIS-Elements software. Also, the number of metastases per mouse was counted for mice sacrificed at the eight-week endpoint.

Metastatic brain tumor burden for mice at the eight-week endpoint was measured using the Nikon NIS-Elements software. Briefly, the area of each metastatic focus was determined by using the object count automation within the software. The areas from each of the foci, visible from either the top or bottom two-dimensional images of the brain, were added to give the total tumor burden, in terms of square millimeters.

Images were prepared by setting a lower threshold for GFP intensity in order to subtract the autofluorescence background and then by overlaying the result on a differential interference contrast (DIC) image.

F. Statistical Analysis

The Fisher's exact test was used to compare the incidence of metastatic colonization to the brain and lung in the different treatment groups. The non-parametric Kruskal-Wallis test was used to evaluate the overall effect of different treatments on the number and size of brain metastases, and Dunn's test was used to compare the number and size of brain metastases between each group. P-values of less than 0.05 were considered statistically significant.

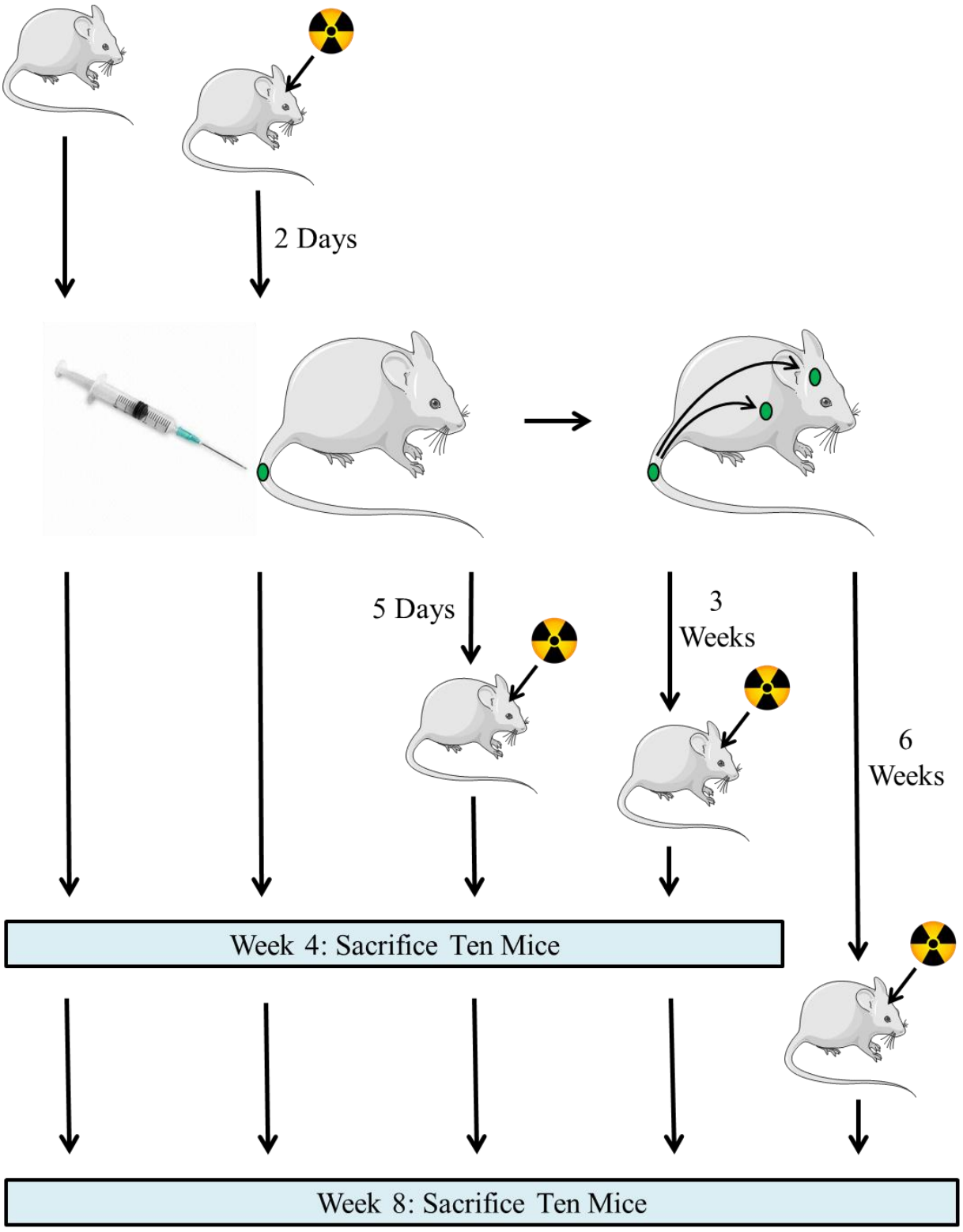

Figure 5: Design of Prophylactic Cranial Irradiation Experiment. SCID/Beige mice were injected with five hundred thousand GFP-labelled MDA-IBC3 cells, via tail vein. Four of the five groups received 4 Gy whole-brain irradiation at different time points. The mice were sacrificed at four and eight weeks after cell injection, at which point the brains and lungs were excised to evaluate metastases.

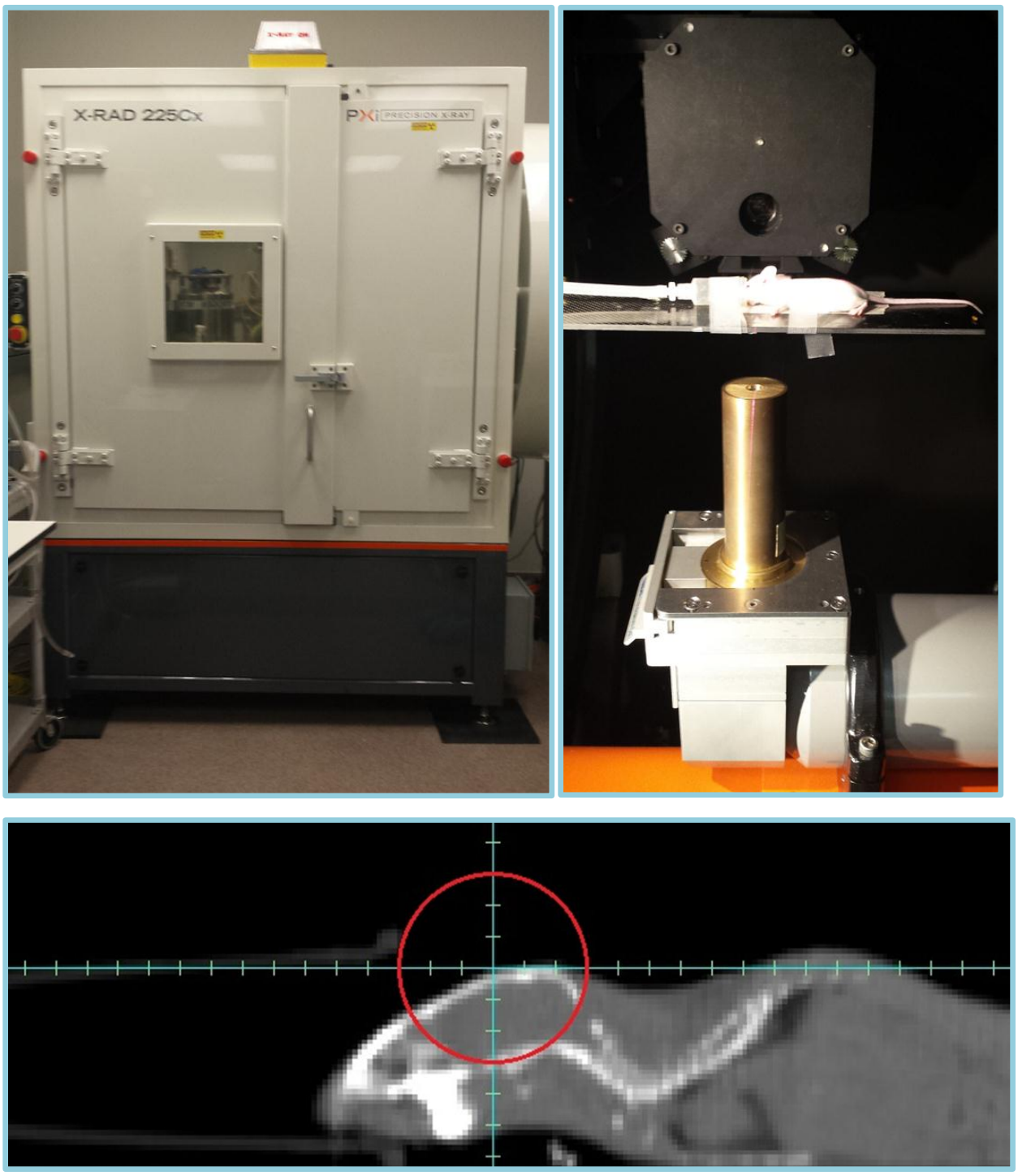

Figure 6: Setup for Irradiation of Mice. Irradiation of mouse brains was carried out in the X-RAD 225Cx, a dedicated small-animal irradiator. In the machine, mice are anesthetized with isoflurane through the nose cone. A scout cone-beam CT image is used to set the isocenter (bottom panel), and a 15-mm collimator (top right) confines the treatment field to the brain. The circle in the bottom panel represents the 15-mm diameter treatment field. All treated mice were irradiated with 4 Gy whole-brain radiation, administered in one fraction with two 2-Gy, opposing lateral fields.

SECTION III. RESULTS

A. Four-Week Endpoint

Thirty-one to -two days after tail-vein injection of 0.5 x 10^6 GFP-labelled MDA-IBC3 cells into SCID/Beige mice, 43 mice were sacrificed. Of these 43 mice, 13 were non-irradiated controls, 10 were irradiated two days prior to cell injection (pre-irradiation group), 10 were irradiated five days after cell injection (prophylactic cranial irradiation [PCI] group), and 10 were irradiated three weeks after injection (3-week treatment group).

After sacrifice, the excised brain and lung tissue from each mouse was evaluated for the presence of GFP-labelled metastases using fluorescence stereomicroscopy. All organs were classified as positive or negative through visual inspection on the stereomicroscope. Representative images of GFP-labelled metastases in brain and lungs four weeks after injection are depicted in Figure 7.

The results for the number of mice in each group with brain metastases are shown in Table 3. Ten mice in the control group developed brain metastases (77%), consistent with the results previously reported by our group [71]. Interestingly, all ten mice in the pre-irradiated group developed brain metastases (not significant compared to control). In the prophylactic cranial irradiation group, only two mice developed brain metastases after four weeks (20%), consistent with my hypothesis that PCI would reduce the incidence of brain metastasis. This was significantly lower than the incidence of brain metastasis in two of the other groups, and suggested a trend in the third (vs. control, $p = 0.01$; vs. pre-irradiation group, $p = 0.0007$; vs. 3-week treatment group, $p = 0.07$). The treatment of mice with 4 Gy WBRT at three weeks after cell injection had no impact on the number of mice that developed brain metastases compared to the control.

The number of brain metastases per mouse was compared between the five different groups (Figure 8). Overall, the number of brain metastases per mouse (p = 0.004) was significantly affected by the treatments at different time points. Further, prophylactic cranial irradiation significantly decreased the number of metastases per mouse compared to two of the three other groups ([number of brain metastases per mouse, PCI: vs. control, $p < 0.03$; vs. pre-irradiation group, $p < 0.003$; vs. 3-week treatment group, $p = 0.25$).

Excised lungs from the sacrificed mice were also examined for the presence of metastases. Because the 4 Gy was administered at various time points only to the brain, we did not expect to see any differences in the incidence of lung metastasis between the four groups. As Table 4 shows, there were no significant differences.

The different groups were also compared based on the number of mice in each group that had *either lung or brain* metastases. As shown in Table 5, there were no significant differences.

We expected to see that mice with lung metastases would have a higher incidence of brain metastasis compared to mice that did not have lung metastases. This was the case for the mice sacrificed at four weeks post-injection (76% vs. 40%, p = 0.06), indicating a trend (Table 6).

Finally, the weight of the mice increased steadily up until the point at which they were sacrificed, indicating that the brain metastases which were present had not yet caused serious morbidity (Figure 9).

Presence of Brain Metastases: 4-Week Endpoint			
0 Gy	10/13	77%	
4 Gy WBI @ 2d Pre-injection	10/10	100%	$p < 0.05$
4 Gy WBI @ 5d Post-injection	2/10	20%	$p < 0.001$
4 Gy WBI @ 3wk Post-injection	7/10	70%	$p < 0.10$

Table 3: Presence of Brain Metastases at Four-Week Endpoint. Four weeks after tail-vein injection of 0.5 x 10^6 GFP-labelled MDA-IBC3 cells into SCID/Beige mice, forty-three mice were sacrificed and the brains were extracted. GFP-expressing metastases in the brains were visually identified with a Nikon fluorescent stereomicroscope. There were thirteen mice in the non-treated control, and ten in each of three groups that received 4 Gy whole-brain irradiation at different time points with respect to cell injection. The prophylactic cranial irradiation group had significantly fewer brain metastases than the treatment and pre-irradiation groups (vs. control, p = 0.01; vs. pre-injection, p = 0.0007; vs. treatment, p = 0.07). Surprisingly, pre-irradiation of the brains caused an increase in the number of mice with brain metastases compared to the control (100% vs. 77%, p = n.s.). Percentages between groups were compared with Fisher's exact test.

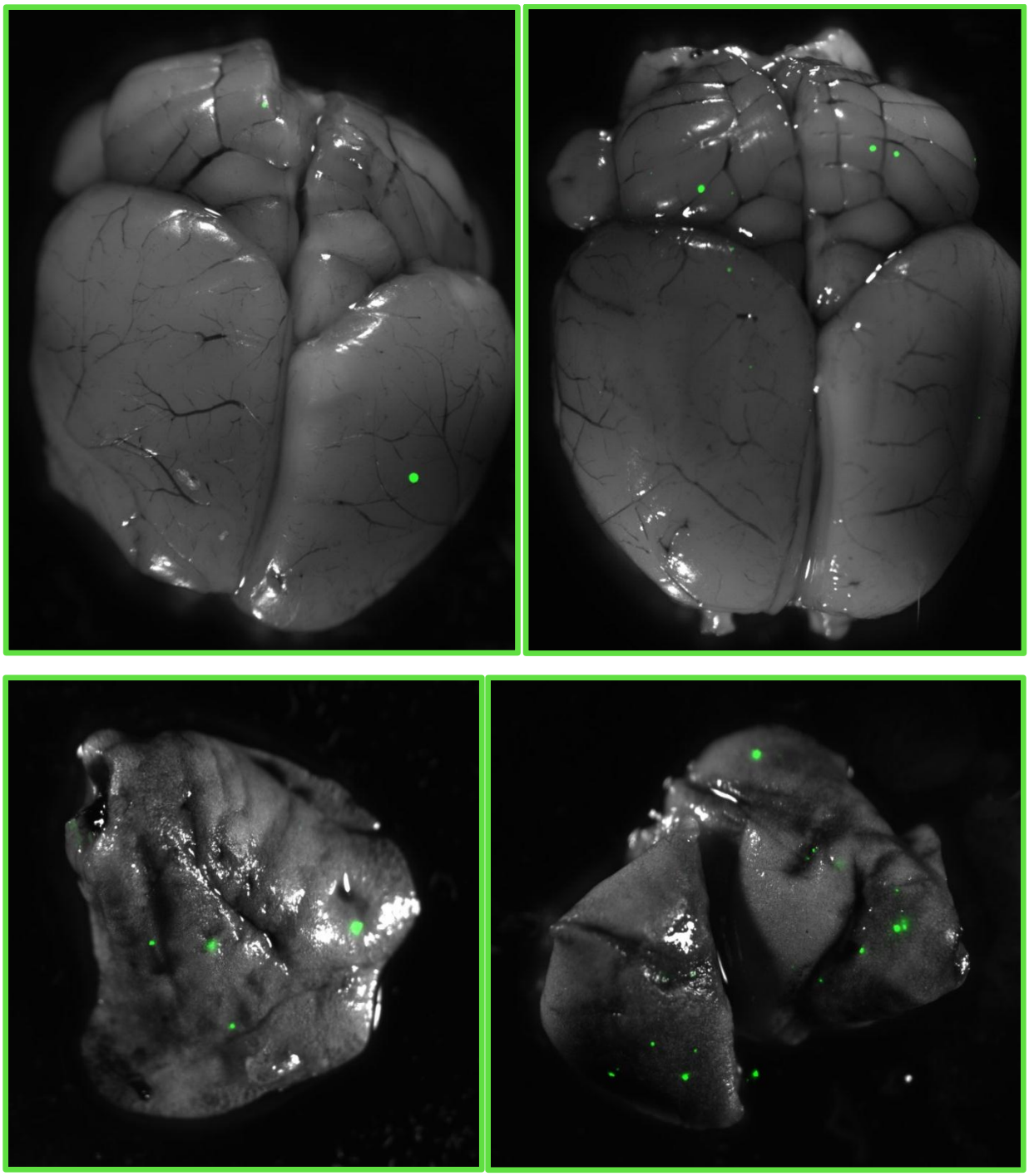

Figure 7: Representative Images of Brain and Lung Metastases at Four-Week Endpoint. Four weeks after tail-vein injection of 0.5 x 10^6 GFP-labelled MDA-IBC3 cells into SCID/Beige mice, forty-three mice were sacrificed and the brains and lungs were extracted. Pictures GFP-expressing metastases in the organs were taken with a Nikon fluorescent stereomicroscope at 20X magnification. The images above were created by merging a brightfield photograph of the organ with the GFP expression profile using the Nikon NIS-Elements software. For the GFP profile, a lower threshold was set so as to eliminate the autofluorescent background and collect only the emission from metastases.

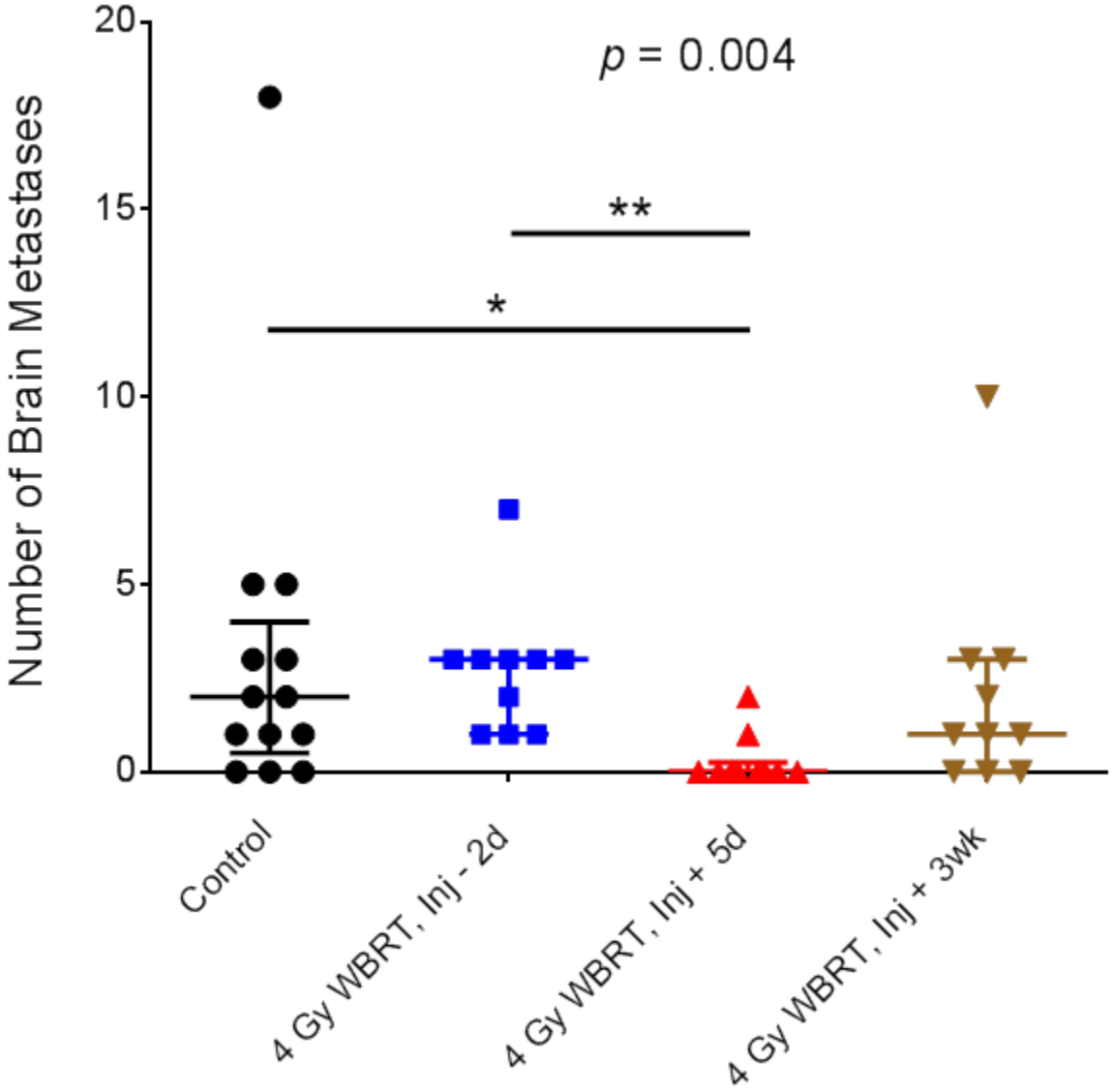

Figure 8: Number of Brain Metastases per Mouse at Four-Week Endpoint. Four weeks after tail-vein injection of 0.5 x 10^6 GFP-labelled MDA-IBC3 cells into SCID/Beige mice, forty-three mice were sacrificed and the brains were extracted. GFP-expressing metastases in the brains were visually identified with a Nikon fluorescent stereomicroscope, and the number of brain metastatic foci per mouse was counted. The different treatment groups had an overall effect on the number of brain metastases per mouse ($p = 0.004$), evaluated using the Kruskal-Wallis test. The prophylactic cranial irradiation group had significantly fewer brain metastases than two of the other groups (vs. control, $p < 0.05$; vs. pre-injection, $p < 0.01$), determined using Dunn's test. Horizontal bars represent median and lower/upper quartiles.

Presence of Lung Metastases: 4-Week Endpoint		
0 Gy	10/13	77%
4 Gy WBI @ 2d Pre-injection	9/10	90%
4 Gy WBI @ 5d Post-injection	7/10	70%
4 Gy WBI @ 3wk Post-injection	7/10	70%

Table 4: Presence of Lung Metastases at Four-Week Endpoint. Four weeks after tail-vein injection of 0.5 x 10^6 GFP-labelled MDA-IBC3 cells into SCID/Beige mice, forty-three mice were sacrificed and the lungs were extracted. GFP-expressing metastases in the lungs were visually identified with a Nikon fluorescent stereomicroscope. There was no significant difference in the number of mice with lung metastases between the non-treated control and the three groups that received 4 Gy whole-brain irradiation at different time points with respect to cell injection. Percentages between groups were compared with Fisher's exact test.

Presence of Any Metastases: 4-Week Endpoint		
0 Gy	12/13	92%
4 Gy WBI @ 2d Pre-injection	10/10	100%
4 Gy WBI @ 5d Post-injection	7/10	70%
4 Gy WBI @ 3wk Post-injection	8/10	80%

Table 5: Presence of Any Metastases at Four-Week Endpoint. Four weeks after tail-vein injection of 0.5 x 10^6 GFP-labelled MDA-IBC3 cells into SCID/Beige mice, forty-three mice were sacrificed and the brains and lungs were extracted. GFP-expressing metastases in the brains and lungs were visually identified with a Nikon fluorescent stereomicroscope. There was no significant difference in the number of mice with any metastases between the non-treated control and the three groups that received 4 Gy whole-brain irradiation at different time points with respect to cell injection. Percentages between groups were compared with Fisher's exact test.

Metastases	# Brain+	# Brain-	% Brain+	
Lung+	25	8	76%	$p = 0.06$
Lung-	4	6	40%	

Table 6: Association between Brain and Lung Metastases at Four-Week Endpoint. SCID/Beige mice that had lungs metastases four weeks after tail-vein injection of 0.5 x 10^6 GFP-labelled MDA-IBC3 cells were more likely to have brain metastases (76%) than the mice that did not have lung metastases (40%). This result is not significant (p = 0.055), as calculated using Fisher's exact test.

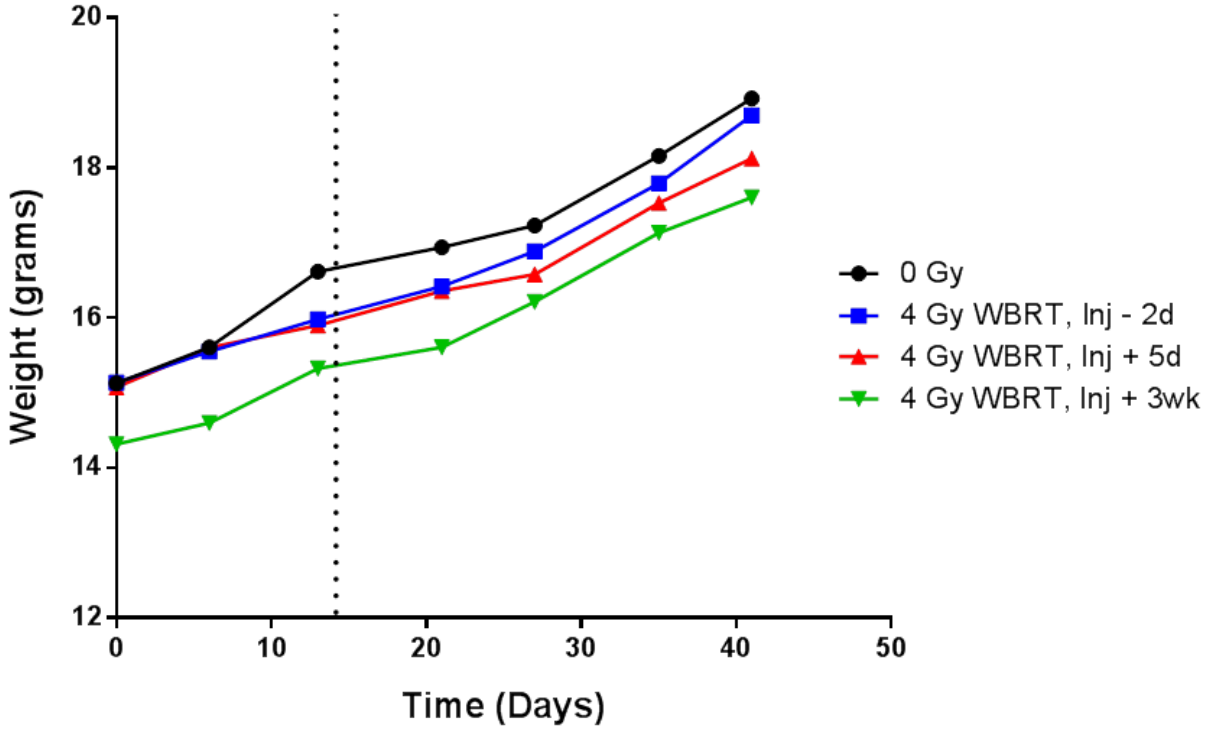

Figure 9: Weight of Mice Sacrificed at Four-Week Endpoint. In each of the four groups, the weight of mice steadily increased over time until sacrifice. The dotted line represents time of tail-vein injection of MDA-IBC3 cells. Error bars not shown.

B. Eight-Week Endpoint

Fifty-nine to sixty days after tail-vein injection of 0.5 x 10^6 GFP-labelled MDA-IBC3 cells into SCID/Beige mice, 45 mice were sacrificed. Of these 45 mice, 10 were non-irradiated controls, 10 were irradiated two days prior to cell injection (pre-irradiation group), 10 were irradiated five days after cell injection (prophylactic cranial irradiation [PCI] group), 7 were irradiated three weeks after injection (3-week treatment group), and 8 were irradiated six weeks after injection (6-week treatment group).

As with the four-week endpoint, the brain and lung tissue was excised in order to evaluate metastases. Representative images of GFP-positive metastases in brain and lungs eight weeks after injection are depicted in Figure 10.

The results for the number of mice in each group with brain metastases are shown in Table 7. Nine out of ten mice in the control group developed brain metastases (90%), greater than what we observed at four weeks. Once again, all ten mice in the pre-irradiated group developed brain metastases, meaning that all twenty mice between the two endpoints that were irradiated two days prior to injection developed metastases. In the prophylactic cranial irradiation group, only three mice developed brain metastases after eight weeks (30%), consistent both with the results from the four-week endpoint and also with my hypothesis that PCI would reduce the incidence of brain metastasis. This was significantly lower than the incidence of brain metastasis in the four other groups (vs. control, $p = 0.02$; vs. pre-irradiation group, $p = 0.003$; vs. 3-week treatment group, $p = 0.009$; vs. 6-week treatment group, $p = 0.02$). The treatment of mice with 4 Gy WBI at three or six weeks after cell injection had no impact on the number of mice that developed brain metastases compared to the control, the same result that we observed at the four-week endpoint.

The number of brain metastases per mouse and the brain metastatic tumor burden per mouse (as measured in square millimeters from the two-dimensional images) were compared

between the five different groups (Figures 11 and 12). Overall, both the number of brain metastases per mouse ($p = 0.0008$) and the brain metastatic tumor burden per mouse ($p = 0.002$) were significantly affected by the treatments at different time points. Further, prophylactic cranial irradiation significantly decreased both number of metastases per mouse and brain metastatic tumor burden per mouse compared to all of the four other groups ([number of brain metastases per mouse, PCI: vs. control, $p = 0.006$; vs. pre-irradiation group, $p = 0.02$; vs. 3-week treatment group, $p = 0.004$; vs. 6-week treatment group, $p = 0.01$]; [brain metastatic tumor burden per mouse, PCI: vs. control, $p = 0.01$; vs. pre-irradiation group, $p = 0.01$; vs. 3-week treatment group, $p = 0.04$; vs. 6-week treatment group, $p = 0.006$]).

When the results from the four- and eight-week endpoints were combined (Table 7), the incidence of brain metastasis was significantly decreased with prophylactic cranial irradiation as compared to all other groups (vs. control, $p = 0.0002$; vs. pre-irradiation group, $p < 0.0001$; vs. 3-week treatment group, $p = 0.0008$; vs. 6-week treatment group, $p = 0.004$). The greater incidence in the pre-irradiation group suggested a trend compared to the 3-week treatment group ($p = 0.08$), although no trend was suggested compared to the control ($p = 0.11$).

Excised lungs from the sacrificed mice were also examined for the presence of metastases. Because the 4 Gy was administered at various time points only to the brain, we did not expect to see any differences in the incidence of lung metastasis between the four groups. However, as Table 9 shows, the mice that received WBI three weeks after cell injection had a 100% incidence of lung metastasis, which was significantly greater than the incidence at three other time points (vs. control, $p < 0.05$; vs. pre-irradiation group, $p < 0.05$; vs. PCI, $p < 0.05$; vs. 6-week treatment group, $p = 0.08$).

The different groups were also compared based on the number of mice in each group that had *either lung or brain* metastases. As shown in Table 10, the group that received PCI had significantly fewer metastases than the pre-irradiation and 3-week treatment groups ($p < 0.05$).

We expected to see that mice with lung metastases would have a higher incidence of brain metastasis compared to mice that did not have lung metastases. The mice with lung metastases did have a greater incidence of brain metastasis compared to the mice without lung metastases (92% vs. 65%, $p = 0.06$), and results suggest a trend (Table 11). When the results from the four- and eight-week endpoints were combined (Table 12), the difference was significant (83% vs. 57%, $p = 0.01$).

The mice steadily gained weight up until five weeks after cell injection, at which point the average weight in the groups either began to decline or plateau (Figure 13). Interestingly, the mice which were irradiated two days before cell injection – those that had 100% incidence of brain metastasis – saw the sharpest decline in weight loss beginning at six weeks: Of the eight mice that lost greater than 10% of their body weight from the peak weight, seven were in that pre-irradiation group (data not shown). Nevertheless, there was no measured correlation between the magnitude of weight loss and the brain metastatic tumor burden.

Presence of Brain Metastases: 8-Week Endpoint		
0 Gy	9/10	90%
4 Gy WBI @ 2d Pre-injection	10/10	100%
4 Gy WBI @ 5d Post-injection	3/10	30%
4 Gy WBI @ 3wk Post-injection	7/7	100%
4 Gy WBI @ 6wk Post-injection	7/8	88%

$p < 0.01$ (2d Pre-injection vs. 5d Post-injection)

$p < 0.01$ (5d Post-injection vs. 3wk Post-injection)

$p < 0.05$ (0 Gy vs. 5d Post-injection)

$p < 0.05$ (5d Post-injection vs. 6wk Post-injection)

Table 7: Presence of Brain Metastases at Eight-Week Endpoint. Eight weeks after tail-vein injection of 0.5 x 10^6 GFP-labelled MDA-IBC3 cells into SCID/Beige mice, forty-five mice were sacrificed and the brains were extracted. GFP-expressing metastases in the brains were visually identified with a Nikon fluorescent stereomicroscope. The prophylactic cranial irradiation group had significantly fewer brain metastases than each of the four other groups (vs. control, $p = 0.02$; vs. pre-injection, $p = 0.003$; vs. 3-week treatment, $p = 0.009$; vs. 6-week treatment, $p = 0.02$). Percentages between groups were compared with Fisher's exact test.

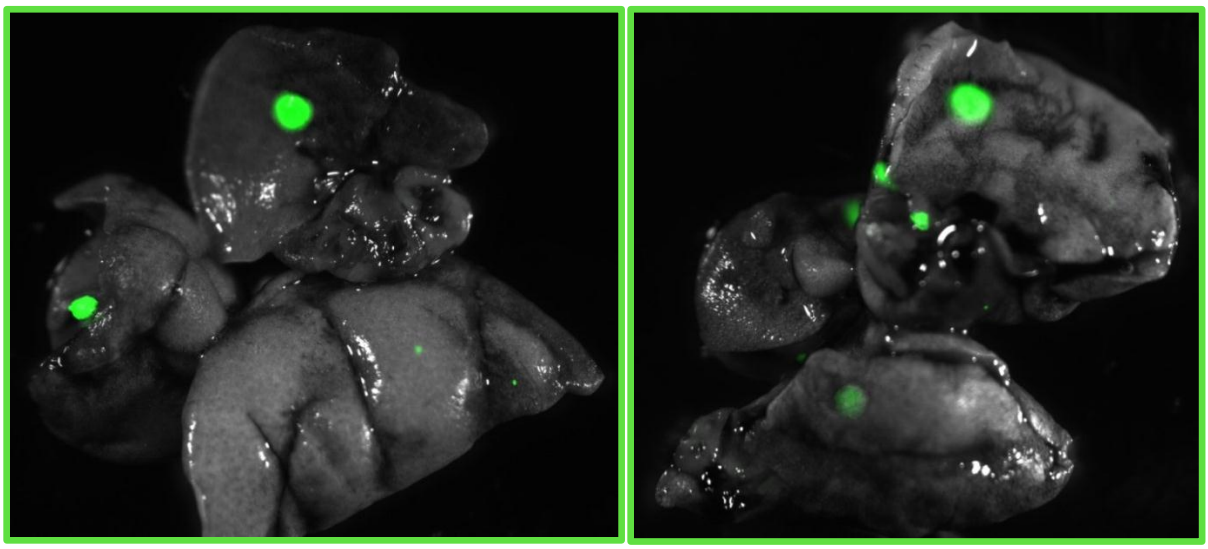

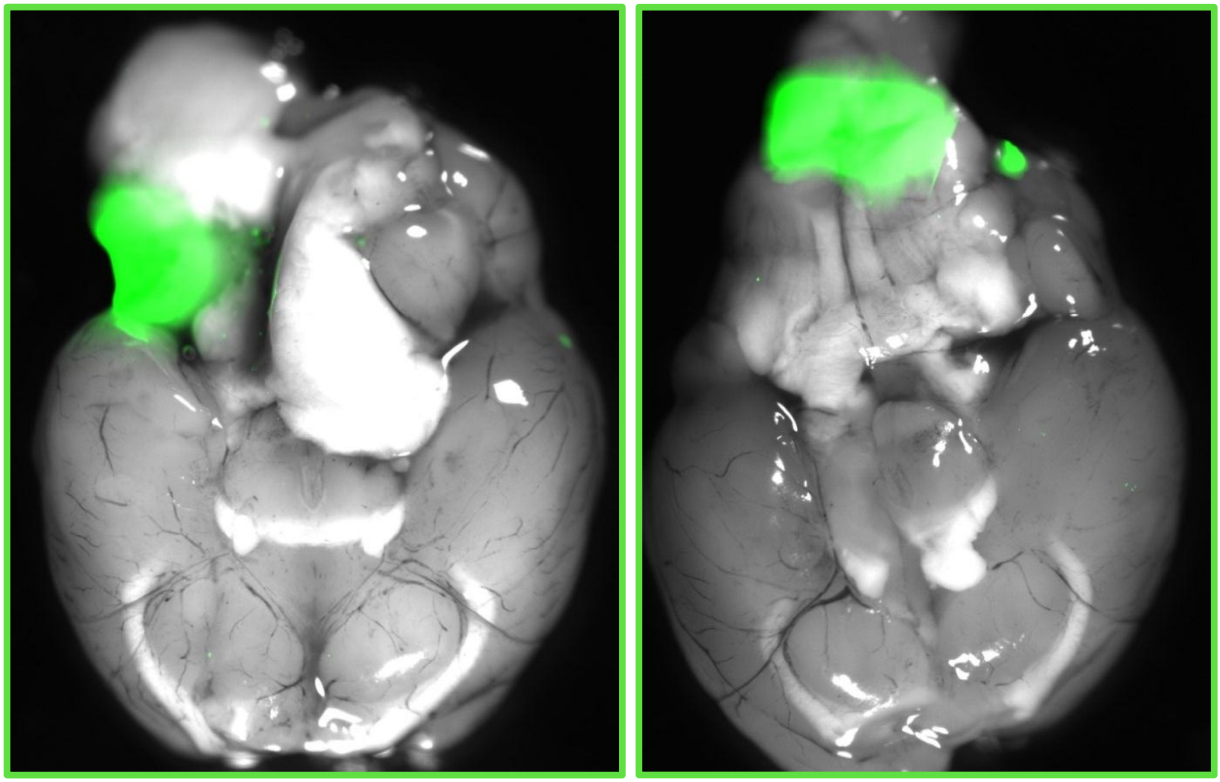

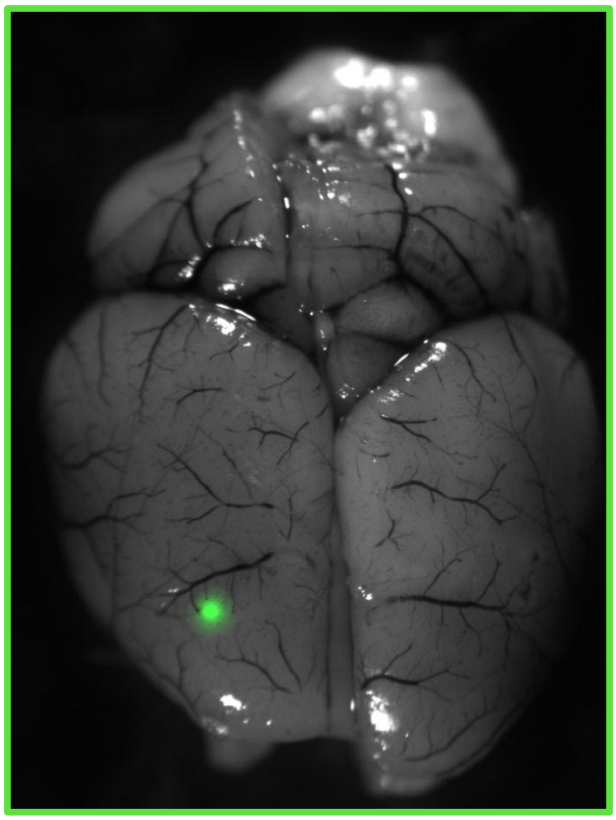

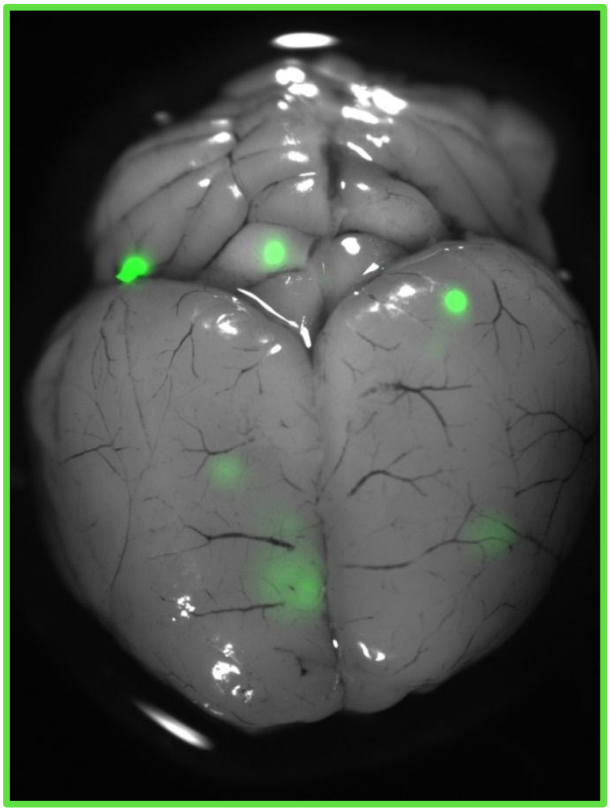

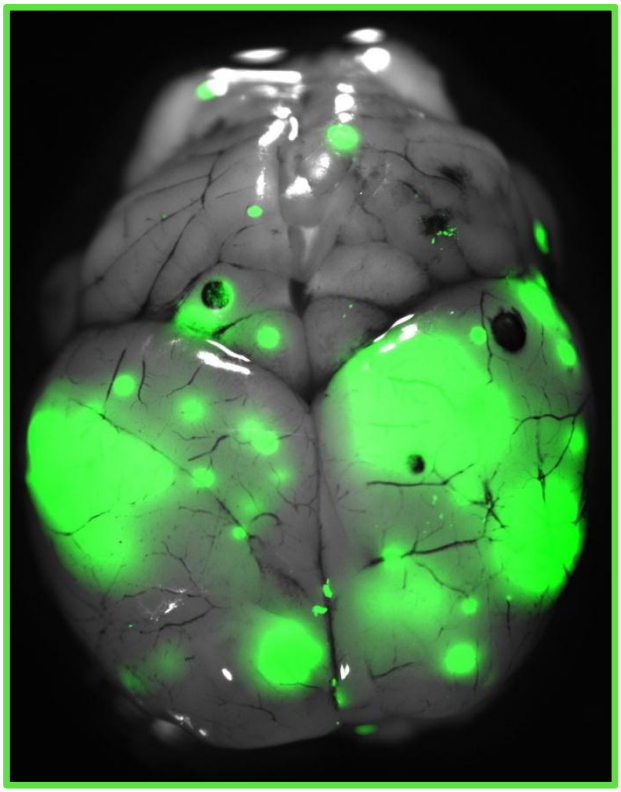

Figure 10: Representative Images of Brain and Lung Metastases at Eight-Week Endpoint. Eight weeks after tail-vein injection of 0.5 x 10^6 GFP-labelled MDA-IBC3 cells into SCID/Beige mice, forty-five mice were sacrificed and the brains and lungs were extracted. Pictures GFP-expressing metastases in the organs were taken with a Nikon fluorescent stereomicroscope at 20X magnification. The images above were created by merging a brightfield photograph of the organ with the GFP expression profile using the Nikon NIS-Elements software. For the GFP profile, a lower threshold was set so as to eliminate the autofluorescent background and collect only the emission from metastases. The brain images on the previous page are from the control (left) and pre-irradiation (right) groups; the images on the current page are from PCI (top left), 3-week treatment (top right), and 6-week treatment (bottom left) groups. Metastatic foci from PCI group visibly smaller.

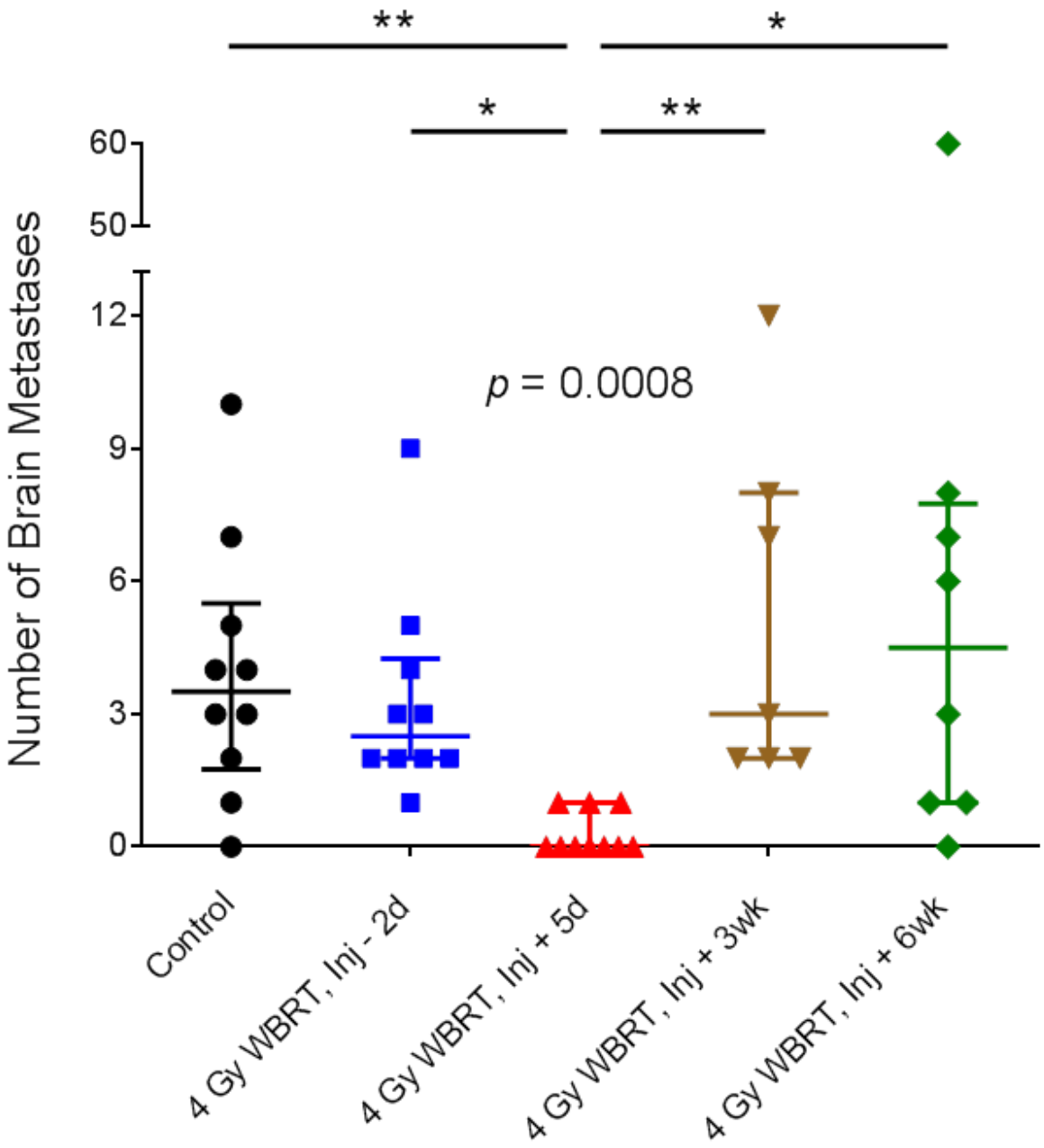

Figure 11: Number of Brain Metastases per Mouse at Eight-Week Endpoint. Eight weeks after tail-vein injection of 0.5 x 10^6 GFP-labelled MDA-IBC3 cells into SCID/Beige mice, forty-five mice were sacrificed and the brains were extracted. GFP-expressing metastases in the brains were visually identified with a Nikon fluorescent stereomicroscope, and the number of brain metastatic foci per mouse was counted. The different treatment groups had an overall effect on the number of brain metastases per mouse ($p = 0.0008$), evaluated using the Kruskal-Wallis test. The prophylactic cranial irradiation group had significantly fewer brain metastases than each of the four other groups (vs. control, $p < 0.01$; vs. pre-injection, $p < 0.05$; vs. 3-week treatment, $p < 0.01$; vs. 6-week treatment, $p < 0.05$), determined using Dunn's test. Horizontal bars represent median and lower/upper quartiles.

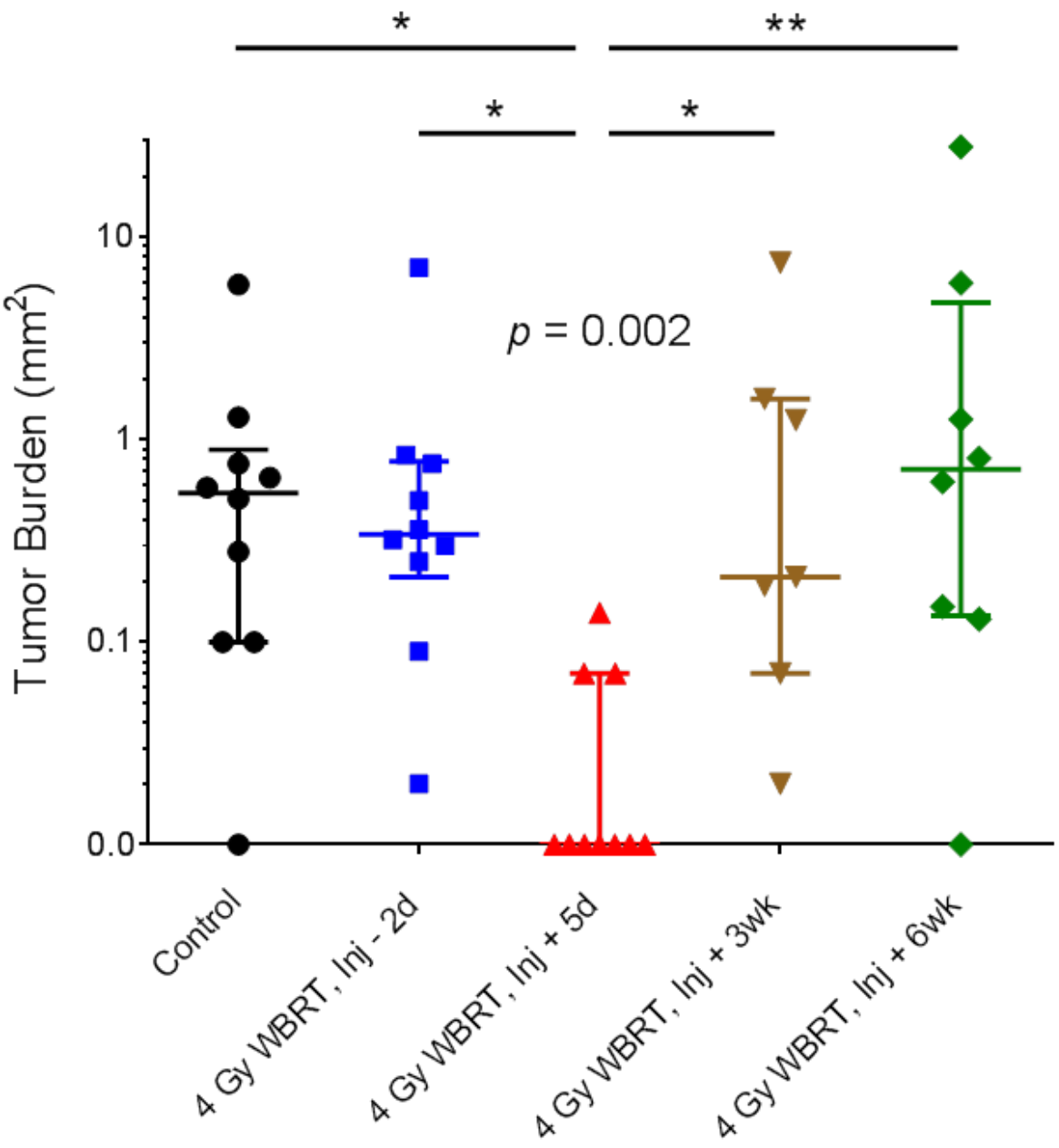

Figure 12: Brain Metastases Burden per Mouse at Eight-Week Endpoint. Eight weeks after tail-vein injection of 0.5 x 10^6 GFP-labelled MDA-IBC3 cells into SCID/Beige mice, forty-five mice were sacrificed and the brains were extracted. GFP-expressing metastases in the brains were visually identified with a Nikon fluorescent stereomicroscope, and the tumor burden per mouse was evaluated with the Nikon software. The different treatment groups had an overall effect on the number of brain metastases per mouse (p = 0.002), evaluated using the Kruskal-Wallis test. The prophylactic cranial irradiation group had significantly fewer brain metastases than each of the four other groups (vs. control, $p < 0.05$; vs. pre-injection, $p < 0.05$; vs. 3-week treatment, $p < 0.05$; vs. 6-week treatment, $p < 0.01$), determined using Dunn's test. Horizontal bars represent median and lower/upper quartiles.

Presence of Brain Metastases at Both Endpoints		
0 Gy	19/23	83%
4 Gy WBI @ 2d Pre-injection	20/20	100%
4 Gy WBI @ 5d Post-injection	5/20	25%
4 Gy WBI @ 3wk Post-injection	14/17	76%
4 Gy WBI @ 6wk Post-injection	7/8	88%

$p < 0.0001$

$p < 0.001$

$p < 0.001$

$p < 0.01$

Table 8: Presence of Brain Metastases in Overall Study. Four to eight weeks after tail-vein injection of 0.5 x 10^6 GFP-labelled MDA-IBC3 cells into SCID/Beige mice, eighty-eight mice were sacrificed and the brains were extracted. GFP-expressing metastases in the brains were visually identified with a Nikon fluorescent stereomicroscope. The prophylactic cranial irradiation group had significantly fewer brain metastases than each of the four other groups (vs. control, $p = 0.0002$; vs. pre-injection, $p < 0.0001$; vs. 3-week treatment, $p = 0.0008$; vs. 6-week treatment, $p = 0.004$). The pre-irradiation group had a greater incidence of brain metastasis compared to the group treated with WBI three weeks after cell injection ($p = 0.08$), suggesting a trend. There is a non-significant difference between the control and pre-irradiation groups ($p = 0.11$). Percentages between groups were compared with Fisher's exact test.

Presence of Lung Metastases: 8-Week Endpoint		
0 Gy	5/10	50%
4 Gy WBI @ 2d Pre-injection	5/10	50%
4 Gy WBI@ 5d Post-injection	4/10	40%
4 Gy WBI @ 3wk Post-injection	7/7	100%
4 Gy WBI @ 6wk Post-injection	4/8	50%

*

*

*

*$p < 0.05$

Table 9: Presence of Lung Metastases at Four-Week Endpoint. Eight weeks after tail-vein injection of 0.5 x 10^6 GFP-labelled MDA-IBC3 cells into SCID/Beige mice, forty-five mice were sacrificed and the lungs were extracted. GFP-expressing metastases in the lungs were visually identified with a Nikon fluorescent stereomicroscope. The group that received 4 Gy WBRT three weeks after tail-vein injection had a significantly greater incidence of lung metastasis compared to three other groups (vs. control, vs. pre-injection, and vs. PCI, $p < 0.05$). The difference in lung incidence between 3- and 6-week WBI groups was not significant ($p = 0.08$). Percentages between groups were compared with Fisher's exact test.

Presence of Any Metastases: 8-Week Endpoint		
0 Gy	9/10	90%
4 Gy WBI @ 2d Pre-injection	10/10	100%
4 Gy WBI @ 5d Post-injection	5/10	50%
4 Gy WBI @ 3wk Post-injection	7/7	100%
4 Gy WBI @ 6wk Post-injection	7/8	88%

$p < 0.05$

$p < 0.05$

Table 10: Presence of Any Metastases at Eight-Week Endpoint. Eight weeks after tail-vein injection of 0.5 x 10^6 GFP-labelled MDA-IBC3 cells into SCID/Beige mice, forty-five mice were sacrificed and the brains and lungs were extracted. GFP-expressing metastases in the brains and lungs were visually identified with a Nikon fluorescent stereomicroscope. The PCI group which was treated with 4 Gy WBI five days post-injection had a significantly lower incidence of metastasis compared to two other groups (vs. pre-injection and vs. 3-week treatment, $p < 0.05$). Percentages between groups were compared with Fisher's exact test.

Metastases	# Brain+	# Brain-	% Brain+
Lung+	23	2	92%
Lung-	13	7	65%

$p = 0.06$

Table 11: Association between Brain and Lung Metastases at Eight-Week Endpoint. SCID/Beige mice that had lungs metastases eight weeks after tail-vein injection of 0.5 x 10^6 GFP-labelled MDA-IBC3 cells were more likely to have brain metastases (92%) than the mice that did not have lung metastases (65%). This result is not significant ($p = 0.057$), as calculated using Fisher's exact test.

Metastases	# Brain+	# Brain-	% Brain+
Lung+	48	10	83%
Lung-	17	13	57%

$p = 0.01$

Table 12: Association between Brain and Lung Metastases in Overall Study. SCID/Beige mice that had lungs metastases four or eight weeks after tail-vein injection of 0.5 x 10^6 GFP-labelled MDA-IBC3 cells were significantly more likely to have brain metastases (80%) than the mice that did not have lung metastases (57%), as calculated using Fisher's exact test ($p = 0.01$).

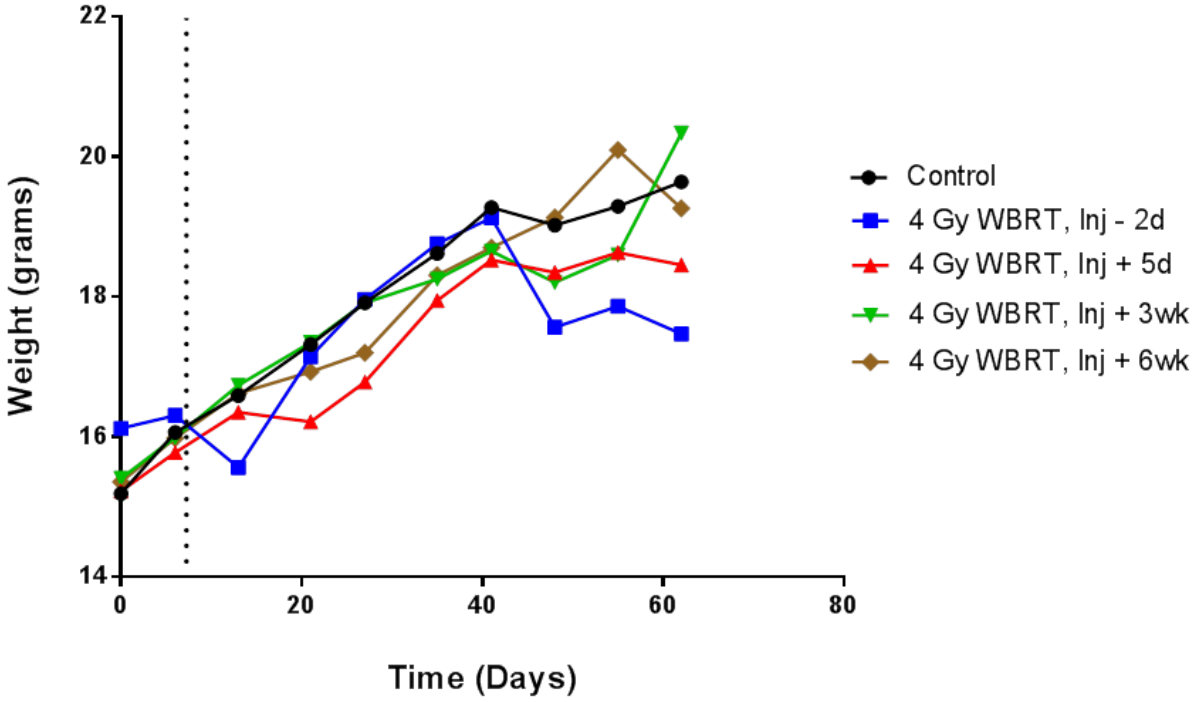

Figure 13: Weight of Mice Sacrificed at Eight-Week Endpoint. In each of the five groups, the weight of mice steadily increased up to five weeks after injection. After that, the weight decreased in the pre-irradiation group, with seven mice losing greater than 10% body weight (four mice were actually treated and regained the weight, explaining the plateau from days 48-55). In the other four groups, the weight leveled off five weeks after injection. The dotted line represents time of tail-vein injection of MDA-IBC3 cells. Error bars not shown.

SECTION IV. CONCLUSIONS

Prophylactic cranial irradiation is a clinical technique used for patients with SCLC and ALL to reduce the incidence of brain metastasis. Because of an emerging group of patients at high risk of developing brain metastasis, PCI is gaining interest as a clinical option for this group.

Through a mouse model of metastatic, HER2+ inflammatory breast cancer, we have demonstrated that PCI has the potential to benefit these patients, supporting the hypothesis. At the four- and eight-week endpoints, PCI reduced the incidence of brain metastasis, the number of metastases per mouse, and the metastatic burden compared to the other endpoints – significantly in most cases. There were no significant differences between the other four groups.

In the original experiment developing this metastatic mouse model [71], two-thirds of the non-treated SCID/Beige mice injected with MDA-IBC3 cells developed brain metastases at the eight-week endpoint. Here, 10/13 (77%) mice had developed brain metastases by the four-week endpoint, and 9/10 by the eight-week endpoint. While the incidence was greater in this study, it further validates the usefulness of this mouse model as a platform for assessing anti-brain metastasis treatments, due to the consistently high incidence in non-treated mice.

The primary endpoint of interest in this *in vivo* experiment was the incidence of brain metastasis in the prophylactic cranial irradiation group, which was set as the group of mice which received 4 Gy whole-brain irradiation five days after cell injection. This time point was chosen because while cells could be expected to have arrested in the brain by this point, very few, if any, would have been able to start growing into metastases of appreciable size. We hypothesized that PCI would reduce the incidence by 50%, and we actually observed a reduction in incidence compared to the control of 74% and 67% at four and eight weeks, respectively. Because the effect was present at both four and eight weeks, it is likely that PCI

has a permanent effect on the incidence of brain metastasis, rather than merely a delay in their growth.

While the significant reduction in incidence in the PCI group supported the hypothesis, it was clear from the microscope images that the PCI also had a major effect on the number of metastases and the metastatic burden. Between the two mice at four weeks and the three mice at eight weeks that were positive for brain metastases in the PCI group, there were *collectively six brain metastases* – six brain metastases among twenty mice. In contrast, there were forty-one brain metastases among ten mice in the control at eight weeks, and forty-one among thirteen mice in the control at four weeks. Further, the metastatic burden at eight weeks was significantly reduced by PCI compared to the other four groups. This is in part due to the fewer brain metastases, as burden is a function of number of metastases. However, the three metastases that were present in the PCI group were all relatively small. This was not necessarily expected, as those cells that retained their clonogenic potential after the early irradiation would still have the full eight weeks to form metastases.

Two groups that were irradiated three and six weeks post-injection were included in the study to serve as something akin to positive controls, in that the presence of brain metastases would already be expected by the time these mice were irradiated. It was necessary to distinguish between prevention and treatment, so these two groups were labelled as the latter. Unsurprisingly, there were no significant differences between the non-irradiated control and the two treatment groups when considering the endpoints of incidence of brain metastasis and the number of brain metastases per mouse. However, there were also no significant differences in tumor burden. While a dose of 4 Gy would not be expected to eradicate all clonogenic cells in the two treatment groups, and thus would not affect incidence and number of metastases, it could be expected to decrease the average volume of metastases through cell kill. This would be reflected by the metastatic burden, but it seems that the 4 Gy dose had negligible effect on

metastatic volumes compared to the non-irradiated control. A couple of possible explanations center around hypoxia and accelerated repopulation, and will be discussed later

Last, a group of mice was irradiated two days prior to cell injection as an attempt to control for any effects that radiation has on the local microenvironment apart from any effects on the tumor cells themselves. Interestingly, the incidence of brain metastasis in this group at both the four- and eight-week endpoints was 100%. Although not a significant difference compared to the non-irradiated control, this taken alone could be suggestive of "priming" of the brain for the growth of metastases. Further, in the group of mice that was pre-irradiated for the eight-week endpoint, there was a sharp decrease in the average mouse weight, possibly indicating greater metastatic burden.

There have been studies looking at the effect of pre-irradiation of host tissues on malignant growth: Barcellos-Hoff and collaborators [115] found that non-transformed mammary epithelial cells preferentially formed tumors in cleared mammary fat pads that were pre-irradiated with 4 Gy (81% vs. 19% incidence). Conversely, the tumor bed effect describes the phenomenon whereby experimental tumors grow slower in pre-irradiated tissues [117]. In the PCI experiment, there was a negligible difference between the number of metastases per mouse and the metastatic burden; therefore, the data does not support the hypothesis that radiation primes the brain for metastatic growth. Also, no connection was observed between weight loss and any of the experimental endpoints.

A sub-aim of the study was to evaluate any correlation between lung and brain metastases, and here there was a significant association between the incidence of lung and brain metastasis. One question this raises is whether many of the brain metastases are secondary metastases, with the lungs as the primary metastatic site. This seems unlikely, however, as the PCI would not have as much of an effect if many of the disseminated tumor cells arrived in the brain via the lungs after the day of irradiation (i.e. five days post-injection). Similarly, the

incidence in lung and brain metastasis appears independent when breaking down the mice into the five experimental groups: PCI had a clear effect on the incidence of brain metastasis, but the incidence of lung metastasis in the PCI group was the same as in the other experimental groups.

As mentioned above, this experiment helps validate the utility of this metastatic mouse model, as not only is the incidence of brain metastasis consistently high in untreated mice, but also experimental treatments clearly are able to show an effect. Likewise, the PCI study validates the small-animal irradiator as an experimental apparatus, as the treatment delivered to the mice was consistent and was able to produce data of clinical relevance.

While the experimental system used in this study was unique and robust, it was not without limitations, especially in the context of the clinical question regarding PCI. First, there was a single day of tail-vein injections of 500,000 GFP-labelled, MDA-IBC3 cells. This does not accurately represent the shedding of breast cancer cells/clumps into the circulation in patients, which likely happens gradually as long as the primary tumor is present, providing a constant source of new circulating tumor cells. A more clinically relevant mouse model would involve spontaneous metastases arising from a primary breast tumor, but no adequate spontaneous metastases models exist. In the clinical situation, the distribution of volumes would be log-normal, as a function of both different growth rates and different times at which point the metastatic site was colonized [118]. In the PCI experiment, the growth rates clearly differ due to the variation in the size of metastases, but all start growing in the same general time frame. Further, there is evidence suggesting that metastases are seeded by clumps rather than single cells [119]; because this is not a spontaneous model, this could not be simulated.

A second limitation of the PCI experiment is that a single dose of 4 Gy was delivered on a single day to each of the treated mice. The clinical scenario for humans would involve several fractions of a much higher dose – for example, 10 fractions of 2.5 Gy each. Also, the single

fraction used in the experiment was for simplicity. A more clinically appropriate scenario might involve five fractions of 1 Gy in mice, or something similar. The combination of a single injection point and a single time of irradiation likely leads to an overestimation of the impact that timing has on the experimental endpoints.

A third limitation involves the primary experimental endpoint chosen – incidence of brain metastasis – and how it differs from the major clinical endpoint – overall survival. While the goal of PCI in the clinic is to directly reduce the incidence of brain metastasis, it would not be beneficial unless it also increased overall survival. In our PCI experiment, we could not monitor the presence of metastases *in vivo*, and consequently we had to sacrifice the mice to evaluate the metastatic burden. A possible future direction would be to conduct the same experiment, but then evaluate the mice for survival; however, this might not be effective unless the entire disease process could be simulated – controlled extracranial disease with chemotherapy and/or Trastuzumab.

A final limitation is that the experiment only tests the effect of PCI on one breast cancer cell line, which does not represent the entire high-risk breast cancer patient cohort. Future experiments could involve the use of other cell lines such as triple-negative breast cancer cell lines.

A next step from this study is to consider what a PCI clinical trial could look like in breast cancer patients at high risk of developing brain metastases; however, I will withhold this conversation until the general discussion. I will mention here that the importance of the timing of PCI has been evaluated before in the case of small cell lung cancer. Withers and collaborators [120] conducted a meta-analysis of clinical trials, focusing on the reduction in incidence of brain metastasis compared to the control as a function of both radiation dose and when the radiation was administered with respect to the completion of chemotherapy. They

found that “early” PCI was more effective than “late” PCI, where the delay actually introduced a dose threshold below which the incidence of brain metastasis was unchanged compared to the control. Because of these results from the SCLC PCI study, and from the significant effect that PCI had in our mouse model of metastatic breast cancer, we wanted to explore more thoroughly how sensitive the experimental endpoints are to the timing of whole-brain irradiation; rather than performing additional mouse studies, I opted to develop a computational model of our experimental system.

CHAPTER 3: MATHEMATICAL MODELING OF SUBCLINICAL BREAST CANCER BRAIN METASTASIS DOSE RESPONSE

SECTION I. INTRODUCTION

The experimental results from the *in vivo* prophylactic cranial irradiation experiment supported the hypothesis that PCI would reduce the incidence of brain metastasis in our mouse model. However, the magnitude of the decrease and the overall effect of PCI on the number of the metastases and metastatic burden was surprising. The effect of PCI – irradiation administered five days after cell injection – stood in sharp contrast to the effect of the whole-brain irradiation administered at either three or six weeks after cell injection. Because of this, we wanted to expand on the experimental results, connecting the radiation time points in order to explore how much of the difference between experimental groups could be attributed to a volume effect – i.e. larger tumors require greater dose because more cells must be inactivated. Further, mapping how the experimental endpoints such as incidence change over time could inform the period where PCI might be most effective. Rather than repeating the *in vivo* experiment with different radiation time points, I have developed a computational model that accurately mimics the experimental results and can be used to increase our knowledge about the radiation dose response of subclinical breast cancer.

In general, computational models are useful as they can incorporate information from different sources into a coherent framework in order to better understand biological processes. Often, they can elucidate the dynamics of a system, and can indicate which might be the most sensitive parameters (e.g. radiation dose, timing) [121]. In this case, information from both our *in vivo* PCI experiment and *in vitro* mammosphere and clonogenic assays, as well as assumptions about tumor growth kinetics, were drawn upon in order to better understand how radiation affects the incidence and number of brain metastases in our mouse model of HER2+,

inflammatory breast cancer. To the best of our knowledge, this is the first attempt to mathematically model subclinical disease radiation dose-response.

The second and third aims will both be addressed in this chapter. The second aim is to *develop a computational model of radiation dose-response for subclinical breast cancer based on the metastatic HER2+ mouse model*. The sub-aims are to recapitulate the experimental non-irradiated mice data by optimizing input parameters and to validate the model assumptions and inputs by performing a limiting dilution assay.

The third aim is to *demonstrate that 4 Gy prophylactic cranial irradiation in the computational model reduces the incidence of brain metastasis by 50%*. The sub-aims are to investigate if the experimental incidence can be explained by the assumptions used to develop the model and to demonstrate that delaying treatment introduces a dose threshold below which no reduction in the incidence is observed.

In developing this computational model, several trade-offs were made. Perhaps the most important involved simplicity vs. information: models should be built on robust experimental data, but including too much information has the potential to dilute the effect of what is most important [121]. For this mathematical model, simplicity was generally favored, in that the foundation of the model is derived primarily from the experimental data, and as few assumptions as possible are made in order to describe metastatic growth. Further, extraneous biological phenomena such as tumor heterogeneity are ignored, in part because of a lack of robust experimental data, and also because incorporating such information would require more assumptions. In this sense, the model is as physical (as opposed to biological) as possible.

The computational model discussed here is *descriptive*, rather than *mechanistic*, in nature. In other words, the focus is on how individual cells grow into metastases and then how the mass of cells respond to radiation in binary terms of life or death. The smallest unit

described here is the single cell, so the underlying mechanisms of colonization biology or DNA damage response, for example, are not considered.

Underlying biological processes are governed in large part by randomness, and I have attempted to incorporate that randomness into this mathematical model. In this sense, the model is *stochastic* when sample sizes are on the order of experimental sample sizes (ten mice per group in this case). However, mathematical modeling affords us the opportunity to run simulations on a much larger sample than would be feasible experimentally. Consequently, the model acts *deterministically* for large sample inputs, as the inherent randomness is averaged out and a "true" mean is approached. In this study, one thousand simulations (i.e. one thousand mice) were conducted to acquire each data point.

After running several simulations, the experimental endpoints of incidence of brain metastasis, number of brain metastases per mouse, and brain metastatic burden from the irradiated groups were compared to the computational model output of the same endpoints. This is possible because the experimental results from only the non-irradiated control mice are used to actually develop the model. Predictions regarding the effect of radiation on cell survival are derived largely from *in vitro* clonogenic data (unpublished). If the computational model output diverges from the experimental results, then the magnitude of that difference becomes important: If small, then the difference could likely be explained by imperfect assumptions that are made in the development of the model; if large, then there may be underlying causes not incorporated into the model, and hypotheses could be generated in an attempt to explain the gap.

Developing this computational model carries other benefits that are not directly related to the PCI experiment. For instance, it could help inform what time period after injection that future experimental treatments should be delivered. Additionally, knowing the effect of different survival fractions on the experimental endpoints could serve as a starting point for selecting an appropriate experimental sample size.

SECTION II. METHODOLOGY

A. Conceptualization of Model

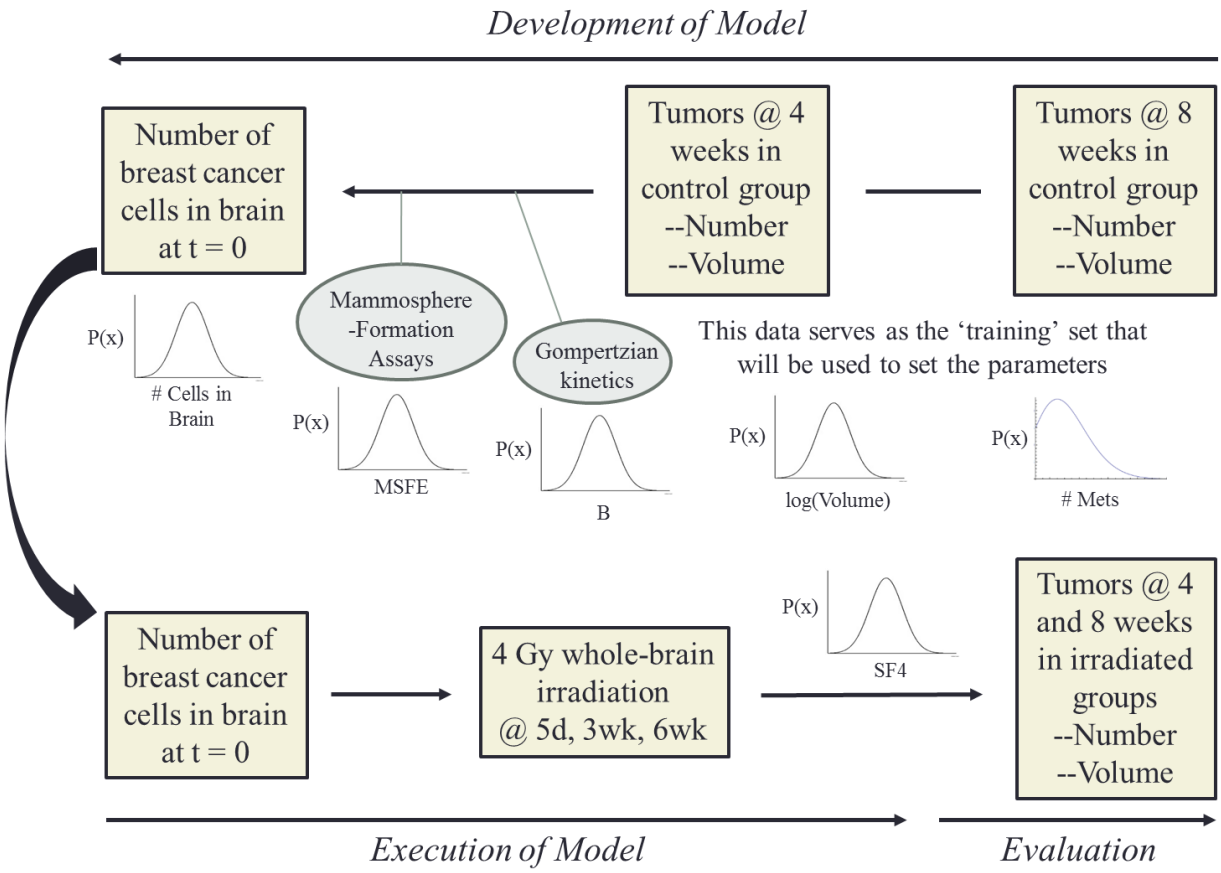

Figure 14: Overview of Development, Execution, and Evaluation of Model. See text for details.

In order to develop a computational model, experimental data from one or more sources must be combined with a set of assumptions. In this case, the experimental data available is the number of metastases per mouse, and the area of each metastasis, from both the non-irradiated and the irradiated mice. Because one goal is to test if the computational model can recapitulate the dose-response results from the PCI experiment, the irradiated mouse data cannot actually be used to develop the model, but only as a comparison against which the model output is evaluated. Therefore, only the non-irradiated mouse data was used in the development of the computational model.

Because of the limited experimental data (10-13 data points for number of metastases per mouse; 40 data points for area of metastases), the data was fit to normal or log-normal curves. This allows for a larger distribution of data in the development of the model which still reflects the experimental results.

From the areas of individual metastases from the microscope images, the volumes are estimated, and from that the number of cells in each metastasis. Assuming the area is the largest cross-section of a spherical metastasis, the area is converted into a radius ($A = \pi r^2$) and then into a volume ($V = 4/3*\pi r^3$). Throughout the model, one cubic millimeter corresponds to one million cells, and one cubic centimeter corresponds to one billion cells.

Because I have volume data from two time points, at four and eight weeks after injection, I can actually solve for the parameters in the Gompertz equation (two equations, two unknowns) by making an assumption about when the cells begin to proliferate in the brain. This will provide a distribution of Gompertz parameters that will be used to define the growth of the metastases.

Next, it is assumed that the probability that a disseminated breast cancer cell in the brain can form a metastasis (metastasis-formation efficiency) is equal to the mammosphere-formation efficiency from our *in vitro* studies. Again, this will be a distribution of probabilities rather than a single value.

Working backwards, it was then possible to approximate the number of disseminated breast cancer cells in the brain soon after cell injection by running the model and comparing the output to the aforementioned normal fit of the experimental number of metastases per mouse. Once the model inputs have been optimized and validated, then radiation can be implemented and compared to the experimental irradiated groups.

All of this is discussed in more detail below, but first I will list the assumptions made in the development of the computational model.

Key Assumptions:

- The model was developed using only the raw data from the non-irradiated control group from the four- and eight-week endpoints. This is considered the "training" set.
- The brain is seeded exclusively by single breast cancer cells, as opposed to clumps, and all metastases arise from those single cells
- The metastases are perfect spheres
- The raw microscope images provide an area for each metastatic focus: from this area an effective radius is calculated, which is converted to a volume of the metastatic sphere
- The effect of scatter on metastasis area on the microscope images is ignored
- Growth of metastases is governed by Gompertzian kinetics
- The distribution of experimental metastatic volumes is best approximated by a log-normal curve
- The distribution of the experimental number of metastases per mouse is best approximated by a normal curve
- The threshold for detection of metastases, from both the experiment and the model, is 50 cells. Metastases with fewer cells than this are not "counted."
- The four- and eight-week endpoint mice were injected with cells on two different days. It is assumed that those cells injected were the same on both days
- Once the cells start proliferating, they continue to proliferate up to the eight-week endpoint without stopping; any four-week volume can lead to any eight-week volume, within limits set by the Gompertz equation
- Although each mouse was an independent observation, the success of PCI depends on eradication of individual metastases; therefore, in this model it is assumed that each metastasis is the individual measurement.

- When radiation is administered, all cells that die do so immediately, without further proliferation
- Each metastasis will have an upper growth limit defined by parameters in the Gompertz equation. Cell kill due to irradiation will not alter this upper growth limit.
- After a tumor is irradiated, each surviving cell has the ability to continue proliferating in an attempt to repopulate the tumor
- Hypoxia: the outer 100 microns of each metastasis is fully oxygenated, while the core (if applicable) is hypoxic, with an oxygen enhancement ratio of 3.0
- Apart from hypoxia, all cells that can form a metastasis are equivalent
- All cells that could form a metastasis will have done so by the eight-week endpoint in the non-irradiated condition
- All breast cancer cells that would arrest in the brain would do so by 3 days post-injection
- ~35% of metastases that would be present at the eight-week endpoint will be below the threshold for detection (50 cells) at the four-week endpoint, in the non-irradiated group

B. Fitting Experimental Data to Distributions

From the PCI *in vivo* experiment, there are two endpoints at four and eight weeks post-injection. At the four-week endpoint, there is data from thirteen mice: thirteen data points for number of metastases per mouse, and forty-one data points for the volumes of individual metastases. At the eight-week endpoint there is data from ten mice: ten data points for number of metastases per mouse and forty-one data points for the volumes of individual metastases.

The number of metastases per mouse data from both time points was fit to a Gaussian probability distribution, using both quantitative correlation and qualitative evaluation (i.e. if this experiment was performed 100 times, would it be reasonable to expect a distribution like this?).

The volume of individual metastases data from both time points was fit to a log-normal probability distribution (log-normal = taking the logarithm of the volumes, and then fit that to a Gaussian) using quantitative correlation. A modification was made to the fit from the four-week time point in order to accommodate the assumption that 35% of eventual metastases are not observable at that time.

C. Generation of Gompertz Parameters

It is assumed that the growth of metastases is governed by Gompertzian kinetics. Here is the Gompertz equation, where N is the number of cells, t is the time, and A & B are parameters:

$$N = N_0 * \exp\left[\left(\frac{A}{B}\right) * (1 - \exp[-B * t]) \right]$$

One can see that at $t = 0$, the equation reduces to $N = N_0 * exp(0) = N_0$. N_0 here is 1 cell, from which all metastases are assumed to grow. When t approaches infinity, $N = N_0 * exp(A/B)$, which is the asymptote defining the upper limit of growth. When B is very small, then the growth is approximated by a pure exponential: $N = N_0 * exp(At)$.

Notice that there are two parameters with unknown values, A & B. It is actually possible to solve for these parameters using a system of two equations: one from each time point relating the number of cells and time interval since the start of cell proliferation, which is assumed to be ten days. In order to determine which sets of equations to use (i.e. which volume at four weeks and which volume at eight weeks to use in the system of equation to calculate one A & B pair), an assumption was made that the any volume at four weeks (from the log-normal curve) could pair with any volume at eight weeks, within the limits of the Gompertz equation. Thus, a distribution of A & B was created based on the log-normal fits of the experimental volumes. These parameters then define the growth of the metastases in the model such that it reflects the experimental volume information.

D. Workflow of Model

Here, the basic operation of the model is described.

Inputs:

- Average number of disseminated tumor cells in the brain
- Average metastasis-formation efficiency of cells
- Average interval between cell injection and start of cellular proliferation
- Day when radiation is administered, if applicable
- Average survival fraction after irradiation, if applicable

Each input, except for day of irradiation, will also have a standard deviation

The metastasis-formation efficiency was extracted directly from the mammosphere-formation efficiency observed in previous *in vitro* work. The number of disseminated tumor cells in the brain and the average interval between cell injection and the start of proliferation were both defined during the optimization process (next section). The day of the radiation and the survival fraction are both selected by the user in order to test a hypothesis.

Model:

- Look at each mouse brain
    - How many disseminated tumor cells are in the brain?
    - Of those, how many can form a metastasis?
    - Look at each disseminated tumor cell that can form a metastasis in that brain
        - When does the cell start proliferating?
        - What are the parameters for Gompertzian growth?
        - What is the surviving fraction after irradiation?
        - How many cells are there each day (i.e. volume) from days 1-56?

Each question is answered by drawing randomly from an input distribution or via calculation.

Outputs:

- Incidence of brain metastasis at four and eight weeks post-injection
- Number of metastases per mouse at four and eight weeks
- Volumes of metastases at four and eight weeks
- Tumor burden of individual mice at eight weeks

The outputs in the model correspond to the outputs from the PCI experiment, so that a comparison can be made where appropriate.

E. Optimization of Model

At this stage, the model has been developed but the inputs have not been optimized to correspond to the experimental data. While the log-normal fit of the experimental volumes was to generate a distribution of Gompertz parameter pairs, the normal fit of the experimental number of metastases per mouse is used here to optimize the inputs of: the number of disseminated tumor cells (DTCs) in the brain after injection and the average interval between cell injection and the start of cellular proliferation. Note that the input of metastasis-formation efficiency is fixed based on *in vitro* experimental work; however, the *product* of metastasis-formation efficiency and the number of DTCs generates the same output over a large range.

The two input distributions (normally distributed: mean and standard deviation are both inputs) were modified until the model output and the experimental number of metastases per mouse were highly correlated.

F. Validation of Model: Limiting Dilution Assay

After the model inputs were optimized, a method of independent validation was sought. In order to accomplish this, a limiting dilution assay was performed, in which different numbers of cells (dilutions) were injected in the tail-vein of SCID/Beige mice, and the incidence of brain metastasis was evaluated. The experimental conditions were the same as those used in the PCI experiment: same cell line, same mouse strain, same endpoint, etc.

There were five different groups: ten mice with 500k cells (same as PCI experiment and assumed as the number of injected cells in the computational model), ten mice with 250k, ten mice with 50k, ten mice with 5k, and five mice with 500 cells. To represent the dilution in the model, the number of disseminated tumor cells and its associated standard deviation was scaled accordingly. The experimental incidence of brain metastasis was then compared against the model output.

G. Execution of Model: Comparison of Model Output to Experimental Results

Having developed, optimized, and validated the model, the hypothesis could then be tested by "administering" radiation to the model. This was done by selecting a series of time points at which the radiation is delivered, and at each time point looking at a range of survival fractions, which correspond to doses based on *in vitro* data.

Irradiation was administered on the following days (experimental time points in bold):

3	**5**	7	9	11	14	17	**21**	27	35	**42**	49	55

Survival fractions used at different days of irradiation (bold values always used):

1.0	**0.75**	**0.5**	0.35	**0.25**	0.15	**0.10**	0.05	0.025	0.01	0.005	0.0025	0.001

Specific combinations correspond to specific questions, as discussed in the results section.

SECTION III. RESULTS

Fitting Experimental Data to Distributions

The volumes of individual metastases and the number of metastases per mouse were fit to log-normal and normal distributions, respectively. The Gaussian fits of the number of metastases per mouse are shown in Figures 15 and 16. The correlation between the four-week endpoint data and the fit was 87%, and the correlation at eight weeks was 66%. In the case of the eight-week endpoint, a significant amount of correlation was "sacrificed" in order to achieve a more reasonable probability distribution (i.e. the peak at n = 3 is represented by the fit, but it is not overemphasized, which would have actually improved the correlation to 75-80%). The mean and standard deviation was 0.0 and 4.0, respectively, at the four-week endpoint; and 3.2 and 3.0, respectively, at the eight-week endpoint. The lower cutoff was zero.

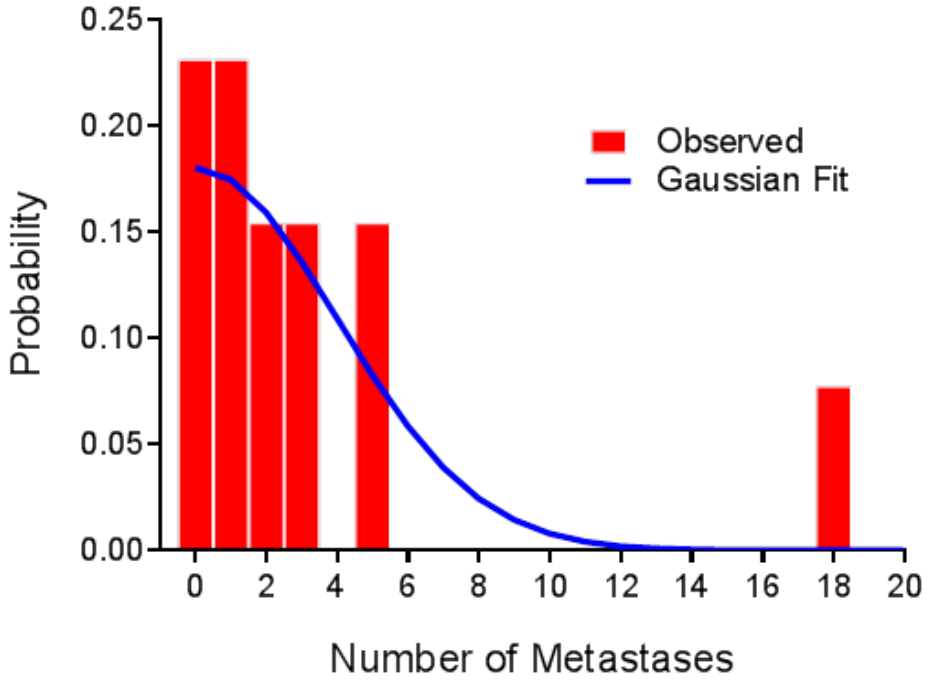

Figure 15: Gaussian Fit of Number of Metastases per Mouse at Four-Week Endpoint. A Gaussian curve (blue line) was fit to the experimental probability distribution (histogram) from the non-irradiated group, using both quantitative and qualitative methods. The correlation between the fit and the experimental data is 0.87. The fit has a mean of 0.0 and a standard deviation of 4.0, with a lower cutoff at zero. This fit was used to optimize the model inputs.

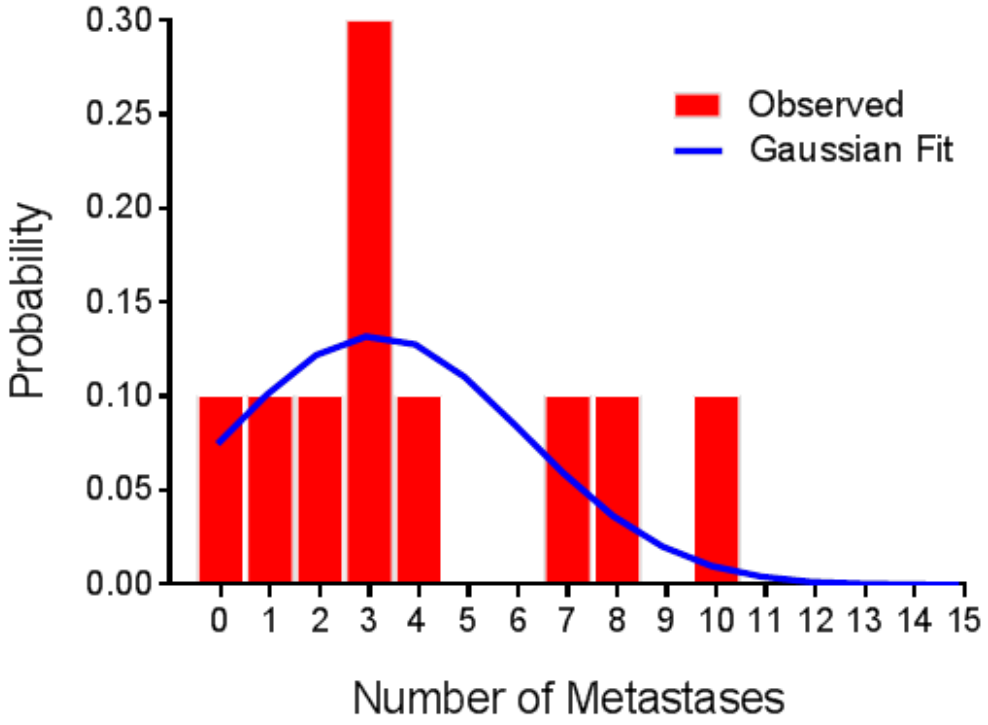

Figure 16: Gaussian Fit of Number of Metastases per Mouse at Eight-Week Endpoint. A Gaussian curve (blue line) was fit to the experimental probability distribution (histogram) from the non-irradiated group, using both quantitative and qualitative methods. The correlation between the fit and the experimental data is 0.66. The fit has a mean of 3.2 and a standard deviation of 3.0, with a lower cutoff at zero. This fit was used to optimize the model inputs.

The fits for the number of metastases per mouse were not used in the development of the model, but rather as a comparison to model outputs in order to optimize model input. The optimization results are described below and shown in Figures 19 and 20.

The volumes of individual metastases at the four- and eight-week endpoints were fit to log-normal distributions (Figure 17). The red circles represent the experimental data points, the x-axis shows the log-base 10 of the number of cells (i.e. volume [mm^3] * 10^6), and the y-axis simply represents the cumulative probability of the number of cells. Remember that the volumes were generated from the areas of the metastases on the microscope images, assuming

the metastases are perfect spheres. The correlation between the fit and the experimental data was 97.6% at four weeks, and 97.1% at eight weeks.

An assumption was made, based on the number of metastases per mouse data, that 35% of total metastases would go unobserved at the four-week endpoint (Figure 17, tan box at origin). Therefore, this needed to be represented by the volume data, where 50 cells is the detection threshold (log-value of 1.7). This caused a slight decrease on the goodness of fit. The volume information was used to define the Gompertzian growth kinetics (next section).

Generation of Gompertz Parameters

As a reminder, here is the Gompertz equation:

$$N = N_0 * \exp\left[\left(\frac{A}{B}\right) * (1 - \exp[-B * t]) \right]$$

Again, N represents the number of cells, which is known by converting the volumes from the microscope images (area → volume → number of cells). The time since the start of cell proliferation is given by t, and A & B are the Gompertz parameters that can be solved with a system of two equations based on the two volume fits.

For each pair of volumes, B and then A were calculated. For smaller tumors, the parameter B is essentially zero, meaning that the metastatic focus grows exponentially. The larger the tumor is to become, the more the growth slows over time. This distribution of B is generated in the model, and each disseminated tumor cell in the brain that is to become a metastasis will randomly draw a value of B from this distribution to define its growth parameters. The range of possible metastatic growth curves is shown in Figure 18.

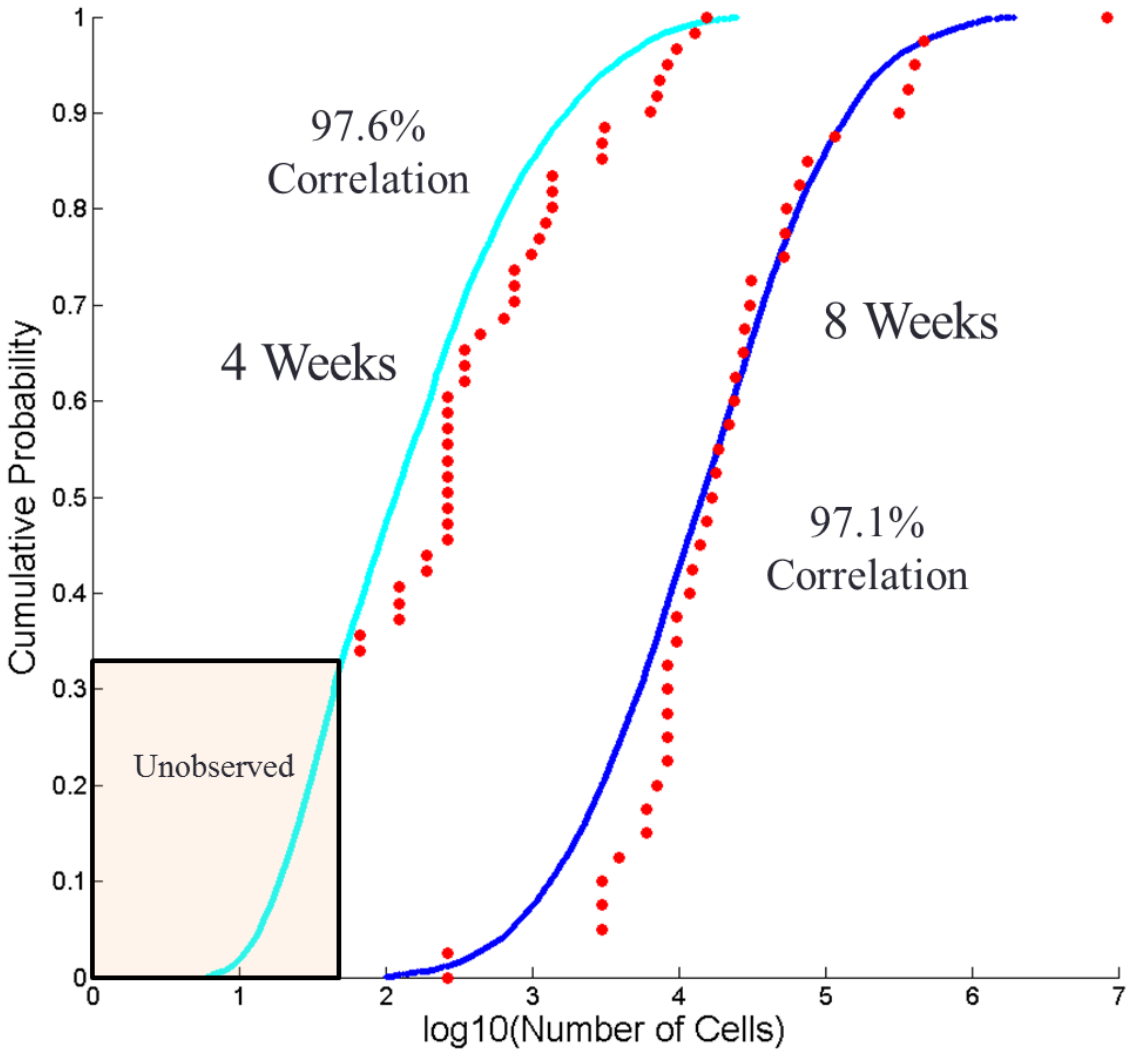

Figure 17: Log-Normal Fit of Experimental Volumes. In order to define the range of growth parameters that will be stored in the model, the experimental volumes of the metastases from the four- and eight-week endpoints (red circles) were fit a log-normal curves (blue lines). The correlation was over 97% for both fits. The green box at the bottom left indicates the range of volumes at the four-week endpoint that were below the threshold for detection. Based on the total number of metastases among the non-irradiated mice at four and eight weeks, it was assumed that 35% of metastases are below that threshold (here, -4.3 corresponds to 50 cells). In this region, the curve was modified so that the four-week volumes are consistent with the eight-week volumes in the pure exponential growth condition.

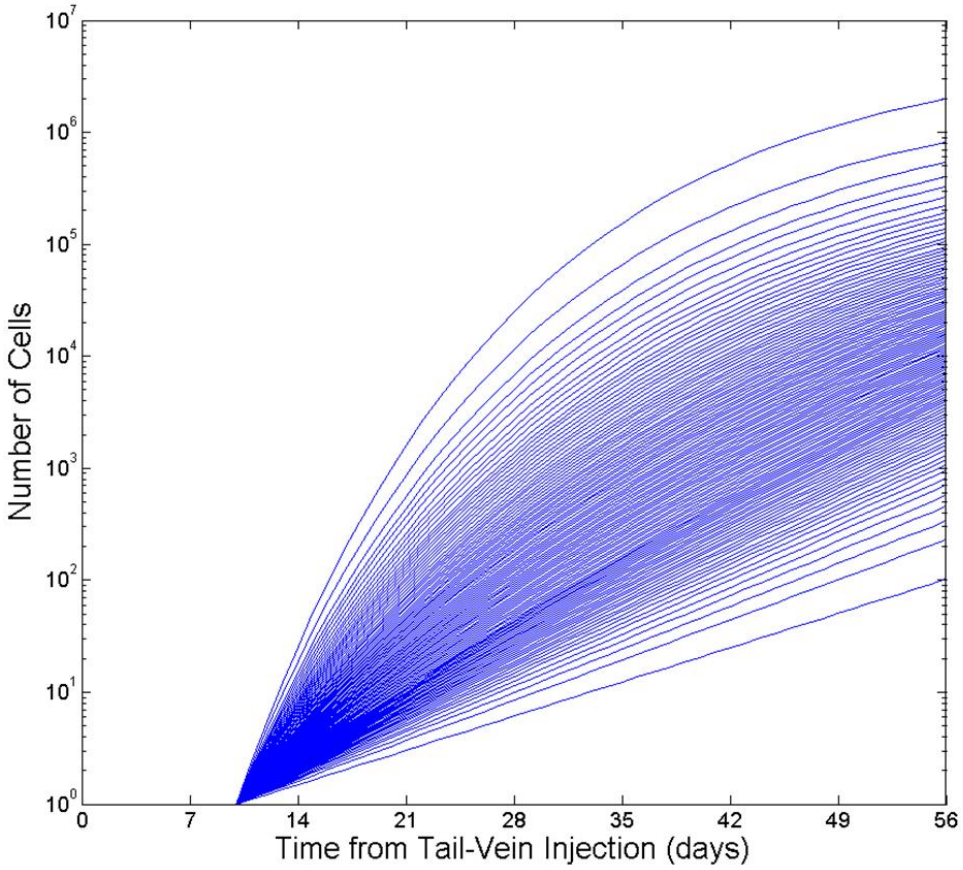

Figure 18: Metastases Growth Curves. Based on the Gompertz parameters, the range of possible growth is shown, assuming proliferations starts ten days post-injection. Note the bunching of volumes at four and eight weeks at the intermediate values, recapitulating the log-normal volume distribution.

Optimization of Model

Once the distribution of Gompertz parameters was generated, the model was optimized by modifying two input parameters. As a reminder, the three principal inputs are the number of breast disseminated tumor cells (DTCs) in the brain shortly after injection, the metastasis-formation efficiency, and the average interval between cell injection and the start of cell proliferation.

The metastasis-formation efficiency was set at 2.2% (*0.5%*), taken directly from in vitro mammosphere-formation efficiency data. This was done mostly for simplicity: the product of

DTCs in the brain and metastasis-formation efficiency gives the expected number of metastases in the brain, so adjusting one of those parameters is enough to optimize the model.

From the experimental data, the average number of metastases per mouse at the eight-week endpoint (when all metastases are assumed to be observable) was between 3.5 and 4.0. Using this information, it seemed reasonable to estimate that the average number of DTCs in the brain was 160-180 (3.5/0.022 = 160). This was the starting range for the optimization. The standard deviation was more difficult to determine, but was in effect the parameter that defined the variability in the model output of number of metastases per mouse. For example, a narrow standard deviation would give an average of 3.5-4.0 metastases per mouse, but with a tight range. The optimized inputs were determined to be 160 DTCs with a standard deviation of 60 cells. This led to excellent coverage of the number of metastases per mouse (Figure 19).

For the interval between cell injection and cell proliferation, the experimental volumes and their associated log-normal fits gave a few hints. Based on the greater deceleration of growth among the relatively large metastases, and the mostly exponential growth among the medium and smaller metastases, it seemed that proliferation started somewhere between five and fifteen days after cell injection. From this, an average interval of ten days was selected with a standard deviation of three days.

The optimized input parameters were those which gave the best correlation between the Gaussian distribution of the number of metastases per mouse (from Figures 15 and 16, corresponding to the four- and eight-week endpoints) and the model output of the same endpoint. With the optimized input parameters described above, the correlation was 95.7% at the four-week time point and 98.2% at the (more important) eight-week time point (Figure 20).

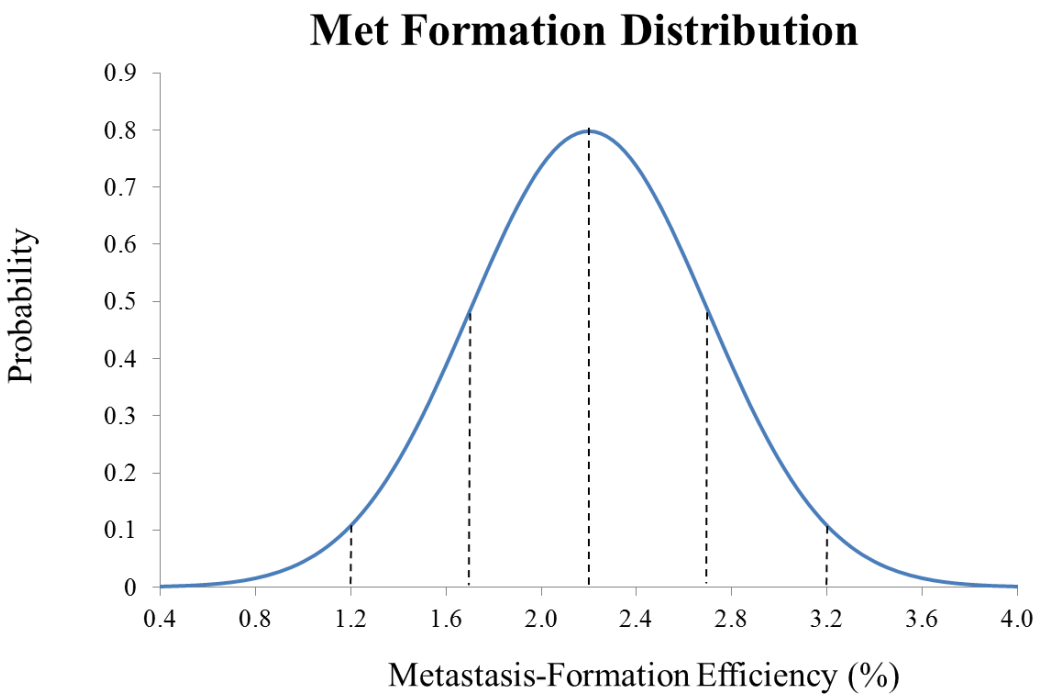
Met Formation Distribution
Probability
0.9
0.8
0.7
0.6
0.5
0.4
0.3
0.2
0.1
0
0.4
0.8
1.2
1.6
2.0
2.4
2.8
3.2
3.6
4.0
Metastasis-Formation Efficiency (%)

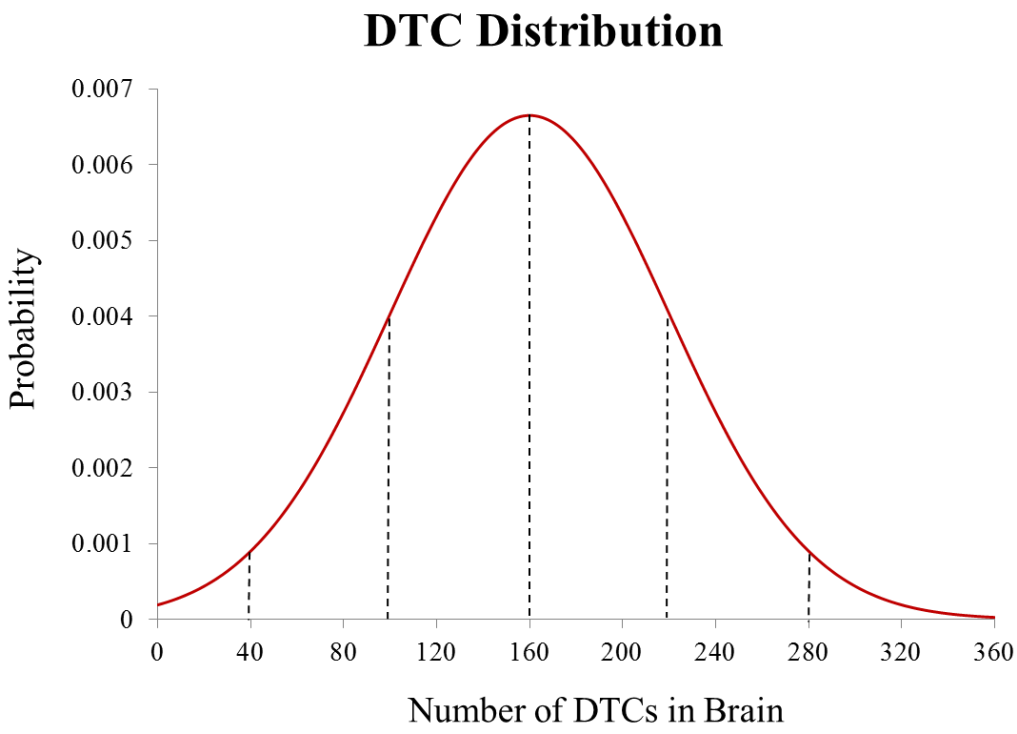
DTC Distribution
Probability
0.007
0.006
0.005
0.004
0.003
0.002
0.001
0
0
40
80
120
160
200
240
280
320
360
Number of DTCs in Brain

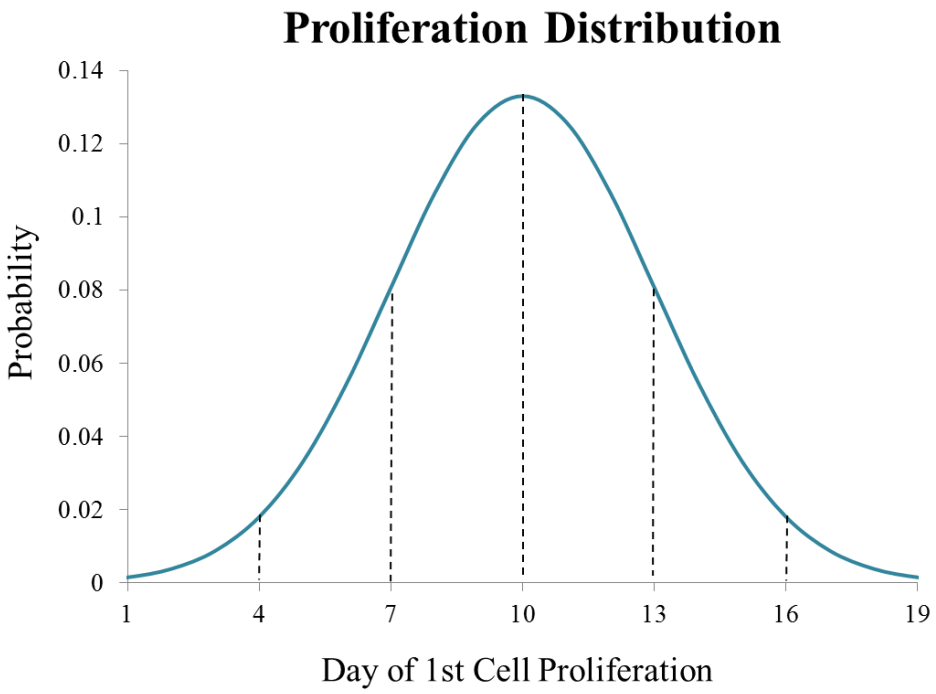

Figure 19: Optimized Input Distributions. The three input parameters to the computational model were optimized by comparing model output to the Gaussian fit at the four- and eight-week endpoint (see Figures 15 and 16). The chosen parameters were 160 disseminated breast cancer cells in the brain shortly after injection, with a standard deviation of 60 cells (previous); a metastasis-formation efficiency of 2.2%, with a standard deviation of 0.5% (previous); and an average interval of 10 days between cell injection and the day when a given disseminated tumor cell in the brain begins to proliferate, with a standard deviation of 3 days (above). The metastasis-formation efficiency was extracted from mammosphere-formation efficiency experiments conducted with the same cell line that was used in the PCI experiment.

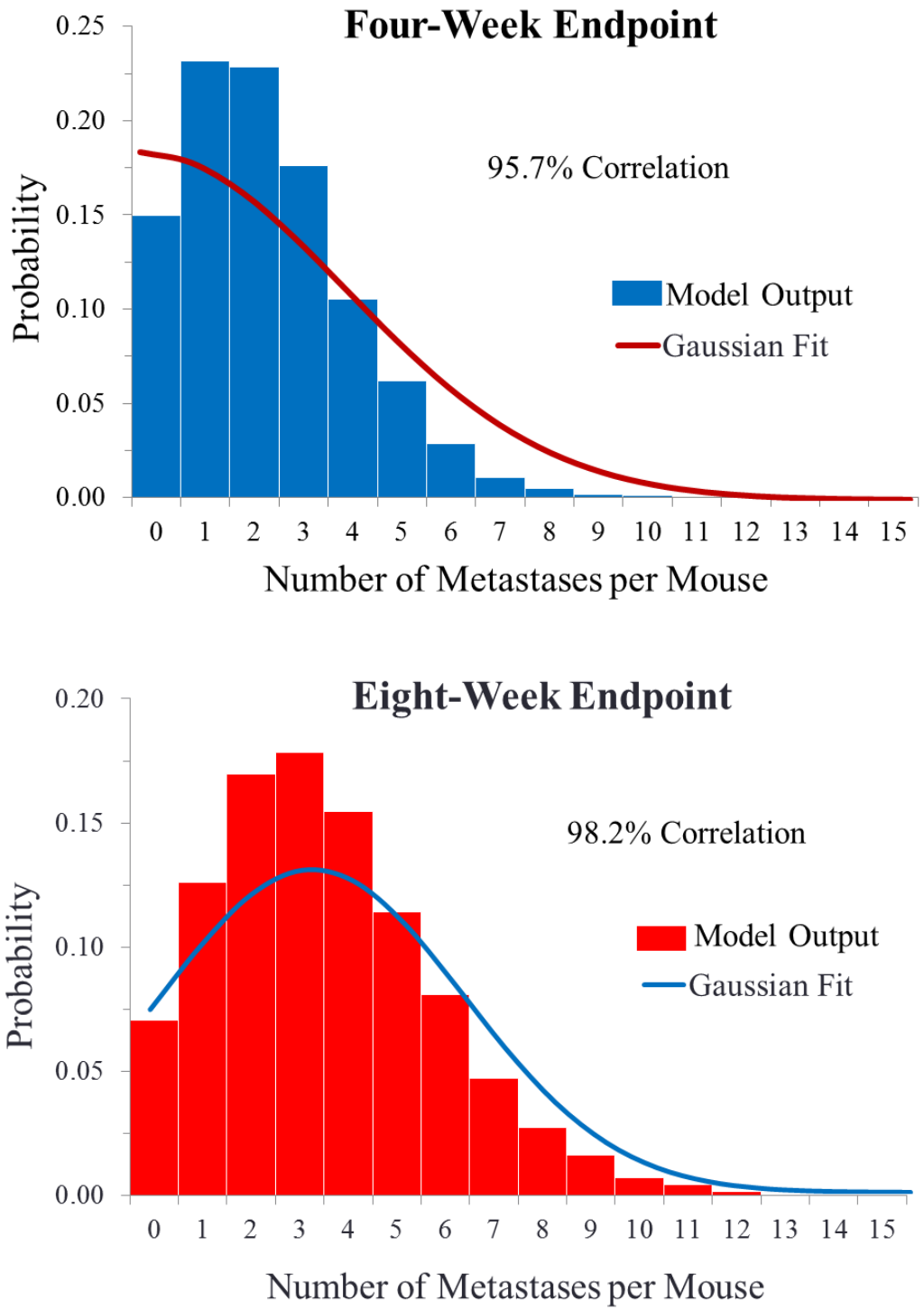

Figure 20: Comparison of Experimental Gaussian Fit to Model Output. The generation of the Gaussian fits were described above (Figures 15 and 16). When the optimized parameters (Figure 19) were input to the model, the model output (histogram) was highly correlated to the fit of the experimental data. Four the four-week endpoint, the correlation was 95.7%, and at eight weeks, the correlation was 98.2%.

Validation of Model: Limiting Dilution Assay

In order to help independently validate the computational model, a limiting dilution assay was performed. When five-hundred thousand MDA-IBC3 cells were injected into the tail vein of SCID/Beige mice, as in the PCI experiment, the incidence was 100%. When only five thousand cells were injected, the incidence was zero (see table below).

To account for the different cell dilutions in the computational model, the number of DTCs was scaled down linearly from 160 (e.g. for 50,000 injected cells, input was 16 DTCs with standard deviation of 6 DTCs). The correlation between the experimental incidence of brain metastasis and the model output was excellent, indicating that the optimized input parameters are appropriate.

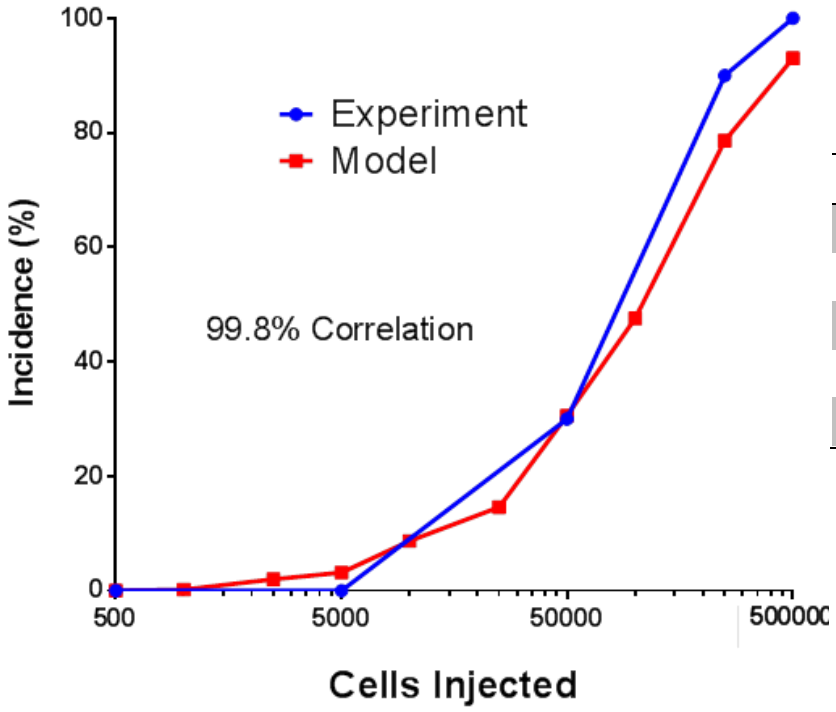

# Cells Injected	Incidence
500,000	10/10
250,000	9/10
50,000	3/10
5,000	0/10
500	0/5

Figure 21: Validation of Computational Model. In order to help validate the model, a limiting dilution assay was performed, in which different numbers of MDA-IBC3 breast cancer cells were injected into the tail vein of SCID/Beige mice. The incidence of brain metastasis in this study is shown by the blue line at 5 data points. To predict the effect of different numbers of injected breast cancer cells, the model input of average (standard deviation) number of disseminated breast cancer cells (Figure 19) was scaled linearly, and the results are shown by the red line. The correlation between the experiment and the model was approximately 100%.

Execution of Model: Comparison of Model Output to Experimental Results

In order to compare the model output to the experimental results in the irradiated groups, and also to expand on those results, simulations of the model were run for different days of radiation administration and different survival fractions (i.e. different doses). For each radiation day-survival fraction combination, n = 1000 mice was used.

The major experimental endpoints that were evaluated in the computational model were incidence of brain metastasis, average number of metastases per mouse, and metastatic burden (sum of volumes in each brain). These comparisons are shown in Figures 22, 23, and 24. In each of these figures, each line represents a single survival fraction in the computational model, where the different radiation time points are connected. The vertical dotted lines show the radiation time points that correspond to the experiment (PCI group: 5 days; 3-week treatment group: 21 days; 6-week treatment group: 42 days). The large red circles on the dotted lines show the experimental data for these radiation time points, while the large red circles adjacent to the y-axis indicate the non-irradiated control experimental results.

For the incidence of brain metastasis (Figure 22), the computational model makes clear that the selected survival fractions make a significant difference only when the radiation is administered early. After about three weeks, the difference in incidence between the non-irradiated control and 90% cell kill is predicted to be negligible. A similar trend is observed for the average number of metastases per mouse (Figure 23), where the survival fractions become insignificant after 4-5 weeks. For both the incidence and the average number of metastases, the experimental results from the PCI group correspond to a 10% survival fraction in the computational model, whereas the two later treatment groups are indistinguishable from the non-irradiated control.

Because metastatic burdens varies widely, even on a logarithmic scale, the model output and experimental results are presented as upper quartile, median, and lower quartile in Figure

24. The computational model recapitulates the burden in the non-irradiated control, while the 3- and 6-week treatment groups, while varying greatly, are not distinguishable from 100% survival. On the other hand, the PCI group is again consistent with a 10% survival fraction. Note that the model predicts zero tumor burden as a median and lower quartile in the 10% survival fraction condition when the radiation is administered five days post-injection. This is indicated by the red circles appearing below the x-axis. The model output also shows that the median for 10% survival and the lower quartiles for 10% and 25% survival dips below a log-value of -4: in these cases, the values actually drop to zero tumor burden.

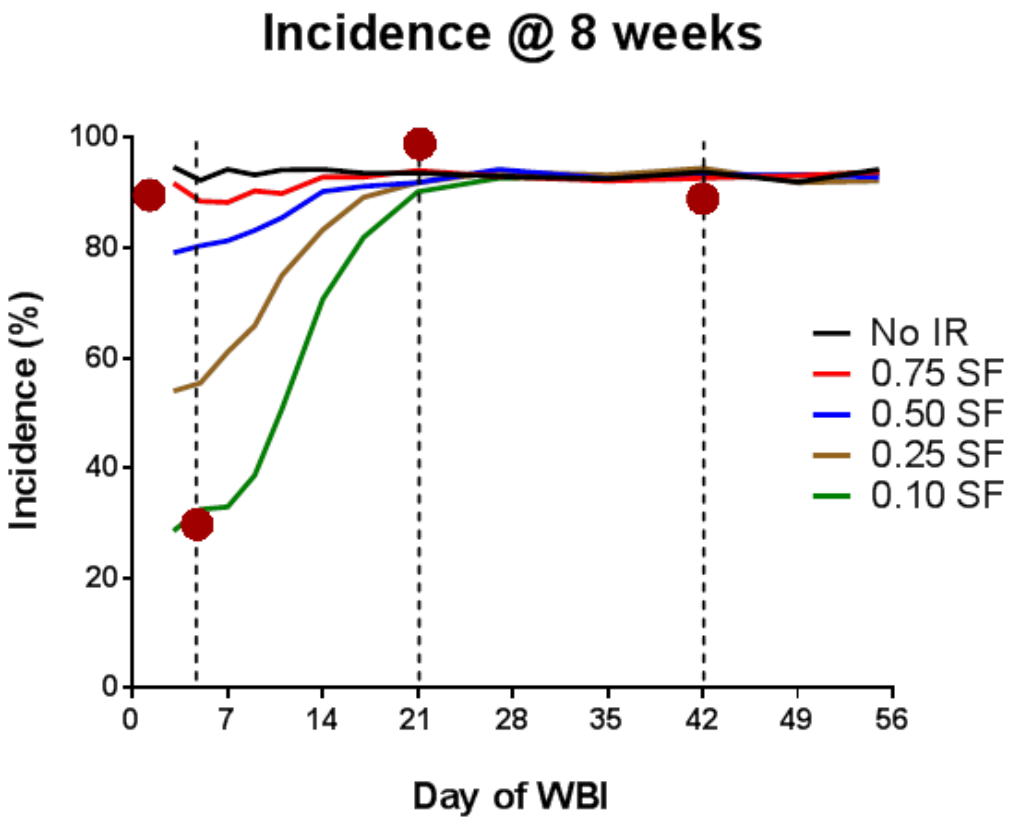

Figure 22: Incidence of Brain Metastasis at Eight-Week Endpoint. When whole-brain irradiation is administered in the few weeks after cell injection, the computational model predicts that the decrease in incidence of brain metastasis compared to the non-irradiated control is very sensitive to both survival fraction and day of irradiation. The dotted lines represent the experimental radiation time points, and the red circles indicate the incidence at those time points (The red circle at the y-axis indicates that the model accurately reflects the incidence in the non-irradiated control.). The incidence in the PCI experimental group is consistent with a 10% survival fraction, whereas the 3- and 6-week treatment groups could be represented by 10-100% survival, due to the insensitivity of dose on the incidence at those times.

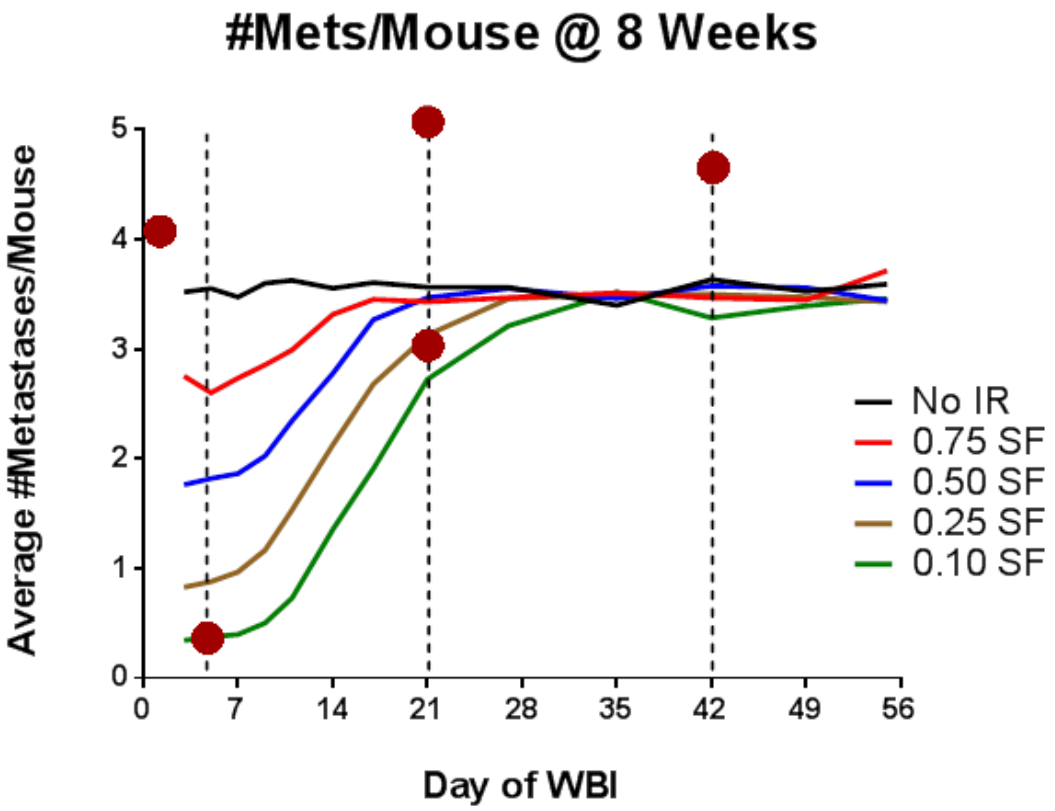

Figure 23: Number of Brain Metastases per Mouse at Eight-Week Endpoint. When whole-brain irradiation is administered in the few weeks after cell injection, the computational model predicts that the decrease in the average number of brain metastases compared to the non-irradiated control is very sensitive to both survival fraction and day of irradiation. The dotted lines represent the experimental radiation time points, and the red circles indicate the incidence at those time points (The red circle at the y-axis indicates that the model slightly underestimates the average number of brain metastases per mouse in the non-irradiated control.). There are two red circles at 21 days to represent both the mean and the median. The number of metastases per mouse in the PCI experimental group is consistent with a 10% survival fraction, whereas the 3- and 6-week treatment groups are consistent with 100% survival.

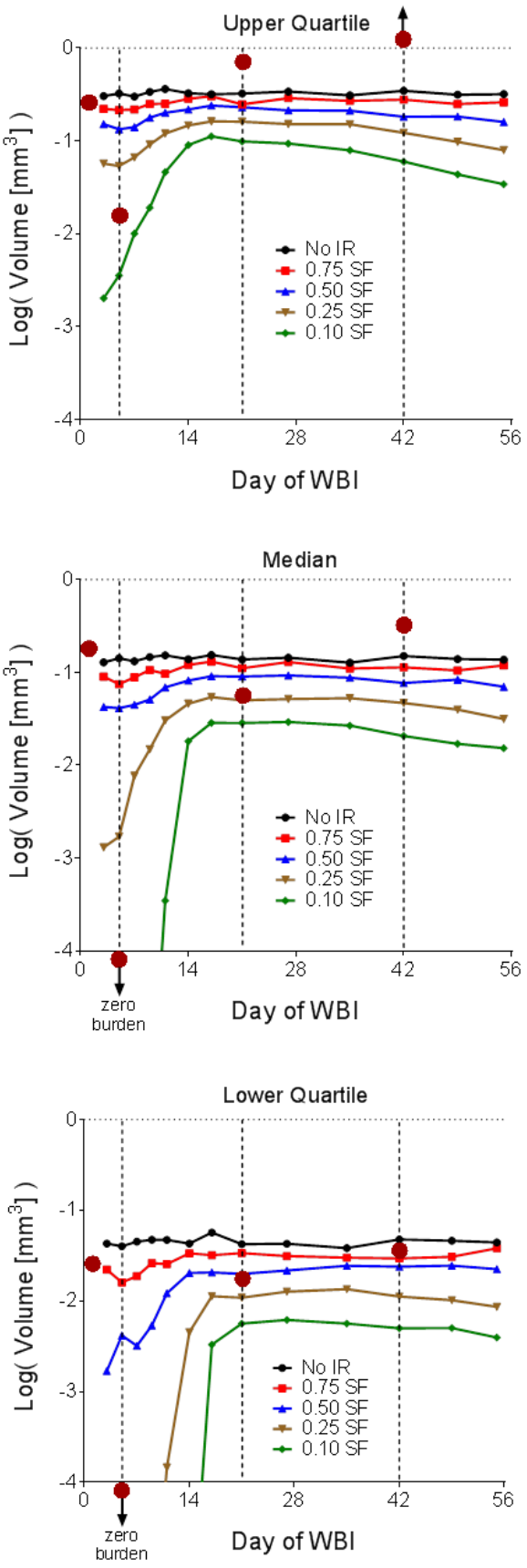

Figure 24: Tumor Burden at Eight-Week Endpoint. When whole-brain irradiation is administered in the few weeks after cell injection, the computational model predicts that the decrease in the metastatic burden is very time-sensitive when the majority of cells are killed. The effect is less pronounced at later time points, where the burden changes little with respect to time. The dotted lines represent the experimental radiation time points, and the red circles indicate the incidence at those time points. A lower cutoff of -4 (100 cells) was chosen, and the lines below that threshold indicate zero burden. The experimental data points (red circles) below the axis indicate zero burden, and the one point above the axis indicates a burden greater than the upper threshold of the graph. The burden in the PCI experimental group is consistent with an approximately 10% survival fraction, whereas the 3- and 6-week treatment groups cannot be distinguished from the non-irradiated condition.

Model Predicts Treatment Delay-Induced Dose-Threshold Effect

Different conclusions can be drawn if the effect of radiation timing is plotted against survival fraction, independent of the experimental results. Figures 25 and 26 show the reduction in incidence and the reduction in the average number of metastases per mouse, respectively, compared to the non-irradiated control. This is displayed for four different radiation time points – days 5, 9, 14, and 21 – and is plotted as a function of survival fraction.

In Figure 25, it is apparent that delaying the whole-brain irradiation introduces a dose-threshold effect, in which a reduction in the incidence of brain metastasis is not observed until a sufficiently low survival fraction (i.e. a sufficiently high radiation dose). In the case of the whole-brain irradiation being administered at twenty one days after cell injection, that threshold appears to correspond to a 10-15% survival fraction. In contrast, a 10-15% survival fraction reduces the incidence of brain metastasis by well over 50% when the dose is administered five days post-injection.

A similar effect is shown in Figure 26, where the reduction in the number of metastases decreases linearly with increasing cell kill (this is intuitive) for early radiation time points, but a dose-threshold is apparent for the twenty-one day irradiation. In this case, the reduction in the number of metastases is not observed until at least 65% cell kill, at which point over 50% reduction would be observed in the five-day irradiation condition.

Extrapolating the fraction cells killed in Figure 25 into a radiation dose can make the information more clinically meaningful. The conversion is done via *in vitro* monolayer clonogenic data (not shown), from which it is assumed that there is an inverse log-linear relationship between radaition dose and survival fraction (i.e. 8 Gy gives 10% survival, 16 Gy gives 1% survival, etc.). The result is shown in Figure 27, where the dose threshold seems to be about 6 Gy. Again, a similar effect would be observed with the number of metastases per mouse data, but this is not shown here.

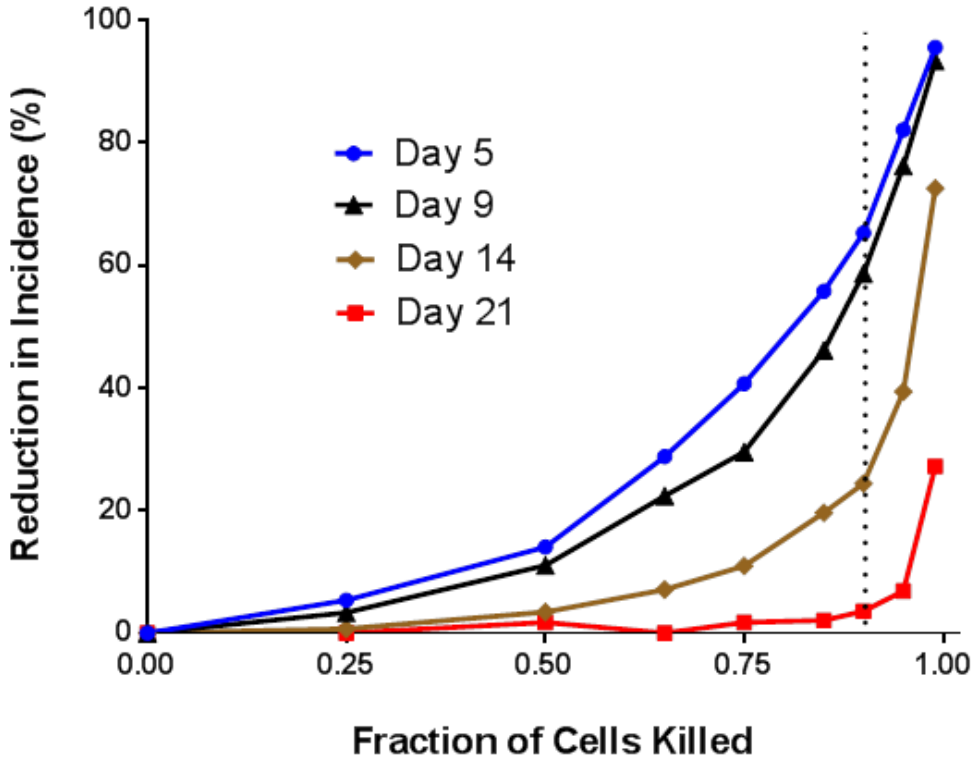

Figure 25: Reduction in Incidence compared to Non-Irradiated Control. The reduction in the incidence of brain metastasis at the eight-week time point is plotted against the fraction of cells killed for four different days of irradiation. The sooner the radiation is administered, the greater the reduction of incidence. The extreme cases, days 5 and 21, represent days of administration in the PCI experiment. The delay of irradiation introduces a dose threshold before which the incidence is reduced: in this case, administering radiation twenty-one days after cell injection would require approximately 90% cell kill (dotted vertical line) before a reduction in the incidence is observed. At this survival fraction, the reduction in incidence caused by radiation delivered five days after cell injection is well over 50%.

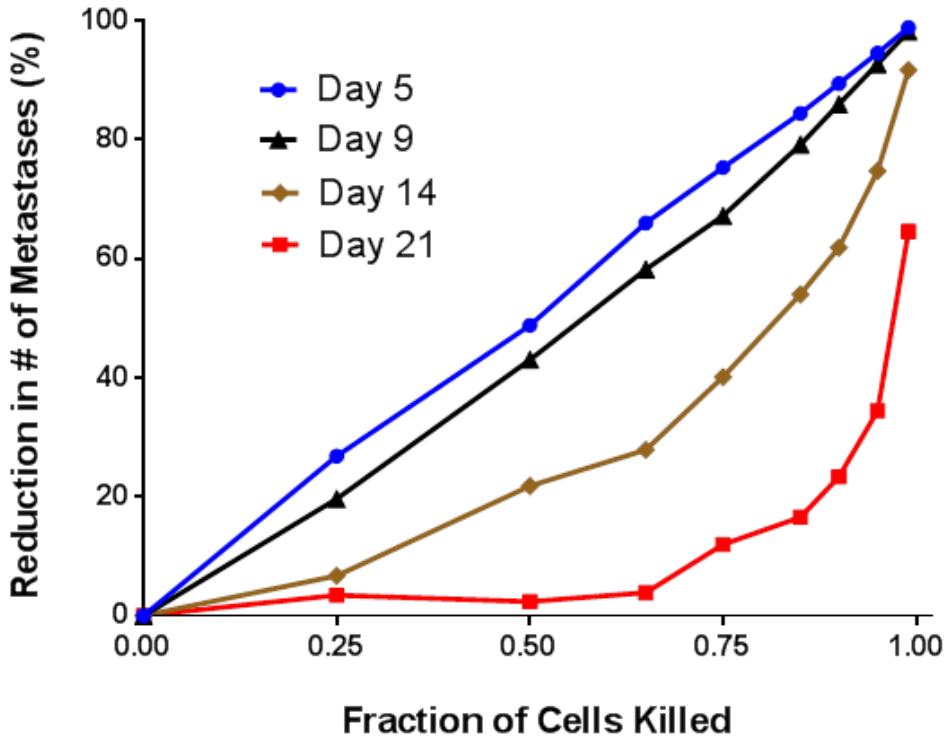

Figure 26: Reduction in Number of Metastases compared to Non-Irradiated Control. The reduction in the number of brain metastases at the eight-week time point is plotted against the fraction of cells killed for four different days of irradiation. The sooner the radiation is administered, the fewer the number of metastases that form. The extreme cases, days 5 and 21, represent days of administration in the PCI experiment. Similar to the reduction in incidence in the previous figure, there appears to be a dose threshold before a reduction in the number of metastases is observed. The dose threshold corresponds to a survival fraction of 30-50%.

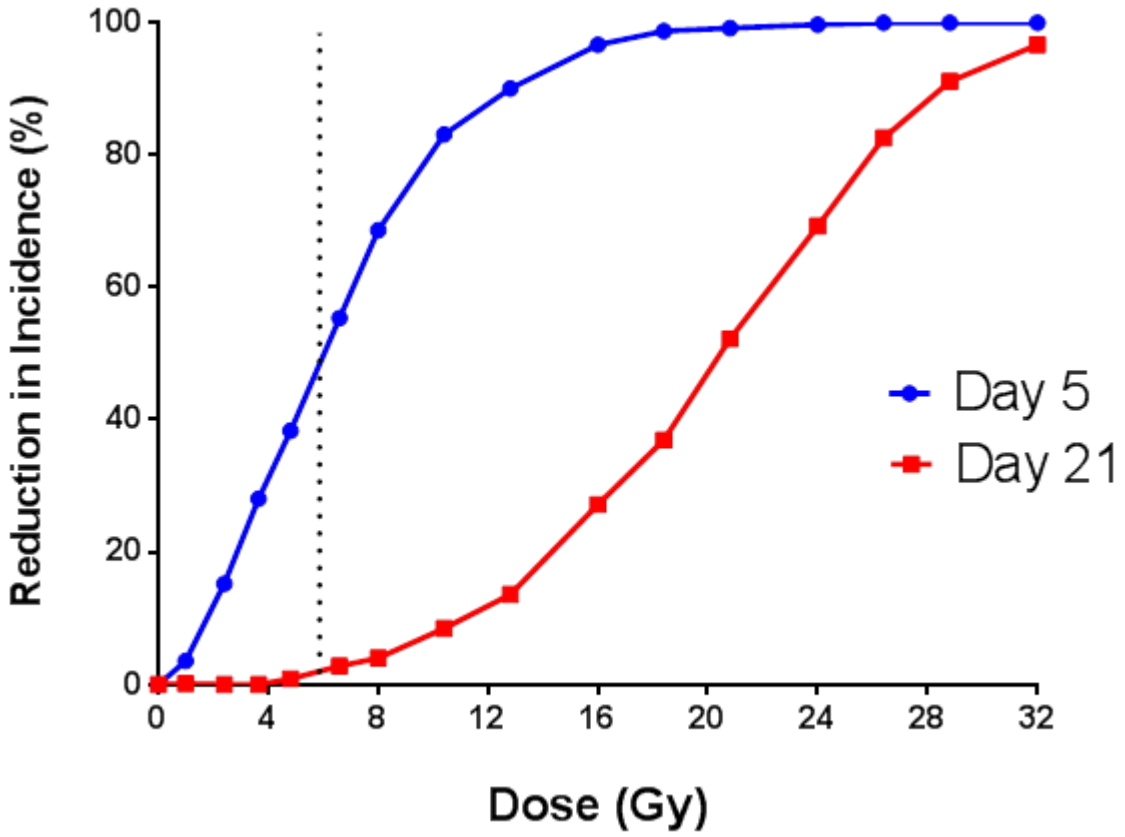

Figure 27: Reduction in Incidence compared to Non-Irradiated Control. The reduction in the incidence of brain metastasis at the eight-week time point is plotted against the radiation dose given on days 5 and 21, which correspond to experimental irradiation times. The dose was estimated by extrapolating monolayer clonogenic survival for the MDA-IBC3 cell line and then converting the input survival fractions in the computational model to dose. While irradiation administered at day 5 results in an immediate reduction in the incidence of brain metastasis, a slight delay introduces a dose threshold of approximately 4-6 Gy. This figure shows a striking similarity to findings by Suwinski and Withers [120] relating to the dose-response of small cell lung cancer to PCI, in which "early" PCI shows an immediate response (Day 5) while "late" PCI exhibits a dose threshold (Day 21).

Inclusion of Hypoxia: Effect on Radiation Response

The effect of hypoxia on radiation resistance was included in the model. It was assumed that the outer 100 microns of the metastasis was fully oxygenated, while the inner, if applicable, was hypoxic (below). The oxygen enhancement ratio was conservatively estimated as 3.0. As seen below, the metastases in this model simply were not large enough for hypoxia to be a factor, as the effect of hypoxia was negligible even when metastases were irradiated late.

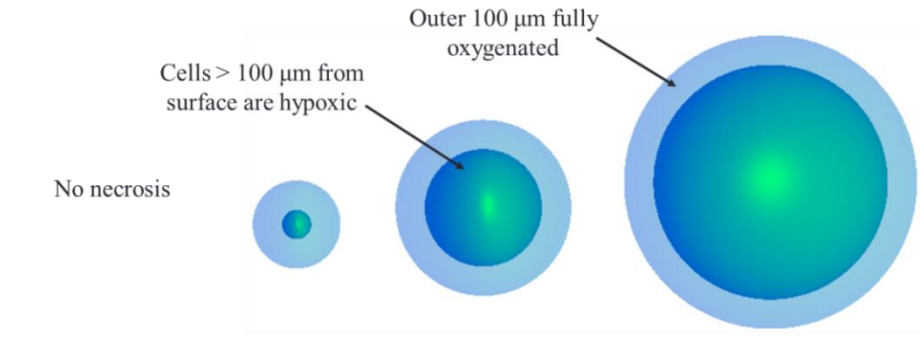

Tumor Radius (μm)	150	300	500
Number of Cells	15,000	115,000	524,000
Hypoxic Fraction	0.037	0.30	0.51

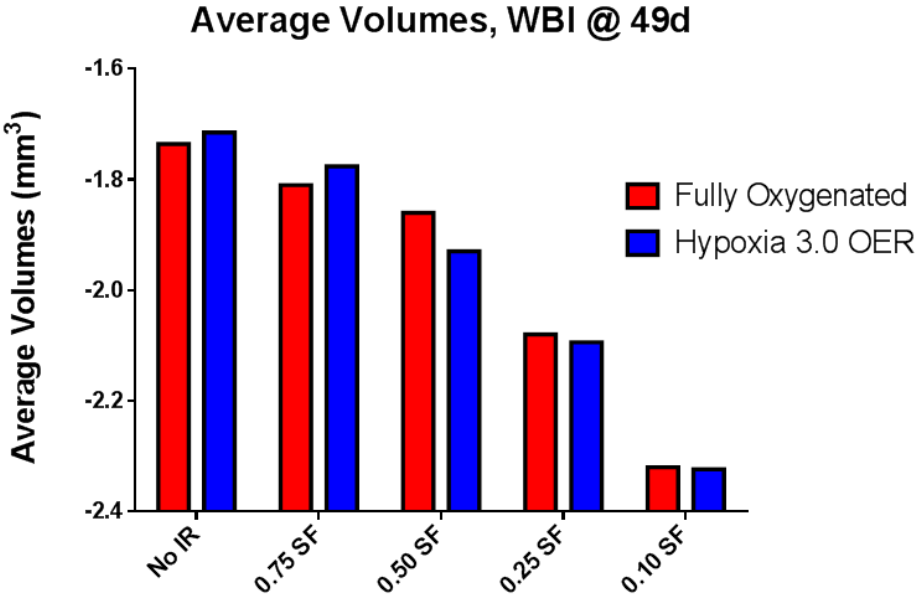

Figure 28: Assumptions about Hypoxia in Model. It was assumed that the outer 100 microns of each metastasis was fully oxygenated, while the core (if applicable) was hypoxic, with an oxygen enhancement ratio of 3.0. Based on previous work done with our metastatic mouse model, it was assumed that no necrosis was present. As shown in the bottom panel, the impact of hypoxia was negligible due to the small size of the metastases.

SECTION IV. CONCLUSIONS

In Chapter 2, I emphasized that the timing of whole-brain irradiation had a significant impact on the experimental endpoints of incidence and number of brain metastases and metastatic burden. Most notably, the sixteen days of additional metastatic growth between 5 and 21 days post-injection produced stark differences in the response to whole-brain irradiation. Unfortunately, due to limited experimental groups, no conclusions could be drawn about the time-course of incidence and other endpoints. Because of previous clinical meta-analyses suggesting that "early" PCI is beneficial in the case of SCLC [120], this information gap in our animal experiment seemed important; in an attempt to bridge that gap, a computational model of subclinical breast cancer dose-response was developed.

Implementing data from the non-irradiated mice in the PCI experiment, I created a mathematical model that recapitulates, and expands upon, the experimental results. Individual volumes of metastases from the four- and eight-week experimental endpoints were fit to log-normal curves, where the correlation between data and the fits was better than 97% at both time points. The log-normal volume fits were then used to generate a range of parameters for the Gompertz equation. Once the model was built, the input parameters were optimized so that the correlation between the model and experimental number of metastases per mouse was better than 95% at both four- and eight-week time points. The mathematical model was validated through a limiting dilution assay, where the correlation between model and experimental incidence was approximately 100%. Because the irradiated mice data was selectively ignored in the *development* of the model, it was then possible to use that data for *evaluation* purposes. By simulating radiation cell kill, predictions were made regarding how the experimental endpoints would change as a function of radiation dose and time of irradiation.

The hypothesis was that the computational model of breast cancer brain metastasis dose-response would underestimate the effect of PCI, and would overestimate the effect of whole-

brain irradiation at three and six weeks post-injection. The comparison of experimental results with model predictions supported the hypothesis: the computational model predicted that 4-Gy whole-brain irradiation would decrease the incidence in the PCI group by 30-50% compared to the non-irradiated control and would decrease the metastatic burden by greater than 40% in the 3- and 6-week treatment groups. In contrast, the experimental reduction in incidence (compared to the non-irradiated control) was 67-74%; the burden in the treatment groups, while highly variable, did not demonstrate clear trends away from the control data in either direction. Further disagreement between the model predictions and experimental results is shown on the next page.

What the data really suggests is that the survival fraction at 4 Gy – predicted as approximately 31% from IBC3 clonogenic assays – is not reflected by the experimental results when comparing against the computational model. The results from the PCI group in the experiment are consistent with a 10% survival fraction in the computational model, whereas the results from the 3- and 6-week treatment groups are highly variable, but more consistent with a 100% than a 31% survival fraction.

PCI Group, Four-Week Endpoint

Change vs. 0-Gy Control	Model	Experimental	Agreement?
Incidence	-38%	-74%	X
Number of Metastases	-65%	-89%	X

PCI Group, Eight-Week Endpoint

Change vs. 0-Gy Control	Model	Experimental	Agreement?
Incidence	-30%	-67%	X
Number of Metastases	-50%	-93%	X
Metastatic Burden, Upper Quartile	-79%	-96%	
Metastatic Burden, Median	-91%	-100%	X
Metastatic Burden, Lower Quartile	-100%	-100%	

Three-Week Treatment Group, Four-Week Endpoint

Change vs. 0-Gy Control	Model	Experimental	Agreement?
Incidence	-12%	-9%	✓
Number of Metastases	-37%	-9%	X

Three-Week Treatment Group, Eight-Week Endpoint

Change vs. 0-Gy Control	Model	Experimental	Agreement?
Incidence	0%	+11%	✓
Number of Metastases	-5%	0%	✓
Metastatic Burden, Upper Quartile	-61%	+340%	
Metastatic Burden, Median	-56%	-69%	X
Metastatic Burden, Lower Quartile	-63%	-46%	

Table X: Comparison between model predictions and experimental results. The experimental results from the PCI and 3-week treatment groups are compared against the same endpoints from the computational model, where both the experimental results and model predictions were normalized against their corresponding non-irradiated control.

The mechanisms behind this are unknown, but some speculation may be appropriate. In the case of the whole-brain irradiation at 3 and 6 weeks post-injection, the 4-Gy dose was not expected (based on the model) to decrease the incidence or the number of metastases per mouse noticeably, but it was expected to decrease the metastatic burden. Two well-known factors involved in radiation response, accelerated repopulation and hypoxia, are worth mentioning. Hypoxia, which is associated with increased survival due to the lack of oxygen (required for DNA damage fixation), was aggressively incorporated into the computational model. Due to the small size of the micrometastases in consideration, it had negligible effect. Accelerated repopulation describes the process by which clonogenic cells attempt to quickly repopulate the tumor after a large fraction of cells are killed [110]. Although not explicitly included in the model, accelerated repopulation is a consequence of the assumption that the radiation dose does not alter the upper limit of tumor growth (i.e. after cell kill, growth rate must increase to reach same upper growth limit as corresponding non-irradiated lesion). Even with the inclusion of these two factors, the difference between observations and predictions remains stark.

Genetic diversity is one factor that may in part explain the difference between the predictions and results. As tumors grow, mutations accumulate, and as a consequence subclones are formed and tumor heterogeneity is observed. This could be significant in terms of radiation response as one or more of the emergent subclones could exhibit relatively greater resistance to the effects of radiation therapy. If so, the resistant clone could then repopulate the tumor [122]. However, in our case the whole-brain irradiation occurs 21 or 42 days after cell injection, and any genetic diversity would likely be limited.

While the model overestimated the effect of irradiation on the later treatment groups, it significantly underestimated the effect of irradiation on the PCI group. Because it is unlikely that the survival fraction *in vivo* is less than the survival fraction in vitro at 4 Gy (roughly 30%), the approximately 10% survival fraction in the PCI experimental group suggests that a non-cell

kill mechanism is a factor. One possibility is that the radiation precludes the colonization step in metastasis, as colonization would be expected to occur in first week or two after cell injection. For example, one group observed that ionizing radiation induces the epithelial-to-mesenchymal transition through TGFβ in mammary epithelial cells [123]. Because the colonization process relies on the *opposite* of EMT – the mesenchymal-to-epithelial transition (MET) – one hypothesis would be that ionizing radiation can reverse or block the colonization process; however, no experimental data supporting this hypothesis exists.

The reduction in the incidence of brain metastasis versus radiation dose curve in Figure 27 mirrors a curve published by Withers and colleagues in a meta-analysis of PCI studies in small-cell lung cancer patients [120]. In both cases, a delay in the treatment (or the initiation of treatment) introduces a dose threshold below which no reduction in the incidence of brain metastasis is observed. In the Withers study, "early" PCI was defined as initiation of treatment in the sixty days after the completion of a chemotherapy regimen (average start 30 days after completion), while "late" PCI was defined as initiation of whole-brain irradiation after sixty days (average 100 days). The dose threshold in that meta-analysis was 20 Gy: there was a linear relationship between dose and the reduction in incidence, but a delay in treatment shifted the curve 20 Gy to the right. That same relationship is observed based on the output of our computational model, where the 16-day delay between the 5- and 21-day irradiations shifts the curve approximately 4-6 Gy to the right. In Figure 27, the two curves are not parallel as might be expected – this is because there is not a log-normal distribution of the number of cells at five days post-injection: the vast majority of cells have not begun to proliferate. In conclusion, this computational model of subclinical breast cancer radiation dose response not only recapitulates the experimental results in the non-irradiation control, but also mirrors the clinical situation for PCI in SCLC, albeit at lower doses and smaller metastasis volumes.

As with any computational model, there are clear limitations that result from imperfect experimental data and the assumptions that form the foundation of the model. In the case of this model of breast cancer micrometastatic dose response, the assumptions, which are listed in the methodology section, are major limitations (bias error). For example, no biological heterogeneity was included in the model: had it been, the reduction in incidence versus dose curve would shift to the right. Many of the assumptions followed from the experimental data, but others were based on the literature and were required to build a usable model. The limitations due to the experimental *system* were discussed in the previous chapter, and will not be repeated here; however, the experimental *results* themselves are limitations as they represent only a small sample of potential outcomes but are the only window we have into the output of the experimental system.

This last point, differentiation between the experimental system and the experimental results from our one *in vivo* study, is very important. When I was attempting to fit the experimental number of metastases per mouse and volumes to normal and log-normal curves, respectively, I am *not* trying to minimize the error of the fits to the experimental results; rather, I am trying to minimize the error of the fits to represent the experimental system (generalization error), which can only be *inferred* from the experimental results. Attempting to optimize the fits to the experimental results would be an example of *overfitting*: the model would be well-tuned to the results, but may not explain anything about the experimental system.

Combined with the data from Chapter 2, the insights drawn from the computational model could carry clinical significance, showing that the timing of irradiation is critical for the treatment of subclinical disease, but that discussion will be withheld until Chapter 6.

CHAPTER 6: GENERAL DISCUSSION

Breast cancer patients who develop brain metastases have abysmal survival times, with only 10-20% surviving beyond one year from the time of diagnosis. Prophylactic cranial irradiation is a clinical technique used to reduce the incidence of brain metastasis in SCLC and ALL patients and, because of an emerging population of breast cancer patients at high risk of developing brain metastasis, there is now interest in extending the technique to select breast cancer patients. The present work addressed the efficacy of PCI in a mouse model of metastatic, HER2+ inflammatory breast cancer.

The central hypothesis of this thesis was that prophylactic cranial irradiation would reduce in the incidence of brain metastasis in our mouse model and, in Chapter 2, I described the results of that *in vivo* study. I found that PCI did significantly decrease the incidence of brain metastasis, the number of metastases per mouse, and the metastatic burden compared to other experimental groups. Expanding on those results in Chapter 3 with a computational model, I mapped the change in the experimental endpoints as a function of survival fraction (i.e. radiation dose) and time of treatment, demonstrating that not only does the computational model mimic a clinical situation for SCLC patients, but it also underestimates the effect that PCI had in the *in vivo* study.

PCI has been utilized in patients with small-cell lung cancer and acute lymphoblastic leukemia for forty years, as it reduces the incidence of brain metastasis and consequently improves overall survival. Now, with receptor subtypes it is known that HER2+ and triple-negative breast cancer patients with extracranial metastases have 30% (or greater) risk of developing brain metastases. Here, I will discuss the potential clinical significance of our data.

First, it is clear from both the experimental data and the computational model that there is a significant benefit to earlier treatment. When considering the incidence of brain metastasis in the model, the timing of irradiation is just as important as the survival fraction. For a given low survival fraction, there is a period of time where the incidence and the number of metastases increase rapidly as the treatment is delayed; beyond that critical period, the radiation has little effect on incidence.

Second, the current clinical scenario is that breast cancer patients will not be referred for brain scans *until they display symptoms consistent with the presence of brain metastases*. Because it is assumed implicitly that all brain metastases are equally bad, it follows that there is no clinical benefit to earlier treatment, and thus no need to image for the presence of brain metastases. This project challenges that assumption, and suggests that there would be a great clinical benefit to referring patients at high risk of developing brain metastases for brain scans as part of their follow-up or continued management. But who are these patients? I opened this discussion in the introduction, but will expand on it below.

If it became the clinical norm that breast cancer patients at high risk of developing brain metastases did receive MRI scans –before the onset of symptoms – the next step would be to consider PCI clinical trials for those patients who had negative scans (those with positive scans would begin WBRT). The design of clinical trials for these patients would involve several factors that need to be addressed. Most important, patient selection becomes critical in light of the potential toxicity of whole-brain irradiation. I mentioned in the introduction that HER2+ and triple-negative breast cancer patients with extracranial metastases are at the highest risk of developing brain metastases, and patients outside this subgroup would be unlikely candidates for PCI. However, it would be desirable to further segment this subgroup in order to better define which patients could benefit from PCI.

The nomogram developed by Ibrahim and colleagues [107] would be a good starting point. In that study, the authors found the patients at the highest risk were:

- Younger
- Higher histologic grade
- Shorter delay between primary diagnosis and first metastasis
- More than one metastatic site

It was estimated that the highest risk patients had 50% probability of developing brain metastases. In addition, it could be possible to combine biomarker information with these clinical factors to better select patients. For example, high miR-141 in the serum of breast cancer patients is associated with significantly lower overall survival and progression-free survival in metastatic breast cancer and inflammatory breast cancer patients [71]. The combination of omics information and clinical data could define a subset of breast cancer patients with a greater than 50% risk of developing brain metastases, which is right in line with the risk of SCLC patients who receive PCI.

One related point that would need to be addressed is whether to restrict PCI to patients with controlled extracranial disease. If not, then the patients with uncontrolled extracranial disease could benefit from early PCI in terms of the incidence of brain metastasis. However, these patients could very well die from their extracranial metastases, and thus the PCI would have little effect on overall survival. At the same time, PCI could reduce the burden of brain metastasis from cells already present in the brain at the time of treatment, but would certainly not be expected to prevent future re-seeding of the brain by the uncontrolled disease. On the other hand, if PCI is restricted to patients with controlled extracranial disease, then those patients with uncontrolled disease may miss their opportunity for early PCI (which could still benefit them, especially in the case where the disease becomes controlled).

While patient selection must be considered from the standpoint of which patients are at the highest risk of developing brain metastasis, the risk of toxicity in individual patients should be considered as well. For example, there is evidence that neurocognitive decline due to WBRT or PCI is more pronounced in patients over 75 years of age [111].

Total dose and fractionation schedule would also have to be determined. In SCLC, patients with extensive disease receive 20-30 Gy in 5-10 fractions [85]. Patients with brain metastases often receive 30 Gy whole-brain radiation therapy in ten fractions. It seems likely that breast cancer patients would receive a similar treatment in terms of dose and fractionation, but clarifying the lowest effective dose (this could certainly change depending on clinical factors) could help reduce toxicity. Further, concrete steps could be taken to reduce the risk of toxicity. For instance, a recent phase II trial demonstrated that hippocampal avoidance during whole-brain radiation therapy was associated with memory preservation and improved quality of life [124], perhaps the two most significant drawbacks of PCI. In addition, the drug memantine – often used in patients with memory disorders – was recently evaluated in a large clinical trial, and the authors found that it delayed the time to cognitive decline and reduced the rate of decline in memory in patients treated with WBRT [125].

Currently, there is not a consensus on how patients with brain metastases should be managed. The current trend is that radiation oncologists are moving away from whole-brain radiation therapy in favor of stereotactic radiosurgery alone. A recent report by Saghal and colleagues [126] found that there was a survival benefit for patients under 50 years of age with SRS alone. Interestingly, those patients under age 50 who were treated with SRS alone had *no increased risk of developing brain metastases* compared to their age-matched cohort in the SRS + WBRT arm; however, the risk was significantly greater in patients over age 50 treated with SRS alone. The authors hypothesize that because there was no significant effect on the distant

brain failure, the adverse effects of WBRT reduce the survival in patients under 50. This point stands in contrast to clinical data presented in the nomogram indicating that younger patients are at higher risk of developing brain metastases [107]. I would note one important difference: the Saghal study looks at only patients who already have brain metastases.

If the radiation oncology community were to accept that PCI could benefit breast cancer patients at high risk of developing brain metastases, then it would seem that those breast cancer patients who already have brain metastases should receive whole-brain radiation therapy, as they would be high risk (for local/distant brain failure) by definition. The Saghal study seems to indicate that this may not be the case for younger patients, and emphasizes how much of an adverse effect that WBRT-associated toxicity can have. If dose reduction techniques or hippocampal avoidance are employed, WBRT may gain favor. Last, if whole-brain irradiation is withheld until disease progression, then the early period where WBRT could show the greatest benefit might be missed.

I included two chapters in this thesis discussing projects that were early transitions in my research, but are only tangentially related, if at all, to the principal topic of PCI. Chapter 4 discusses our findings on how survivin affects radiation response in breast cancer *in vitro*. Because survivin is universally overexpressed in cancers and has been shown to be a radiation resistance factor in many experimental models, there is the possibility that it may promote survival and recurrence in those clones that survived whole-brain irradiation, especially in the PCI group. The survivin project fits under the umbrella of attempting to improve the efficacy of radiation therapy in breast cancer patients, through better understanding of radiobiology and informing the possible development of radiosensitizers.

The other chapter deals with the hedgehog signaling pathway, and our attempts to quantify its activity *in vivo* through the use of radiotracers. The rationale behind this paper and

related previous studies was that hedgehog signaling could be a surrogate for cancer stem cells, which are associated with resistance to irradiation. Further, hedgehog activity could potentially serve as a predictor for treatment response and could help select which patients could benefit from anti-hedgehog therapies. While survivin could promote recurrence, quantification of hedgehog activity before and after irradiation could help predict which patients recur. Because these studies were transitions, they are far from complete and would need to be expanded upon in order to address the initial hypotheses.

In this work, I have utilized a unique experimental system – a robust mouse model of brain metastasis and a small-animal irradiator – in order to address the question of whether PCI could reduce the incidence of brain metastasis. The overall hypothesis, that PCI would reduce the incidence of brain metastasis in a mouse model of HER2+ IBC, was supported, and the computational modeling indicates a divergence between experimental results and model predictions, and helps to indicate the time period where the experimental endpoints are most sensitive to changes in radiation dose. These findings have the potential to inform the debate surrounding SRS +/- WBRT and the management of breast cancer patients at high risk of developing brain metastases.

BIBLIOGRAPHY

1. American Cancer Society. *Breast Cancer Facts & Figures 2013-2014*: Atlanta: American Cancer Society, Inc. 2013.
2. Howlader N, N.A., Krapcho M, Garshell J, Neyman N, Altekruse SF, Kosary CL, Yu M, Ruhl J, Tatalovich Z, Cho H, Mariotto A, Lewis DR, Chen HS, Feuer EJ, Cronin KA, *SEER Cancer Statistics Review, 1975-2010*. Bethesda, MD: National Cancer Institute; 2013. http://seer.cancer.gov/csr/1975_2010/, based on June 2013 SEER data submission.
3. Carey, L.A., C.M. Perou, C.A. Livasy, L.G. Dressler, D. Cowan, K. Conway, G. Karaca, M.A. Troester, K.T. Chiu, S. Edmiston, S.L. Deming, J. Geradts, M.C.U. Cheang, T.O. Nielsen, P.G. Moorman, H.S. Earp, and R.C. Millikan, *Race, breast cancer subtypes, and survival in the Carolina Breast Cancer Study*. Journal of the American Medical Association, 2006. **295**(21): p. 2492-2502.
4. Robertson, F.M., M. Bondy, W. Yang, H. Yamauchi, S. Wiggins, S. Kamrudin, S. Krishnamurthy, H. Le-Petross, L. Bidaut, A.N. Player, S.H. Barsky, W.A. Woodward, T. Buchholz, A. Lucci, N. Ueno, and M. Cristofanilli, *Inflammatory breast cancer the disease, the biology, the treatment*. CA Cancer Journal for Clinicians, 2010. **60**(6): p. 351-375.
5. Green, F., D. Page, and I. Flemming, *American Joint Committee on cancer staging manual*. 6th ed. 2002, New York: Springer.
6. Van Laere, S.J., N.T. Ueno, P. Finetti, P. Vermeulen, A. Lucci, F.M. Robertson, M. Marsan, T. Iwamoto, S. Krishnamurthy, H. Masuda, P. Van Dam, W.A. Woodward, P. Viens, M. Cristofanilli, D. Birnbaum, L. Dirix, J.M. Reuben, and F. Bertucci, *Uncovering the molecular secrets of inflammatory breast cancer biology: An integrated*

analysis of three distinct affymetrix gene expression datasets. Clinical Cancer Research, 2013. **19**(17): p. 4685-4696.

7. Woodward, W.A., S. Krishnamurthy, H. Yamauchi, R. El-Zein, D. Ogura, E. Kitadai, S.I. Niwa, M. Cristofanilli, P. Vermeulen, L. Dirix, P. Viens, S. Van Laere, F. Bertucci, J.M. Reuben, and N.T. Ueno, *Genomic and expression analysis of microdissected inflammatory breast cancer.* Breast Cancer Research and Treatment, 2013. **138**(3): p. 761-772.
8. Parton, M., M. Dowsett, S. Ashley, M. Hills, F. Lowe, and I.E. Smith, *High incidence of HER-2 positivity in inflammatory breast cancer.* Breast, 2004. **13**(2): p. 97-103.
9. Makower, D. and J.A. Sparano, *How do i treat inflammatory breast cancer?* Current Treatment Options in Oncology, 2013. **14**(1): p. 66-74.
10. Cristofanilli, M., V. Valero, A.U. Buzdar, S.W. Kau, K.R. Broglio, A.M. Gonzalez-Angulo, N. Sneige, R. Islam, N.T. Ueno, T.A. Buchholz, S.E. Singletary, and G.N. Hortobagyi, *Inflammatory breast cancer (IBC) and patterns of recurrence: Understanding the biology of a unique disease.* Cancer, 2007. **110**(7): p. 1436-1444.
11. Hance, K.W., W.F. Anderson, S.S. Devesa, H.A. Young, and P.H. Levine, *Trends in inflammatory breast carcinoma incidence and survival: The surveillance, epidemiology, and end results program at the National Cancer Institute.* Journal of the National Cancer Institute, 2005. **97**(13): p. 966-975.
12. Kim, T., A.E. Giuliano, and G.H. Lyman, *Lymphatic mapping and sentinel lymph node biopsy in early-stage breast carcinoma: A metaanalysis.* Cancer, 2006. **106**(1): p. 4-16.
13. Darby, S., P. McGale, C. Correa, C. Taylor, R. Arriagada, M. Clarke, D. Cutter, C. Davies, M. Ewertz, J. Godwin, R. Gray, L. Pierce, T. Whelan, Y. Wang, R. Peto, K. Albain, S. Anderson, W. Barlow, J. Bergh, J. Bliss, M. Buyse, D. Cameron, E. Carrasco, A. Coates, R. Collins, J. Costantino, J. Cuzick, N. Davidson, K. Davies, A. Delmestri, A.

Di Leo, M. Dowsett, P. Elphinstone, V. Evans, R. Gelber, L. Gettins, C. Geyer, A. Goldhirsch, C. Gregory, D. Hayes, C. Hill, J. Ingle, R. Jakesz, S. James, M. Kaufmann, A. Kerr, E. MacKinnon, T. McHugh, L. Norton, Y. Ohashi, S. Paik, H.C. Pan, E. Perez, M. Piccart, K. Pritchard, G. Pruneri, V. Raina, P. Ravdin, J. Robertson, E. Rutgers, Y. F Shao, S. Swain, P. Valagussa, G. Viale, E. Winer, and W. Wood, *Effect of radiotherapy after breast-conserving surgery on 10-year recurrence and 15-year breast cancer death: Meta-analysis of individual patient data for 10 801 women in 17 randomised trials.* The Lancet, 2011. **378**(9804): p. 1707-1716.

14. Fisher, B., S. Anderson, J. Bryant, R.G. Margolese, M. Deutsch, E.R. Fisher, J.H. Jeong, and N. Wolmark, *Twenty-year follow-up of a randomized trial comparing total mastectomy, lumpectomy, and lumpectomy plus irradiation for the treatment of invasive breast cancer.* New England Journal of Medicine, 2002. **347**(16): p. 1233-1241.

15. Hortobagyi, G.N., *Treatment of breast cancer.* New England Journal of Medicine, 1998. **339**(14): p. 974-984.

16. Von Minckwitz, G., M. Untch, J.U. Blohmer, S.D. Costa, H. Eidtmann, P.A. Fasching, B. Gerber, W. Eiermann, J. Hilfrich, J. Huober, C. Jackisch, M. Kaufmann, G.E. Konecny, C. Denkert, V. Nekljudova, K. Mehta, and S. Loibl, *Definition and impact of pathologic complete response on prognosis after neoadjuvant chemotherapy in various intrinsic breast cancer subtypes.* Journal of Clinical Oncology, 2012. **30**(15): p. 1796-1804.

17. Early Breast Cancer Trialists' Collaborative Group (EBCTCG), *Relevance of breast cancer hormone receptors and other factors to the efficacy of adjuvant tamoxifen: Patient-level meta-analysis of randomised trials.* The Lancet, 2011. **378**(9793): p. 771-784.

18. Dowsett, M., J. Cuzick, J. Ingle, A. Coates, J. Forbes, J. Bliss, M. Buyse, M. Baum, A. Buzdar, M. Colleoni, C. Coombes, C. Snowdon, M. Gnant, R. Jakesz, M. Kaufmann, F. Boccardo, J. Godwin, C. Davies, and R. Peto, *Meta-analysis of breast cancer outcomes in adjuvant trials of aromatase inhibitors versus tamoxifen.* Journal of Clinical Oncology, 2010. **28**(3): p. 509-518.

19. Romond, E.H., E.A. Perez, J. Bryant, V.J. Suman, C.E. Geyer Jr, N.E. Davidson, E. Tan-Chiu, S. Martino, S. Paik, P.A. Kaufman, S.M. Swain, T.M. Pisansky, L. Fehrenbacher, L.A. Kutteh, V.G. Vogel, D.W. Visscher, G. Yothers, R.B. Jenkins, A.M. Brown, S.R. Dakhil, E.P. Mamounas, W.L. Lingle, P.M. Klein, J.N. Ingle, and N. Wolmark, *Trastuzumab plus adjuvant chemotherapy for operable HER2-positive breast cancer.* New England Journal of Medicine, 2005. **353**(16): p. 1673-1684.

20. Dawood, S., S.D. Merajver, P. Viens, P.B. Vermeulen, S.M. Swain, T.A. Buchholz, L.Y. Dirix, P.H. Levine, A. Lucci, S. Krishnamurthy, F.M. Robertson, W.A. Woodward, W.T. Yang, N.T. Ueno, and M. Cristofanilli, *International expert panel on inflammatory breast cancer: Consensus statement for standardized diagnosis and treatment.* Annals of Oncology, 2011. **22**(3): p. 515-523.

21. Hurley, J., P. Doliny, I. Reis, O. Silva, C. Gomez-Fernandez, P. Velez, G. Pauletti, M.D. Pegram, and D.J. Slamon, *Docetaxel, cisplatin, and trastuzumab as primary systemic therapy for human epidermal growth factor receptor 2-positive locally advanced breast cancer.* Journal of Clinical Oncology, 2006. **24**(12): p. 1831-1838.

22. Langley, R.R. and I.J. Fidler, *Tumor cell-organ microenvironment interactions in the pathogenesis of cancer metastasis.* Endocrine Reviews, 2007. **28**(3): p. 297-321.

23. Fidler, I.J., *The pathogenesis of cancer metastasis: The 'seed and soil' hypothesis revisited.* Nature Reviews Cancer, 2003. **3**(6): p. 453-458.

24. Chambers, A.F., A.C. Groom, and I.C. MacDonald, *Dissemination and growth of cancer cells in metastatic sites.* Nature Reviews Cancer, 2002. **2**(8): p. 563-572.

25. Luzzi, K.J., I.C. MacDonald, E.E. Schmidt, N. Kerkvliet, V.L. Morris, A.F. Chambers, and A.C. Groom, *Multistep nature of metastatic inefficiency: Dormancy of solitary cells after successful extravasation and limited survival of early micrometastases.* American Journal of Pathology, 1998. **153**(3): p. 865-873.

26. Langley, R.R. and I.J. Fidler, *The seed and soil hypothesis revisited-The role of tumor-stroma interactions in metastasis to different organs.* International Journal of Cancer, 2011. **128**(11): p. 2527-2535.

27. Weinberg, R.A., *The Biology of Cancer*. 2007, New York: Garland Science.

28. Talmadge, J.E. and I.J. Fidler, *AACR centennial series: The biology of cancer metastasis: Historical perspective.* Cancer Research, 2010. **70**(14): p. 5649-5669.

29. Kawaguchi, T. and K. Nakamura, *Analysis of the lodgement and extravasation of tumor cells in experimental models of hematogenous metastasis.* CANCER AND METASTASIS REVIEW, 1986. **5**(2): p. 77-94.

30. Honn, K.V., D.G. Tang, I. Grossi, Z.M. Duniec, J. Timar, C. Renaud, M. Leithauser, I. Blair, C.R. Johnson, C.A. Diglio, V.A. Kimler, J.D. Taylor, and L.J. Marnett, *Tumor cell-derived 12(S)-hydroxyeicosatetraenoic acid induces microvascular endothelial cell retraction.* Cancer Research, 1994. **54**(2): p. 565-574.

31. Al-Mehdi, A.B., K. Tozawa, A.B. Fisher, L. Shientag, A. Lee, and R.J. Muschel, *Intravascular origin of metastasis from the proliferation of endothelium-attached tumor cells: A new model for metastasis.* Nature Medicine, 2000. **6**(1): p. 100-102.

32. Chambers, A.F., I.C. MacDonald, E.E. Schmidt, S. Koop, V.L. Morris, R. Khokha, and A.C. Groom, *Steps in tumor metastasis: New concepts from intravital videomicroscopy.* Cancer and Metastasis Reviews, 1995. **14**(4): p. 279-301.

33. Barkan, D., J.E. Green, and A.F. Chambers, *Extracellular matrix: A gatekeeper in the transition from dormancy to metastatic growth.* European Journal of Cancer, 2010. **46**(7): p. 1181-1188.

34. Hedley, B.D. and A.F. Chambers, *Chapter 3 Tumor Dormancy and Metastasis*. 2009. p. 67-101.

35. Paget, S., *THE DISTRIBUTION OF SECONDARY GROWTHS IN CANCER OF THE BREAST*. The Lancet, 1889. **133**(3421): p. 571-573.

36. Schackert, G. and I.J. Fidler, *Site-specific metastasis of mouse melanomas and a fibrosarcoma in the brain or meninges of syngeneic animals.* Cancer Research, 1988. **48**(12): p. 3478-3484.

37. Gavrilovic, I.T. and J.B. Posner, *Brain metastases: Epidemiology and pathophysiology.* Journal of Neuro-Oncology, 2005. **75**(1): p. 5-14.

38. Barnholtz-Sloan, J.S., A.E. Sloan, F.G. Davis, F.D. Vigneau, P. Lai, and R.E. Sawaya, *Incidence proportions of brain metastases in patients diagnosed (1973 to 2001) in the Metropolitan Detroit Cancer Surveillance System*. Journal of Clinical Oncology, 2004. **22**(14): p. 2865-2872.

39. Schouten, L.J., J. Rutten, H.A.M. Huveneers, and A. Twijnstra, *Incidence of brain metastases in a cohort of patients with carcinoma of the breast, colon, kidney, and lung and melanoma.* Cancer, 2002. **94**(10): p. 2698-2705.

40. Patchell, R.A., P.A. Tibbs, J.W. Walsh, R.J. Dempsey, Y. Maruyama, R.J. Kryscio, W.R. Markesbery, J.S. Macdonald, and B. Young, *A randomized trial of surgery in the treatment of single metastases to the brain.* New England Journal of Medicine, 1990. **322**(8): p. 494-500.

41. Eichler, A.F., E. Chung, D.P. Kodack, J.S. Loeffler, D. Fukumura, and R.K. Jain, *The biology of brain metastases-translation to new therapies.* Nature Reviews Clinical Oncology, 2011. **8**(6): p. 344-356.

42. Chang, E.L., J.S. Wefel, M.H. Maor, S.J. Hassenbusch Iii, A. Mahajan, F.F. Lang, S.Y. Woo, L.A. Mathews, P.K. Allen, A.S. Shiu, and C.A. Meyers, *A pilot study of neurocognitive function in patients with one to three new brain metastases initially treated with stereotactic radiosurgery alone.* Neurosurgery, 2007. **60**(2): p. 277-283.

43. Mehta, M.P., P. Rodrigus, C.H.J. Terhaard, A. Rao, J. Suh, W. Roa, L. Souhami, A. Bezjak, M. Leibenhaut, R. Komaki, C. Schultz, R. Timmerman, W. Curran, J. Smith, S.C. Phan, R.A. Miller, and M.F. Renschler, *Survival and neurologic outcomes in a randomized trial of motexafin gadolinium and whole-brain radiation therapy in brain metastases.* Journal of Clinical Oncology, 2003. **21**(13): p. 2529-2536.

44. Steeg, P.S., K.A. Camphausen, and Q.R. Smith, *Brain metastases as preventive and therapeutic targets.* Nature Reviews Cancer, 2011. **11**(5): p. 352-363.

45. Ito, S., H. Nakanishi, Y. Ikehara, T. Kato, Y. Kasai, K. Ito, S. Akiyama, A. Nakao, and M. Tatematsu, *Real-time observation of micrometastasis formation in the living mouse liver using a green fluorescent protein gene-tagged rat tongue carcinoma cell line.* International Journal of Cancer, 2001. **93**(2): p. 212-217.

46. Kienast, Y., L. Von Baumgarten, M. Fuhrmann, W.E.F. Klinkert, R. Goldbrunner, J. Herms, and F. Winkler, *Real-time imaging reveals the single steps of brain metastasis formation.* Nature Medicine, 2010. **16**(1): p. 116-122.

47. Carbonell, W.S., O. Ansorga, N. Sibson, and R. Muschel, *The vascular basement membrane as "soil" in brain metastasis.* PLoS ONE, 2009. **4**(6).

48. Heyn, C., J.A. Ronald, S.S. Ramadan, J.A. Snir, A.M. Barry, L.T. MacKenzie, D.J. Mikulis, D. Palmieri, J.L. Bronder, P.S. Steeg, T. Yoneda, I.C. MacDonald, A.F.

Chambers, B.K. Rutt, and P.J. Foster, *In vivo MRI of cancer cell fate at the single-cell level in a mouse model of breast cancer metastasis to the brain.* Magnetic Resonance in Medicine, 2006. **56**(5): p. 1001-1010.

49. Aupérin, A., R. Arriagada, J.P. Pignon, C. Le Péchoux, A. Gregor, R.J. Stephens, P.E.G. Kristjansen, B.E. Johnson, H. Ueoka, H. Wagner, and J. Aisner, *Prophylactic cranial irradiation for patients with small-cell lung cancer in complete remission.* New England Journal of Medicine, 1999. **341**(7): p. 476-484.

50. Fitzgerald, D.P., D. Palmieri, E. Hua, E. Hargrave, J.M. Herring, Y. Qian, E. Vega-Valle, R.J. Weil, A.M. Stark, A.O. Vortmeyer, and P.S. Steeg, *Reactive glia are recruited by highly proliferative brain metastases of breast cancer and promote tumor cell colonization.* Clinical and Experimental Metastasis, 2008. **25**(7): p. 799-810.

51. Seike, T., K. Fujita, Y. Yamakawa, M.A. Kido, S. Takiguchi, N. Teramoto, H. Iguchi, and M. Noda, *Interaction between lung cancer cells and astrocytes via specific inflammatory cytokines in the microenvironment of brain metastasis.* Clinical and Experimental Metastasis, 2011. **28**(1): p. 13-25.

52. Lin, Q., K. Balasubramanian, D. Fan, S. Kim, L. Guo, H. Wang, M. Bar-Eli, K.D. Aldape, and I.J. Fidler, *Reactive astrocytes protect melanoma cells from chemotherapy by sequestering intracellular calcium through gap junction communication channels.* Neoplasia, 2010. **12**(9): p. 748-754.

53. Pukrop, T., F. Dehghani, H.N. Chuang, R. Lohaus, K. Bayanga, S. Heermann, T. Regen, D. Van Rossum, F. Klemm, M. Schulz, L. Siam, A. Hoffmann, L. Trümper, C. Stadelmann, I. Bechmann, U.K. Hanisch, and C. Binder, *Microglia promote colonization of brain tissue by breast cancer cells in a Wnt-dependent way.* GLIA, 2010. **58**(12): p. 1477-1489.

54. Fidler, I.J., *The role of the organ microenvironment in brain metastasis.* Seminars in Cancer Biology, 2011. **21**(2): p. 107-112.

55. Kim, S.J., J.S. Kim, E.S. Park, J.S. Lee, Q. Lin, R.R. Langley, M. Maya, J. He, S.W. Kim, Z. Weihua, K. Balasubramanian, D. Fan, G.B. Mills, M.C. Hung, and I.J. Fidler, *Astrocytes upregulate survival genes in tumor cells and induce protection from chemotherapy.* Neoplasia, 2011. **13**(3): p. 286-298.

56. Lockman, P.R., R.K. Mittapalli, K.S. Taskar, V. Rudraraju, B. Gril, K.A. Bohn, C.E. Adkins, A. Roberts, H.R. Thorsheim, J.A. Gaasch, S. Huang, D. Palmieri, P.S. Steeg, and Q.R. Smith, *Heterogeneous blood-tumor barrier permeability determines drug efficacy in experimental brain metastases of breast cancer.* Clinical Cancer Research, 2010. **16**(23): p. 5664-5678.

57. Yano, S., H. Shinohara, R.S. Herbst, H. Kuniyasu, C.D. Bucana, L.M. Ellis, D.W. Davis, D.J. McConkey, and I.J. Fidler, *Expression of vascular endothelial growth factor is necessary but not sufficient for production and growth of brain metastasis.* Cancer Research, 2000. **60**(17): p. 4959-4967.

58. DiStefano, A., H.Y. Yap, G.N. Hortobagyi, and G.R. Blumenschein, *The natural history of breast cancer patients with brain metastases.* Cancer, 1979. **44**(5): p. 1913-1918.

59. Issa, C.M., R. Semrau, R. Kath, and K. Höffken, *Isolated brain metastases as the sole manifestation of a late relapse in breast cancer.* Journal of Cancer Research and Clinical Oncology, 2002. **128**(1): p. 61-63.

60. Niwińska, A., M. Murawska, and K. Pogoda, *Breast cancer brain metastases: Differences in survival depending on biological subtype, RPA RTOG prognostic class and systemic treatment after whole-brain radiotherapy (WBRT).* Annals of Oncology, 2009. **21**(5): p. 942-948.

61. Berghoff, A., Z. Bago-Horvath, C. De Vries, P. Dubsky, U. Pluschnig, M. Rudas, A. Rottenfusser, M. Knauer, H. Eiter, F. Fitzal, K. Dieckmann, R.M. Mader, M. Gnant, C.C. Zielinski, G.G. Steger, M. Preusser, and R. Bartsch, *Brain metastases free survival differs between breast cancer subtypes.* British Journal of Cancer, 2012. **106**(3): p. 440-446.

62. Kim, H.J., S.A. Im, B. Keam, Y.J. Kim, S.W. Han, T.M. Kim, D.Y. Oh, J.H. Kim, S.H. Lee, E.K. Chie, W. Han, D.W. Kim, T.Y. Kim, D.Y. Noh, D.S. Heo, I.A. Park, Y.J. Bang, and S.W. Ha, *Clinical outcome of central nervous system metastases from breast cancer: Differences in survival depending on systemic treatment*. Journal of Neuro-Oncology, 2012. **106**(2): p. 303-313.

63. Bendell, J.C., S.M. Domchek, H.J. Burstein, L. Harris, J. Younger, I. Kuter, C. Bunnell, M. Rue, R. Gelman, and E. Winer, *Central nervous system metastases in women who receive trastuzumab-based therapy for metastatic breast carcinoma.* Cancer, 2003. **97**(12): p. 2972-2977.

64. Patanaphan, V., O.M. Salazar, and R. Risco, *Breast cancer: Metastatic patterns and their prognosis.* Southern Medical Journal, 1988. **81**(9): p. 1109-1112.

65. Tsukada, Y., A. Fouad, J.W. Pickren, and W.W. Lane, *Central nervous system metastasis from breast carcinoma. Autopsy study.* Cancer, 1983. **52**(12): p. 2349-2354.

66. Lee, Y.T.N., *Breast carcinoma: Pattern of metastasis at autopsy.* Journal of Surgical Oncology, 1983. **23**(3): p. 175-180.

67. Clayton, A.J., S. Danson, S. Jolly, W.D.J. Ryder, P.A. Burt, A.L. Stewart, P.M. Wilkinson, R.S. Welch, B. Magee, G. Wilson, A. Howell, and A.M. Wardley, *Incidence of cerebral metastases in patients treated with trastuzumab for metastatic breast cancer.* British Journal of Cancer, 2004. **91**(4): p. 639-643.

68. Miller, K.D., T. Weathers, L.G. Haney, R. Timmerman, M. Dickler, J. Shen, and G.W. Sledge Jr, *Occult central nervous system involvement in patients with metastatic breast cancer: Prevalence, predictive factors and impact on overall survival.* Annals of Oncology, 2003. **14**(7): p. 1072-1077.

69. Bos, P.D., X.H.F. Zhang, C. Nadal, W. Shu, R.R. Gomis, D.X. Nguyen, A.J. Minn, M.J. Van De Vijver, W.L. Gerald, J.A. Foekens, and J. Massagué, *Genes that mediate breast cancer metastasis to the brain.* Nature, 2009. **459**(7249): p. 1005-1009.

70. Palmieri, D., J.L. Bronder, J.M. Herring, T. Yoneda, R.J. Weil, A.M. Stark, R. Kurek, E. Vega-Valle, L. Feigenbaum, D. Halverson, A.O. Vortmeyer, S.M. Steinberg, K. Aldape, and P.S. Steeg, *Her-2 overexpression increases the metastatic outgrowth of breast cancer cells in the brain.* Cancer Research, 2007. **67**(9): p. 4190-4198.

71. Debeb, B., L. Lacerda, S. Anfossi, P. Diagaradjane, K. Chu, L. Huo, C. Wei, R. Larson, A. Wolfe, W. Xu, D. Smith, L. Li, C. Ivan, X. Zhang, G. Calin, S. Krishnamurthy, N. Ueno, T. Buchholz, J. Reuben, and W. Woodward, *The microRNA miR-141 is a regulator of breast cancer metastases to the brain.* Journal of the National Cancer Institute, 2015.

72. Lin, N.U., *Targeted therapies in brain metastases.* Current Treatment Options in Neurology, 2014. **16**(1).

73. Noordijk, E.M., C.J. Vecht, H. Haaxma-Reiche, G.W. Padberg, J.H.C. Voormolen, F.H. Hoekstra, J.T.J. Tans, N. Lambooij, J.A.L. Metsaars, A.R. Wattendorff, R. Brand, and J. Hermans, *The choice of treatment of single brain metastasis should be based on extracranial tumor activity and age.* International Journal of Radiation Oncology Biology Physics, 1994. **29**(4): p. 711-717.

74. Andrews, D.W., C.B. Scott, P.W. Sperduto, A.E. Flanders, L.E. Gaspar, M.C. Schell, M. Werner-Wasik, W. Demas, J. Ryu, J.P. Bahary, L. Souhami, M. Rotman, M.P. Mehta,

and W.J. Curran Jr, *Whole brain radiation therapy with or without stereotactic radiosurgery boost for patients with one to three brain metastases: Phase III results of the RTOG 9508 randomised trial.* Lancet, 2004. **363**(9422): p. 1665-1672.

75. Patil, C.G., K. Pricola, J.M. Sarmiento, S.K. Garg, A. Bryant, and K.L. Black, *Whole brain radiation therapy (WBRT) alone versus WBRT and radiosurgery for the treatment of brain metastases.* Cochrane database of systematic reviews (Online), 2012. **9**.

76. Tsao, M.N., D. Rades, A. Wirth, S.S. Lo, B.L. Danielson, L.E. Gaspar, P.W. Sperduto, M.A. Vogelbaum, J.D. Radawski, J.Z. Wang, M.T. Gillin, N. Mohideen, C.A. Hahn, and E.L. Chang, *Radiotherapeutic and surgical management for newly diagnosed brain metastasis(es): An American Society for Radiation Oncology evidence-based guideline.* Practical Radiation Oncology, 2012. **2**(3): p. 210-225.

77. Aoyama, H., H. Shirato, M. Tago, K. Nakagawa, T. Toyoda, K. Hatano, M. Kenjyo, N. Oya, S. Hirota, H. Shioura, E. Kunieda, T. Inomata, K. Hayakawa, N. Katoh, and G. Kobashi, *Stereotactic radiosurgery plus whole-brain radiation therapy vs stereotactic radiosurgery alone for treatment of brain metastases: A randomized controlled trial.* Journal of the American Medical Association, 2006. **295**(21): p. 2483-2491.

78. Kocher, M., R. Soffietti, U. Abacioglu, S. Villà, F. Fauchon, B.G. Baumert, L. Fariselli, T. Tzuk-Shina, R.D. Kortmann, C. Carrie, M. Ben Hassel, M. Kouri, E. Valeinis, D. Van Den Berge, S. Collette, L. Collette, and R.P. Mueller, *Adjuvant whole-brain radiotherapy versus observation after radiosurgery or surgical resection of one to three cerebral metastases: Results of the EORTC 22952-26001 study.* Journal of Clinical Oncology, 2011. **29**(2): p. 134-141.

79. Pajouhesh, H. and G.R. Lenz, *Medicinal chemical properties of successful central nervous system drugs.* NeuroRx, 2005. **2**(4): p. 541-553.

80. Szakács, G., J.K. Paterson, J.A. Ludwig, C. Booth-Genthe, and M.M. Gottesman, *Targeting multidrug resistance in cancer.* Nature Reviews Drug Discovery, 2006. **5**(3): p. 219-234.

81. Noguchi, K., K. Katayama, J. Mitsuhashi, and Y. Sugimoto, *Functions of the breast cancer resistance protein (BCRP/ABCG2) in chemotherapy.* Advanced Drug Delivery Reviews, 2009. **61**(1): p. 26-33.

82. Deeken, J.F. and W. Löscher, *The blood-brain barrier and cancer: Transporters, treatment, and trojan horses.* Clinical Cancer Research, 2007. **13**(6): p. 1663-1674.

83. Bria, E., F. Cuppone, M. Fornier, C. Nisticò, P. Carlini, M. Milella, I. Sperduti, E. Terzoli, F. Cognetti, and D. Giannarelli, *Cardiotoxicity and incidence of brain metastases after adjuvant trastuzumab for early breast cancer: The dark side of the moon? A meta-analysis of the randomized trials.* Breast Cancer Research and Treatment, 2008. **109**(2): p. 231-239.

84. Taskar, K.S., V. Rudraraju, R.K. Mittapalli, R. Samala, H.R. Thorsheim, J. Lockman, B. Gril, E. Hua, D. Palmieri, J.W. Polli, S. Castellino, S.D. Rubin, P.R. Lockman, P.S. Steeg, and Q.R. Smith, *Lapatinib distribution in HER2 overexpressing experimental brain metastases of breast cancer.* Pharmaceutical Research, 2012. **29**(3): p. 770-781.

85. Bovi, J.A. and J. White, *Radiation therapy in the prevention of brain metastases.* Current Oncology Reports, 2012. **14**(1): p. 55-62.

86. Jabbour, E., D. Thomas, J. Cortes, H.M. Kantarjian, and S. O'Brien, *Central nervous system prophylaxis in adults with acute lymphoblastic leukemia: Current and emerging therapies.* Cancer, 2010. **116**(10): p. 2290-2300.

87. Bleyer, W.A. and D.G. Poplack, *Prophylaxis and treatment of leukemia in the central nervous system and other sanctuaries.* Seminars in Oncology, 1985. **12**(2): p. 131-148.

88. Ritchey, A.K., B.H. Pollock, S.J. Lauer, Y. Andejeski, and G.R. Buchanan, *Improved survival of children with isolated CNS relapse of acute lymphoblastic leukemia: A pediatric oncology group study.* Journal of Clinical Oncology, 1999. **17**(12): p. 3745-3752.

89. Aur, R.J.A., H.O. Hustu, and M.S. Verzosa, *Comparison of two methods of preventing central nervous system leukemia.* Blood, 1973. **42**(3): p. 349-357.

90. Pui, C.H., C.G. Mullighan, W.E. Evans, and M.V. Relling, *Pediatric acute lymphoblastic leukemia: Where are we going and how do we get there?* Blood, 2012. **120**(6): p. 1165-1174.

91. Pui, C.H., C. Cheng, W. Leung, S.N. Rai, G.K. Rivera, J.T. Sandlund, R.C. Ribeiro, M.V. Relling, L.E. Kun, W.E. Evans, and M.M. Hudson, *Extended follow-up of long-term survivors of childhood acute lymphoblastic leukemia.* New England Journal of Medicine, 2003. **349**(7): p. 640-649.

92. Pui, C.H., D. Campana, D. Pei, W.P. Bowman, J.T. Sandlund, S.C. Kaste, R.C. Ribeiro, J.E. Rubnitz, S.C. Raimondi, M. Onciu, E. Coustan-Smith, L.E. Kun, S. Jeha, C. Cheng, S.C. Howard, V. Simmons, A. Bayles, M.L. Metzger, J.M. Boyett, W. Leung, R. Handgretinger, J.R. Downing, W.E. Evans, and M.V. Relling, *Treating childhood acute lymphoblastic leukemia without cranial irradiation.* New England Journal of Medicine, 2009. **360**(26): p. 2730-2741.

93. Veerman, A.J., W.A. Kamps, H. van den Berg, E. van den Berg, J.P. Bökkerink, M.C. Bruin, M.M. van den Heuvel-Eibrink, C.M. Korbijn, E.T. Korthof, K. van der Pal, T. Stijnen, M.H. van Weel Sipman, J.F. van Weerden, E.R. van Wering, and A. van der Does-van den Berg, *Dexamethasone-based therapy for childhood acute lymphoblastic leukaemia: results of the prospective Dutch Childhood Oncology Group (DCOG) protocol ALL-9 (1997-2004).* The Lancet Oncology, 2009. **10**(10): p. 957-966.

94. Govindan, R., N. Page, D. Morgensztern, W. Read, R. Tierney, A. Vlahiotis, E.L. Spitznagel, and J. Piccirillo, *Changing epidemiology of small-cell lung cancer in the United States over the last 30 years: Analysis of the surveillance, epidemiologic, and end results database.* Journal of Clinical Oncology, 2006. **24**(28): p. 4539-4544.

95. Arriagada, R., T. Le Chevalier, F. Borie, A. Rivière, P. Chomy, I. Monnet, A. Tardivon, F. Viader, M. Tarayre, and S. Benhamou, *Prophylactic cranial irradiation for patients with small-cell lung cancer in complete remission.* Journal of the National Cancer Institute, 1995. **87**(3): p. 183-190.

96. Paumier, A., X. Cuenca, and C. Le Péchoux, *Prophylactic cranial irradiation in lung cancer.* Cancer Treatment Reviews, 2011. **37**(4): p. 261-265.

97. Slotman, B., C. Faivre-Finn, G. Kramer, E. Rankin, M. Snee, M. Hatton, P. Postmus, L. Collette, E. Musat, and S. Senan, *Prophylactic cranial irradiation in extensive small-cell lung cancer.* New England Journal of Medicine, 2007. **357**(7): p. 664-672.

98. Greenspoon, J.N., W.K. Evans, W. Cai, and J.R. Wright, *Selecting patients with extensive-stage small cell lung cancer for prophylactic cranial irradiation by predicting brain metastases.* Journal of Thoracic Oncology, 2011. **6**(4): p. 808-812.

99. Ramalingam, S. and C. Belani, *Systemic chemotherapy for advanced non-small cell lung cancer: Recent advances and future directions.* Oncologist, 2008. **13**(SUPPL. 1): p. 5-13.

100. Law, A., D.D. Karp, T. Dipetrillo, and B.T. Daly, *Emergence of increased cerebral metastasis after high-dose preoperative radiotherapy with chemotherapy in patients with locally advanced nonsmall cell lung carcinoma.* Cancer, 2001. **92**(1): p. 160-164.

101. Cox, J.D., K. Stanley, Z. Petrovich, C. Paig, and R. Yesner, *Cranial irradiation in cancer of the lung of all cell types.* Journal of the American Medical Association, 1981. **245**(5): p. 469-472.

102. Umsawasdi, T., M. Valdivieso, T.T. Chen, H.T. Barkley Jr, D.J. Booser, D.F. Chiuten, H.M. Dhingra, W.K. Murphy, C.L. Dixon, P. Farha, G. Spitzer, and D.T. Carr, *Role of elective brain irradiation during combined chemoradiotherapy for limited disease non-small cell lung cancer.* Journal of Neuro-Oncology, 1984. **2**(3): p. 253-259.

103. Miller, T.P., J.J. Crowley, and J. Mira, *A randomized trial of chemotherapy and radiotherapy for stage III non-small cell lung cancer.* Cancer Therapeutics, 1998. **1**: p. 229-236.

104. Russell, A.H., T.E. Pajak, H.M. Selim, J.C. Paradelo, K. Murray, P. Bansal, J.D. Cooper, S. Silverman, and J.A. Clement, *Prophylactic cranial irradiation for lung cancer patients at high risk for development of cerebral metastasis: Results of a prospective randomized trial conducted by the Radiation Therapy Oncology Group.* International Journal of Radiation Oncology Biology Physics, 1991. **21**(3): p. 637-643.

105. Gore, E.M., K. Bae, and S. Wong, *A phase III comparison of prophylactic cranial irradiation versus observation in patients with locally advanced non-small cell lung cancer: Initial analysis of Radiation Therapy Oncology Group 0214.* J Clin Oncol, 2009. **27**(15 S).

106. Pöttgen, C., W. Eberhardt, A. Grannass, S. Korfee, G. Stüben, H. Teschler, G. Stamatis, H. Wagner, B. Passlick, V. Petersen, V. Budach, H. Wilhelm, I. Wanke, H. Hirche, H.J. Wilke, and M. Stuschke, *Prophylactic Cranial Irradiation in Operable Stage IIIA Non-Small-Cell Lung Cancer Treated with Neoadjuvant Chemoradiotherapy: Results from a German Multicenter Randomized Trial.* Journal of Clinical Oncology, 2007. **25**(31): p. 4987-4992.

107. Graesslin, O., B.S. Abdulkarim, C. Coutant, F. Huguet, Z. Gabos, L. Hsu, O. Marpeau, S. Uzan, L. Pusztai, E.A. Strom, G.N. Hortobagyi, R. Rouzier, and N.K. Ibrahim,

Nomogram to predict subsequent brain metastasis in patients with metastatic breast cancer. Journal of Clinical Oncology, 2010. **28**(12): p. 2032-2037.

108. Huang, F., M. Alrefae, A. Langleben, and D. Roberge, *Prophylactic Cranial Irradiation in Advanced Breast Cancer: A Case for Caution*. International Journal of Radiation Oncology Biology Physics, 2009. **73**(3): p. 752-758.

109. Niwińska, A., M. Tacikowska, and M. Murawska, *The Effect of Early Detection of Occult Brain Metastases in HER2-Positive Breast Cancer Patients on Survival and Cause of Death*. International Journal of Radiation Oncology Biology Physics, 2010. **77**(4): p. 1134-1139.

110. Hall, E.J. and A.J. Giaccia, *Radiobiology for the Radiologist*. 6th ed. 2005.

111. Wright, J. and A. Wolfson, *Prophylactic Cranial Irradiation: Do Benefits Outweigh Neurocognitive Impact?* Current Problems in Cancer, 2012. **36**(3): p. 106-116.

112. Johnson, B.E., B. Becker, W.B. Goff Ii, N. Petronas, M.A. Krehbiel, R.W. Makuch, G. McKenna, E. Glatstein, and D.C. Ihde, *Neurologic, neuropsychologic, and computed cranial tomography scan abnormalities in 2- to 10-year survivors of small-cell lung cancer*. Journal of Clinical Oncology, 1985. **3**(12): p. 1659-1667.

113. Le Péchoux, C., A. Dunant, S. Senan, A. Wolfson, E. Quoix, C. Faivre-Finn, T. Ciuleanu, R. Arriagada, R. Jones, R. Wanders, D. Lerouge, and A. Laplanche, *Standard-dose versus higher-dose prophylactic cranial irradiation (PCI) in patients with limited-stage small-cell lung cancer in complete remission after chemotherapy and thoracic radiotherapy (PCI 99-01, EORTC 22003-08004, RTOG 0212, and IFCT 99-01): a randomised clinical trial*. The Lancet Oncology, 2009. **10**(5): p. 467-474.

114. Verhaegen, F., P. Granton, and E. Tryggestad, *Small animal radiotherapy research platforms*. Physics in Medicine and Biology, 2011. **56**(12): p. R55-R83.

115. Barcellos-Hoff, M.H. and S.A. Ravani, *Irradiated mammary gland stroma promotes the expression of tumorigenic potential by unirradiated epithelial cells.* Cancer Research, 2000. **60**(5): p. 1254-1260.

116. Klopp, A.H., L. Lacerda, A. Gupta, B.G. Debeb, T. Solley, L. Li, E. Spaeth, W. Xu, X. Zhang, M.T. Lewis, J.M. Reuben, S. Krishnamurthy, M. Ferrari, R. Gaspar, T.A. Buchholz, M. Cristofanilli, F. Marini, M. Andreeff, and W.A. Woodward, *Mesenchymal stem cells promote mammosphere formation and decrease E-Cadherin in normal and malignant breast cells.* PLoS ONE, 2010. **5**(8).

117. Milas, L., N. Hunter, and L.J. Peters, *The tumor bed effect: Dependence of tumor take, growth rate, and metastasis on the time interval between irradiation and tumor cell transplantation.* International Journal of Radiation Oncology, Biology, Physics, 1987. **13**(3): p. 379-383.

118. Kendal, W.S., *Empirically-based estimates for the burden of subclinical metastases.* International Journal of Radiation Biology, 2007. **83**(6): p. 383-393.

119. Liotta, L.A., J. Kleinerman, and G.M. Saidel, *The significance of hematogenous tumor cell clumps in the metastatic process.* Cancer Research, 1976. **36**(3): p. 889-894.

120. Suwinski, R., S.P. Lee, and H.R. Withers, *Dose-response relationship for prophylactic cranial irradiation in small cell lung cancer.* International Journal of Radiation Oncology Biology Physics, 1998. **40**(4): p. 797-806.

121. Scott, J.G., P. Gerlee, D. Basanta, A.G. Fletcher, P.K. Maini, and A.R.A. Anderson, *Mathematical Modeling of the Metastatic Process*, in *Experimental Metastasis: Modeling and Analysis*. 2013.

122. Kreso, A. and J.E. Dick, *Evolution of the cancer stem cell model.* Cell Stem Cell, 2014. **14**(3): p. 275-291.

123. Andarawewa, K.L., A.C. Erickson, W.S. Chou, S.V. Costes, P. Gascard, J.D. Mott, M.J. Bissell, and M.H. Barcellos-Hoff, *Ionizing radiation predisposes nonmalignant human mammary epithelial cells to undergo transforming growth factor β-induced epithelial to mesenchymal transition.* Cancer Research, 2007. **67**(18): p. 8662-8670.

124. Gondi, V., S.L. Pugh, W.A. Tome, C. Caine, B. Corn, A. Kanner, H. Rowley, V. Kundapur, A. DeNittis, J.N. Greenspoon, A.A. Konski, G.S. Bauman, S. Shah, W. Shi, M. Wendland, L. Kachnic, and M.P. Mehta, *Preservation of memory with conformal avoidance of the hippocampal neural stem-cell compartment during whole-brain radiotherapy for brain metastases (RTOG 0933): A phase II multi-institutional trial.* Journal of Clinical Oncology, 2014. **32**(34): p. 3810-3816.

125. Brown, P.D., S. Pugh, N.N. Laack, J.S. Wefel, D. Khuntia, C. Meyers, A. Choucair, S. Fox, J.H. Suh, D. Roberge, V. Kavadi, S.M. Bentzen, M.P. Mehta, and D. Watkins-Bruner, *Memantine for the prevention of cognitive dysfunction in patients receiving whole-brain radiotherapy: A randomized, double-blind, placebo-controlled trial.* Neuro-Oncology, 2013. **15**(10): p. 1429-1437.

126. Sahgal, A., H. Aoyama, M. Kocher, B. Neupane, S. Collette, M. Tago, P. Shaw, J. Beyene, and E.L. Chang, *Phase 3 trials of stereotactic radiosurgery with or without whole-brain radiation therapy for 1 to 4 brain metastases: Individual patient data meta-analysis.* International Journal of Radiation Oncology Biology Physics, 2015. **91**(4): p. 710-717.

APPENDIX I: DIFFERENTIAL EFFECT OF PHOSPHORYLATION-DEFECTIVE SURVIVIN ON RADIATION RESPONSE IN ESTROGEN RECEPTOR-POSITIVE AND -NEGATIVE BREAST CANCER.

This appendix is based upon:

Debeb BG, Smith DL, Li L, Larson R, Xu W, Woodward WA (2015) Differential Effect of Phosphorylation-Defective Survivin on Radiation Response in Estrogen Receptor-Positive and -Negative Breast Cancer. *PLoS ONE* 10(3): e0120719. doi:10.1371/journal.pone.0120719

PLOS | ONE

RESEARCH ARTICLE

Differential Effect of Phosphorylation-Defective Survivin on Radiation Response in Estrogen Receptor-Positive and -Negative Breast Cancer

Bisrat G. Debeb[☯], **Daniel L. Smith**[☯], **Li Li, Richard Larson, Wei Xu, Wendy A. Woodward***

Department of Radiation Oncology, University of Texas M.D. Anderson Cancer Center, Houston, TX, United States of America

☯ These authors contributed equally to this work.
* wwoodward@mdanderson.org

Citation: Debeb BG, Smith DL, Li L, Larson R, Xu W, Woodward WA (2015) Differential Effect of Phosphorylation-Defective Survivin on Radiation Response in Estrogen Receptor-Positive and -Negative Breast Cancer. PLoS ONE 10(3): e0120719. doi:10.1371/journal.pone.0120719

Received: August 4, 2014

Accepted: January 26, 2015

Published: March 12, 2015

Data Availability Statement: All relevant data are within the paper.

Funding: This work was supported by the National Institutes of Health R01CA138239-01; and The State of Texas Grant for Rare and Aggressive Breast Cancer Research Program. Bisrat G. Debeb and Wei Xu are recipients of Susan G. Komen for the cure® Postdoctoral Fellowships, KG101478 and KG111387, respectively. Daniel L. Smith is a recipient of a fellowship from the M.D. Anderson Cancer Center, Center for Stem Cell and Developmental Biology and the Estate of CW Johnson. The funders had no role in study design, data collection and analysis, decision to publish, or preparation of the manuscript.

Abstract

Survivin is a key member of the inhibitor of apoptosis protein family, and is considered a promising therapeutic target due to its universal overexpression in cancers. Survivin is implicated in cellular radiation response through its role in apoptosis, cell division, and DNA damage response. In the present study, analysis of publically available data sets showed that survivin gene expression increased with breast cancer stage ($p < 0.00001$) and was significantly higher in estrogen receptor-negative cancers as compared to estrogen receptor-positive cancers ($p = 9e\text{-}46$). However, survivin was prognostic in estrogen receptor-positive tumors ($p = 0.03$) but not in estrogen receptor-negative tumors ($p = 0.28$). We assessed the effect of a survivin dominant-negative mutant on colony-formation (2D) and mammosphere-formation (3D) efficiency, and radiation response in the estrogen receptor-positive MCF7 and estrogen receptor-negative SUM149 breast cancer cell lines. The colony-formation efficiency was significantly lower in the dominant-negative survivin-transduced cells versus control MCF7 cells (0.42 vs. 0.58, $p < 0.01$), but it was significantly higher in dominant-negative population versus control-transduced SUM149 cells (0.29 vs. 0.20, $p < 0.01$). A similar, non-significant, trend in mammosphere-formation efficiency was observed. We compared the radiosensitivity of cells stably expressing dominant-negative survivin with their controls in both cell lines under 2D and 3D culture conditions following exposure to increasing doses of radiation. We found that the dominant-negative populations were radioprotective in MCF7 cells but radiosensitive in SUM149 cells compared to the control-transduced population; further, Taxol was synergistic with the survivin mutant in SUM149 but not MCF7. Our data suggests that survivin modulation influences radiation response differently in estrogen receptor-positive and estrogen receptor-negative breast cancer subtypes, warranting further investigation.

Competing Interests: The authors have declared that no competing interests exist.

Introduction

Survivin is the smallest member of the inhibitor of apoptosis protein (IAP) family at 16.5 kDa and is encoded by *BIRC5* (baculoviral inhibitor of apoptosis repeat-containing protein-5) [1]. It is implicated in the regulation of several cellular networks, and is prominent for its universal over-expression in human cancers. Survivin harbors many phosphorylation sites and interacts with a variety of different proteins, enabling its diverse functions that include its involvement in cellular division, apoptosis, intracellular signaling, and adaptation to unfavorable environments [2].

Survivin is clinically relevant in breast cancer and may be predictive of response to therapy. One of the seminal studies found that survivin is expressed in approximately 70% of breast carcinomas compared to no expression in adjacent normal tissue, and that survivin expression is a significant prognostic parameter of worse outcome in breast cancer patients [3]. Further, Kennedy and colleagues [4] found that nuclear survivin expression is prognostic of favorable outcome for breast cancer patients. A more recent study reported that survivin expression could function as a predictive biomarker of complete pathologic response to neoadjuvant chemotherapy in patients with stage II or stage III breast cancer [5]. Interestingly, survivin is a component of the 21-gene recurrence score validated in ER+ node-negative patients as a prognostic and predictive marker of recurrence and response to chemotherapy [6]. More recently, retrospective analysis of clinical trials from which these studies were validated revealed the recurrence score also predicts for risk of local recurrence among patients treated with lumpectomy and radiation [7].

Survivin, due in part to its role in apoptosis, and cell division, has long been proposed as a predictive factor for response to radiation therapy treatments, and anti-survivin treatments have been explored as possible radiosensitizers in preclinical studies [8]. More recently, it has been reported that survivin also plays a role in DNA double-strand break repair [9], adding another mechanism by which survivin may increase cellular radio-resistance. Several preclinical studies have shown that survivin is associated with radiation resistance in pancreatic cancer [10], colorectal cancer [11], melanoma [12], lung cancer [13], glioblastoma [14], and epidermoid carcinoma [15]. Further, several of these and other preclinical studies [16] [17] [18] [19] tested the efficacy of anti-survivin treatments—including the use of antisense oligonucleotides, siRNA, ribozymes, dominant-negative mutants, and small-molecule inhibitors—in combination with radiation. In each case, the combination treatment was more effective than radiation alone, and increased apoptosis as well as decreased cell survival and growth were observed in the combined regimen. In murine mammary epithelial cells, Woodward and colleagues [20] [21] reported that survivin is selectively upregulated following irradiation in stem cell-enriched populations; however, no group has specifically examined if survivin is a radiation resistance factor in breast cancer cells.

In the present study, we examined public gene expression datasets and report that although survivin expression is higher in estrogen receptor-negative (ER–) than estrogen-receptor-positive (ER+) breast cancer, it is only prognostic in ER+ breast cancer. Based on the differential impact that survivin expression has on overall survival in ER+ and ER– breast cancer patients, we hypothesized that survivin perturbation would exert different effects on an ER+ versus an ER– cell line. We evaluated how a phosphorylation-defective mutant of survivin (survivin-DN) affects apoptosis, self-renewal capacity, and radiation response in ER+ and ER– breast cancer cell lines.

Materials and Methods

Data Mining

BIRC5 expression in different breast cancer patient cohorts was extracted from two public databases, Oncomine [22] and Gene Expression-Based Outcome for Breast Cancer Online

(GOBO) [23]. In Oncomine, data was specifically extracted from The Cancer Genome Atlas, Bittner (unpublished), and Curtis [24] breast datasets. *BIRC5* expression was then stratified based on three characteristics: presence of invasive carcinoma, stage, and receptor status.

Breast cancer patient survival information (all breast cancer patients, ER+ patients, or ER– patients) was evaluated in the Kaplan-Meier Plotter (K-M Plot) [25] and GOBO public databases, where patients were stratified into groups of high and low *BIRC5* expression using a database-selected "cutoff" point.

Cell culture

The estrogen receptor-positive breast cancer cell line MCF7 was acquired from ATCC and cultured in Modified Eagle Medium (MEM) supplemented with 10% fetal bovine serum, 0.1 mM nonessential amino acids, 1 mM sodium pyruvate, 1 μg/mL hydrocortisone, 5 μg/mL insulin, and 1% antibiotic-antimycotic. The triple-negative, inflammatory breast cancer cell line SUM149 was obtained from Asterand (Detroit, MI, USA) and was cultured in Ham's F-12 media supplemented with 10% fetal bovine serum (FBS), 1 μg/mL hydrocortisone, 5 μg/mL insulin, and 1% antibiotic-antimycotic. Cell lines were maintained at 37°C in a humidified atmosphere (5% carbon dioxide).

Construct

In order to generate a survivin dominant-negative mutant, an adenoviral construct with a survivin-T34A point mutation, kindly provided by Dr. Altieri and colleagues [26], was acquired. The green fluorescent protein from the pFUGW backbone [27] was removed, after which the survivin dominant-negative construct (survivin-DN) was cloned into the HindIII-BamHI site. pFUGW was used as a negative control throughout the study.

Western blot

Western blots were run to validate induction of the survivin-DN construct and to evaluate caspase cleavage as a marker for apoptosis in both MCF7 and SUM149 cell lines. The lysate was collected with 1X RIPA lysis buffer (diluted from 10X RIPA from Cell Signaling, Danvers, MA) containing 1 uM phenylmethyl sulfonyl fluoride and was transferred to microcentrifuge tubes. The samples were rotated for one hour at 4°C and centrifuged at 10,000 *g* for 10 minutes. Fifty-μg aliquots of the protein lysate supernatants were electrophoresed on 4–20% gradient sodium dodecyl sulfate-polyacyrlamide gels (Invitrogen, Life Technologies, Carlsbad, CA) and transferred to polyvinylidene fluoride membranes (Bio-Rad Laboratories, Hercules, CA). The membranes were incubated in 5% non-fat milk for one hour at room temperature and then incubated at 4°C for 16 hours with the primary antibody: rabbit anti-survivin mAb (Cell Signaling #2808, Danvers, MA), rabbit anti-caspase 3 mAb (Cell Signaling #9662) and rabbit anti-cleaved capsase 3 mAb (Cell Signaling #9664). The membranes were then washed three times and incubated with the corresponding secondary antibody conjugated with horseradish peroxidase (Santa Cruz, CA) in 5% non-fat milk at room temperature. Next, the membranes were washed three times and immunoreactivity was detected by enhanced chemiluminescence. For all western blots, mouse anti-β-actin mAb (Sigma-Aldrich #A5316, St. Louis, MO) was used as a loading control.

Cell cycle assay

Cell cycle analyses were performed as described previously [28]. Briefly, cells were enzymatically dissociated and centrifuged for 5 minutes at 4°C. After washing once with PBS, cells were

fixed with 70% cold ethanol and were left overnight at 4°C. Cells were then centrifuged and re-suspended in a Propidium Iodide solution (50 μg/mL Propidium Iodide). RNase (20 μg/mL) was added and samples incubated at 37°C for 1 hour. Samples were then immediately analyzed for DNA content using FACSAria II flow cytometer from Becton-Dickinson (BD Biosciences, San Jose, CA), and the distribution of cells across cell phases was analyzed using FlowJo software (Treestar, Ashland, OR).

Mammosphere cultures

Cancer stem/progenitor cells can be enriched by propagating cells in serum-free, growth factor-enriched conditions—called mammospheres (3D) cultures in the case of breast cancer [29]. To generate mammospheres from MCF7 and SUM149 cells, 2 x 10^4 cells/mL were cultured in serum-free MEM supplemented with 20 ng/mL basic fibroblast growth factor (Invitrogen), 20 ng/mL epidermal growth factor (Invitrogen), and B27 (Invitrogen) in six-well, ultra-low attachment plates.

Clonogenic assays

The radiosensitivity of the survivin-DN construct in both monolayer (2D) and mammosphere (3D) cultures was evaluated as described previously [30]. For both 2D and 3D radiosensitivity assays, single cells from dissociated MCF7 and SUM149 monolayer cultures were seeded into 6-well tissue culture plates. The 6-well plates containing seeded cells were irradiated with γ-irradiation (0, 2, 4, or 6 Gy) four hours after plating with a ^{137}Cs source (Shepherd Irradiator, J. L. Shepherd and Associates, San Fernando, CA). For 2D monolayer culture, the plates were incubated for 14 days, after which the colonies were stained with crystal violet and then counted manually. For 3D mammosphere cultures, the cells were incubated in mammosphere media for 7 days, and then the spheres were stained with MTT to improve visualization.

In a separate set of experiments, mammosphere cultures were incubated with either 10 nM Taxol (Cayman Chemical, Ann Arbor, MI) or 1 μM GSI (CalBiochem, Darmstadt, Germany). Spheres with a minimal size of 50 μm were counted using a GelCount colony counter (Oxford Optronix, Oxford, UK). Linear-quadratic survival curves were generated using SigmaPlot, version 8.0 (Systat Software, San Jose, CA).

Tissue Staining

Primary MCF7 and SUM149 tumor xenograft tissue was used for immunohistochemical staining to detect survivin and phospho (pT34)-survivin with the rabbit anti-survivin mAb (Cell Signaling #2808, Danvers, MA) and rabbit anti-pT34-survivin (Santa Cruz, sc-23758) antibodies, respectively.

Statistical Analysis

Statistical analyses were performed in GraphPad Prism version 6. Two-tailed Student's *t* test was used to evaluate colony- and mammosphere-formation efficiency and to compare group means in the clonogenic assay, with $p < 0.05$ considered statistically significant.

Results

We investigated the relevance of survivin to breast cancer by extracting *BIRC5* expression information from three public databases: Oncomine [22], Gene Expression-Based Outcome for Breast Cancer Online (GOBO) [23], and Kaplan-Meier Plotter (K-M Plot) [25]. We found that *BIRC5* was expressed significantly higher in invasive breast carcinoma compared to normal breast

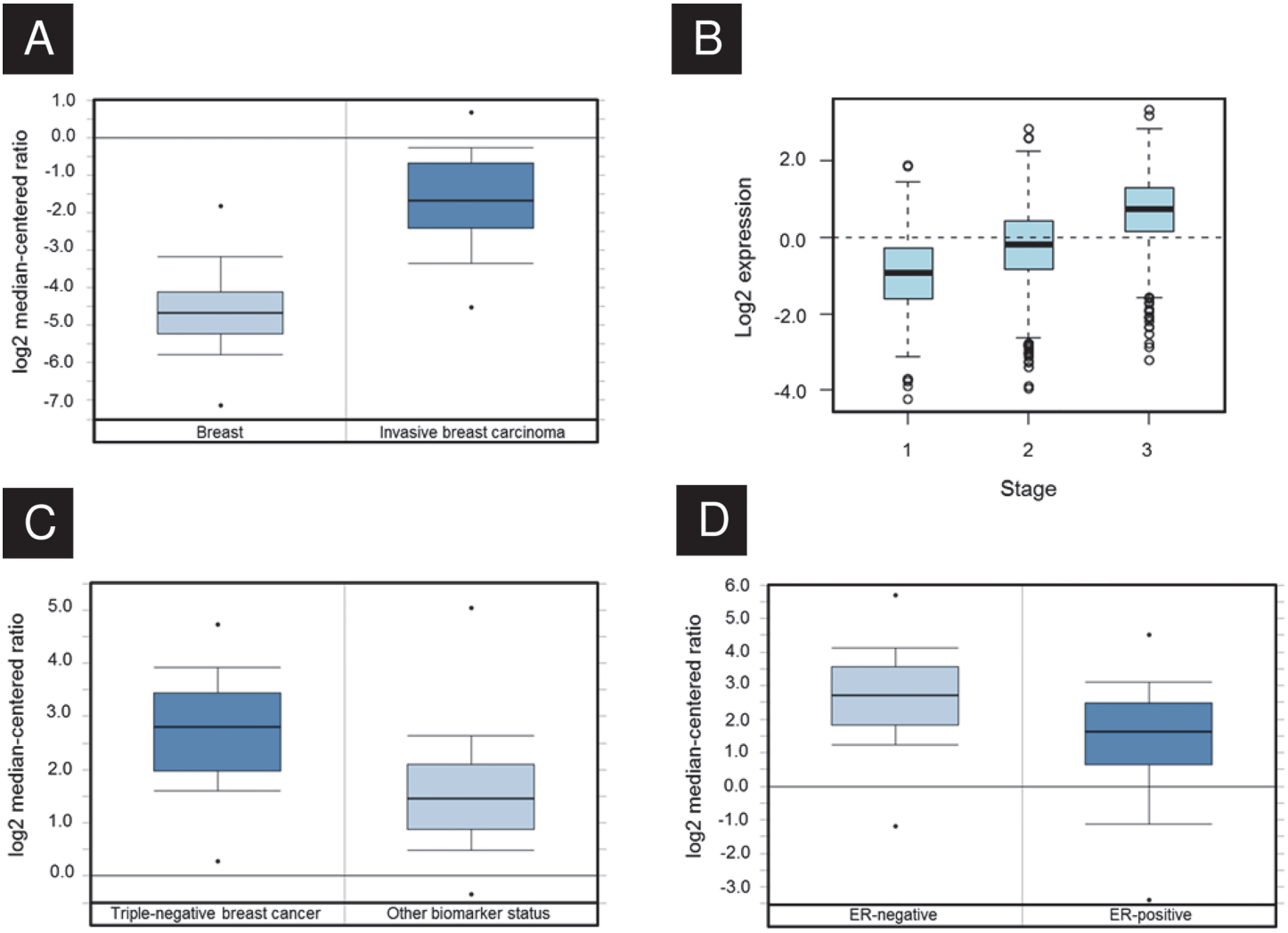

Fig 1. Survivin expression in breast cancer from public databases. A) Survivin expression is approximately seven-fold higher in invasive breast carcinoma compared to normal breast (p = 5.5e-31) from the TCGA data set in the Oncomine public database. **B)** From the GOBO public dataset, survivin expression increases with breast cancer stage ($p < 0.00001$). **C)** Survivin is expressed 2.3-fold higher in triple-negative breast cancer compared to all other molecular subtypes (p = 3.5e-8) in the Bittner breast data set in Oncomine. **D)** Similarly, survivin expression is 2.3-fold higher in estrogen receptor-negative compared to estrogen receptor-positive breast cancers (p = 9e-46) in the Curtis breast data set [24] in Oncomine.

doi:10.1371/journal.pone.0120719.g001

tissues (Fig. 1A, p = 5.5e-31) and increased with breast cancer stage (Fig. 1B, $p < 0.00001$). Moreover, *BIRC5* was expressed significantly higher in triple-negative breast cancer, a type of breast cancer known to be more aggressive and with poor prognosis, compared to all other combined subtypes (Fig. 1C, p = 3.5e-8). Furthermore, *BIRC5* was expressed over two-fold higher in estrogen receptor-negative (ER–) breast cancers compared to estrogen receptor-positive (ER+) breast cancers (Fig. 1D, p = 9e-46).

To determine whether survivin expression correlates with prognosis in patients with ER+ and ER– tumors, we analyzed two public breast cancer databases which had outcome data [22] [25]. In K-M Plot, we found that high *BIRC5* expression is associated with poor overall survival in all breast cancers patients (Fig. 2A, p = 0.0002) and in patients with ER+ breast cancer (Fig. 2C, p = 0.03), but was not associated with response in ER– patients (Fig. 2E, p = 0.28).

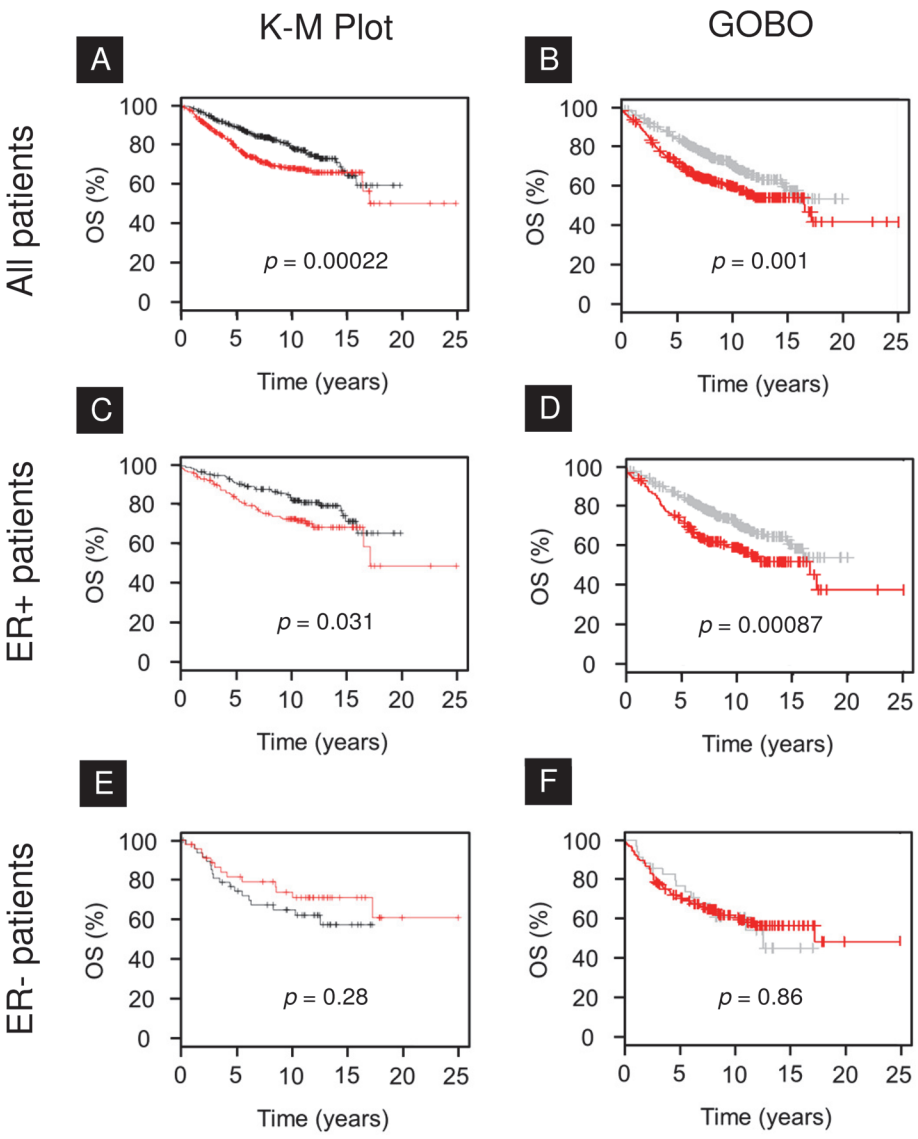

Fig 2. Overall survival in breast cancer stratified by survivin expression using two public databases. Kaplan-Meier Plotter (A,C,E) and Gene Expression-Based Outcome for Breast Cancer Online (B,D,F) data are shown. Red = high survivin expression at selected cutoff expression. **A,B)** High survivin expression is prognostic for poor outcome in all breast cancer patients. **C,D)** Likewise, high survivin expression predicts for poor outcome in patients with estrogen receptor-positive breast cancer. **E,F)** In patients with estrogen receptor-negative breast cancer, survivin expression is not associated with clinical outcome.

doi:10.1371/journal.pone.0120719.g002

Similar results were observed in the second database with respect to overall survival in all breast cancer patients, ER+ patients, and ER– patients (Fig. 2B, D, F).

To functionally assess whether survivin plays a significant role in the radiation response of breast cancer, we generated a survivin dominant-negative construct by cloning a T34A mutant into a pFUGW lentiviral backbone. As has been observed in T34A-transfected 293T cells by Altieri's group [26], we found induction of the dominant-negative mutant in MCF7 and SUM149 cell lines (Fig. 3A). Normally, this threonine residue would be phosphorylated by p34(cdc2)-cyclin B1, which is important in survivin protein stability and trafficking [31]. We first assessed the effect of the dominant-negative mutant on the frequency of apoptosis in MCF7 and SUM149 cell

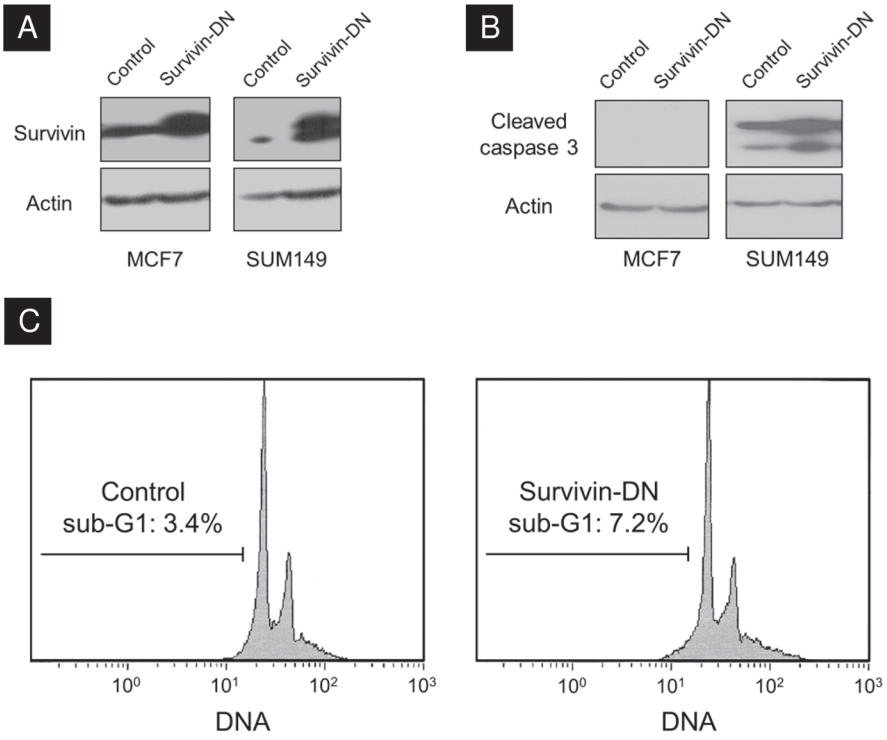

Fig 3. Cells transduced with the survivin dominant-negative construct display higher levels of apoptotic markers. A) MCF7 and SUM149 breast cancer cell lines were successfully transduced with the survivin dominant-negative construct, as shown by Western blot. **B)** Survivin-DN cells display greater levels of cleaved caspase 3 compared to the control; MCF7 shows no expression of caspase 3, consistent with the literature [32]. **C)** Survivin-DN cells have a greater fraction of sub-G1 (i.e. apoptotic) cells compared to the control, when stained with Propidium iodide.

doi:10.1371/journal.pone.0120719.g003

lines with caspase cleavage and cell cycle assays. In the caspase cleavage assay, the survivin-DN-transduced SUM149 cells showed greater levels of caspase cleavage compared to the pFUGW control (Fig. 3B). MCF7 did not express caspase 3, consistent with the literature [32].

In cell cycle assays we stained both cell lines with Propidium Iodide, and measured the number of cells in the sub-G1 phase of the cell cycle as a surrogate for apoptosis. In the SUM149 survivin-DN population, 7.2% of cells were in the sub-G1 phase, compared to only 3.4% of cells in the control population (Fig. 3C). Similarly, there was also a higher percentage of cells in sub-G1 phase for the survivin-DN population compared to the control in MCF7 cells (Fig. 3D).

We then evaluated the effect of the T34A survivin mutation on colony- and mammosphere-formation assays. In the ER+ MCF7 cell line, colony-formation efficiency was significantly lower in the survivin-DN population as compared to the control (Fig. 4A, 0.42 vs. 0.58, $p < 0.01$). In the ER– SUM149 cell line, however, the survivin-DN cells had significantly greater colony-formation efficiency (Fig. 4B, 0.29 vs. 0.20, $p < 0.01$). No significant difference in mammosphere-formation efficiency was observed between survivin-DN and control in either cell line (Fig. 4C, 4D, $p > 0.05$).

Next, we sought to investigate how the survivin-DN construct affects radiation sensitivity in MCF7 and SUM149. For both cell lines, clonogenic assays were performed with single-dose irradiation in monolayer and mammosphere conditions, and with fractionated radiation under mammosphere conditions. In all three conditions in MCF7, survivin-DN was radio-protective, with the survivin-DN-transduced MCF7 cells showing more resistance to irradiation than

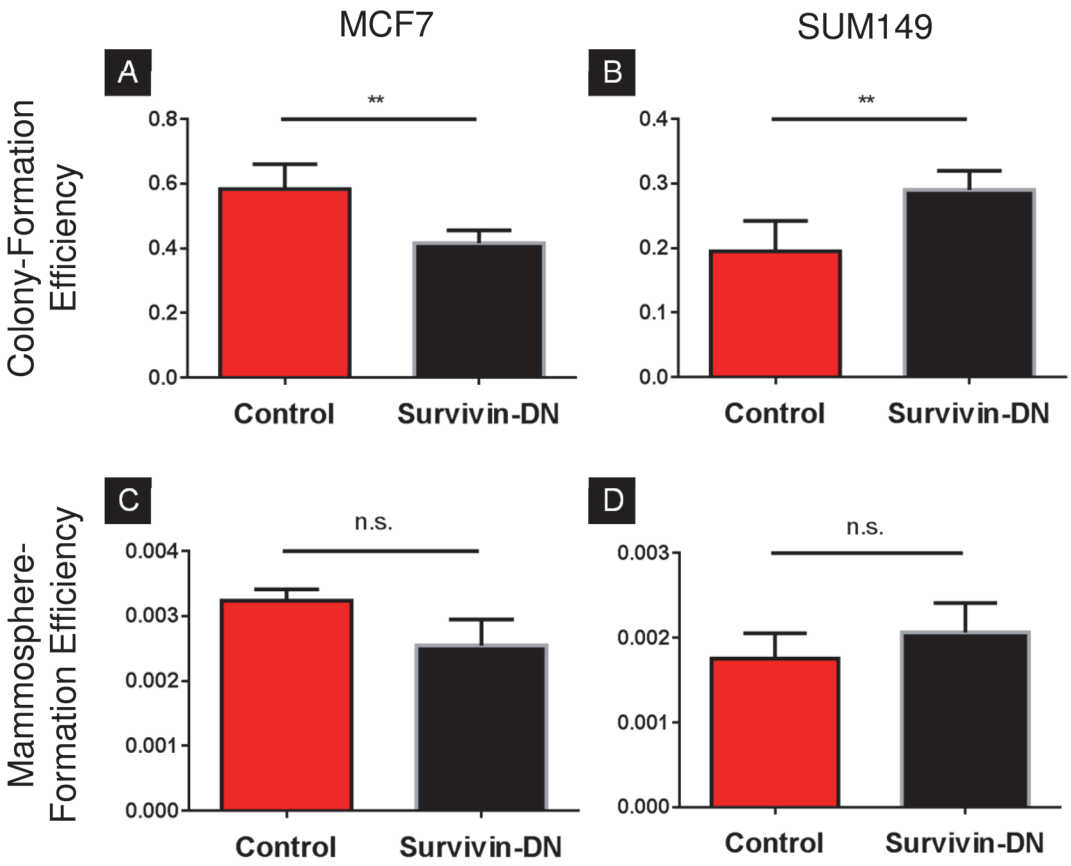

Fig 4. Colony- and mammosphere-formation efficiency in MCF7 and SUM149 breast cancer cell lines. A) In MCF7, the FUGW control forms significantly more colonies than the survivin-DN-transfected cells ($p < 0.01$). **B)** In SUM149, the survivin-DN cells form significantly more colonies than the control ($p < 0.01$). **C,D)** In both MCF7 and SUM149, there is no statistical difference in mammosphere-formation efficiency between the control and survivin-DN clone. Error bars indicate standard deviation.

doi:10.1371/journal.pone.0120719.g004

control-transduced MCF7 cells (Fig. 5A, C, E). In the SUM149 monolayer cultures, however, survivin-DN-transduced cells were radiosensitized compared to the control-transduced cells (Fig. 5B, 5D). Radiation response between different groups can also be compared by calculating surviving fraction at 2 Gy (SF2) values. For MCF7, survivin-DN was slightly radioprotective under all plating conditions, while survivin-DN was slightly radiosensitized compared to the control in SUM149 (Table 1).

We investigated the synergy of survivin perturbation and chemotherapy by adding Taxol to both the control and survivin-DN populations in MCF7 and SUM149 cell lines. In Taxol-treated cells, there were no significant differences between control and survivin-DN MCF7 cells (Fig. 6A, $p > 0.05$). In SUM149 cells, however, the combined regimen with Taxol and survivin-DN significantly decreased mammosphere-formation efficiency compared with survivin-DN alone (Fig. 6B, 0.002 vs. 0.004, $p < 0.001$). We also evaluated the synergy of a gamma secretase inhibitor with survivin-DN in both cell lines, but no significant differences were observed (Fig. 6C, 6D, $p > 0.05$).

After staining SUM149 and MCF7 tissues for pT34-survivin in order to quantify the background activity of survivin, no differences were observed (S1 Fig.). Further, the total survivin and phospho-survivin was localized in the nucleus in both the control and survivin-DN SUM149 clones (S2 Fig.).

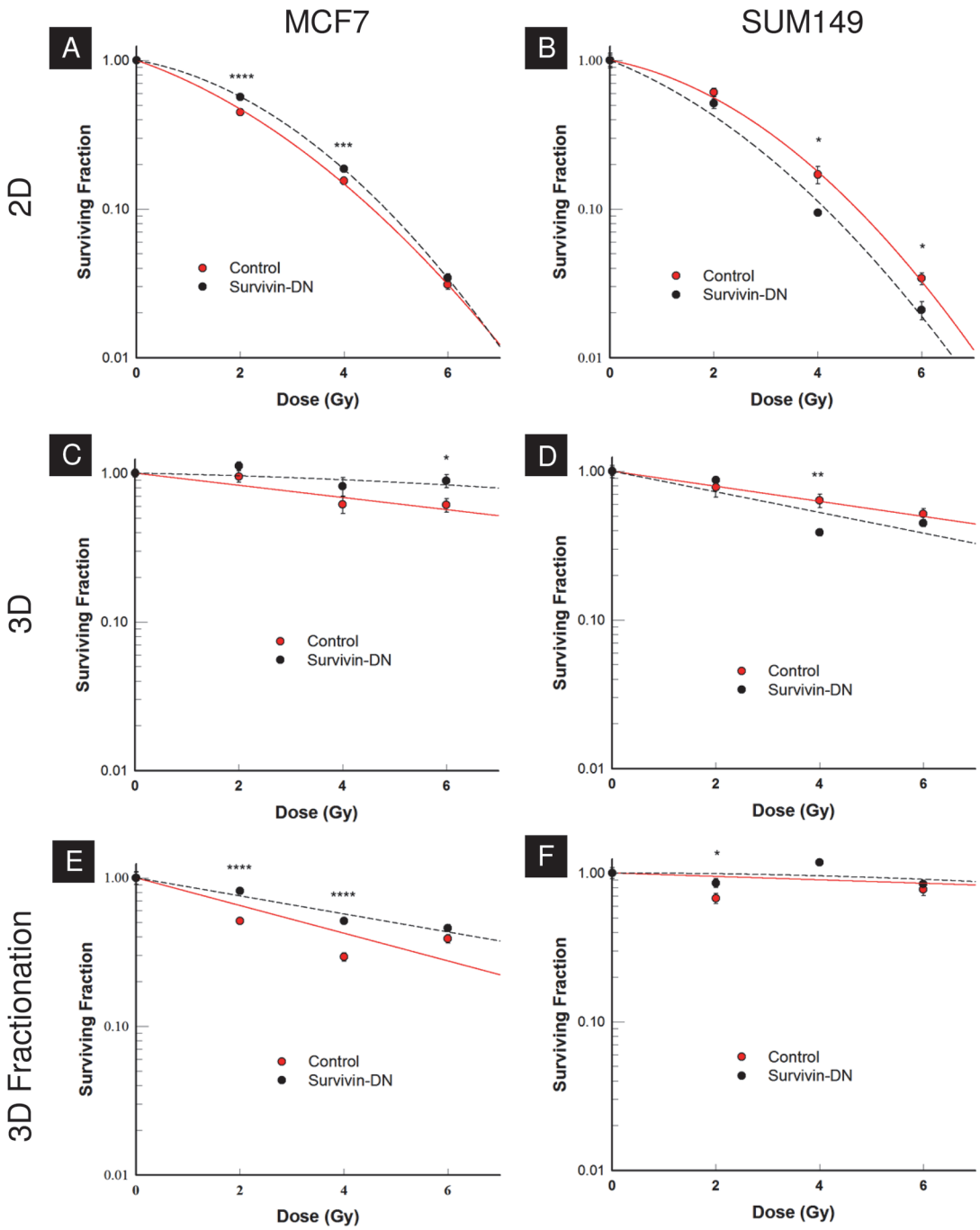

Fig 5. Representative figures for monolayer and mammosphere clonogenic assays in MCF7 and SUM149. A,C,E) MCF7 survivin-DN cells are radioprotective in monolayer cultures, mammosphere cultures, and also mammosphere cultures undergoing a fractionated regimen. **B)** SUM149 survivin-DN cells are radiosensitive compared to the control in monolayer cultures. **D,F)** SUM149 survivin-DN cells show no statistical difference in response to radiation, for both mammosphere cultures and mammosphere cultures exposed to a fractionated regiment. Error bars indicate standard deviation.

doi:10.1371/journal.pone.0120719.g005

Discussion

Here we report that T34A, phosphorylation-defective survivin reduces colony and mammosphere formation in the ER+ MCF7 cell line but not in the ER– SUM149 cell line. Conversely, the phosphorylation-defective survivin synergizes with taxol and radiation in an ER– cell line,

Table 1. Survival Fraction at 2 Gy for survivin-DN in MCF7 and SUM149.

	Control	Survivin-DN
MCF7 2D	0.23 (*13*)	0.30 (*16*)
MCF7 3D	0.60 (*23*)	0.63 (*19*)
SUM149 2D	0.17 (*08*)	0.15 (*12*)
SUM149 3D	0.89 (*19*)	0.82 (*20*)

doi:10.1371/journal.pone.0120719.t001

SUM149, but not in the ER+ MCF7, suggesting that the primary function of survivin in these cell lines and potentially in ER+ and ER− tumors is different.

We extracted information from three public databases regarding expression of *BICR5*, the gene that encodes survivin. We found that increased *BIRC5* expression is associated with advanced stage and ER− disease, but is prognostic only in ER+ breast cancer patients. These data raise important questions about targeting survivin in ER+ and ER− tumors and lead to the speculation that the dominant function of survivin in ER+ tumors may be promotion of progression, while in ER− tumors it may be regulation of response. This is consistent with the well-documented clinical paradox of greater response but worse overall outcomes in patients with ER− breast cancer who receive neoadjuvant chemotherapy.

Evasion from apoptotic death is a key mechanism in the response to therapy, in effect resistance of cancer cells to ionizing radiation and chemotherapy. Indeed, it is considered a

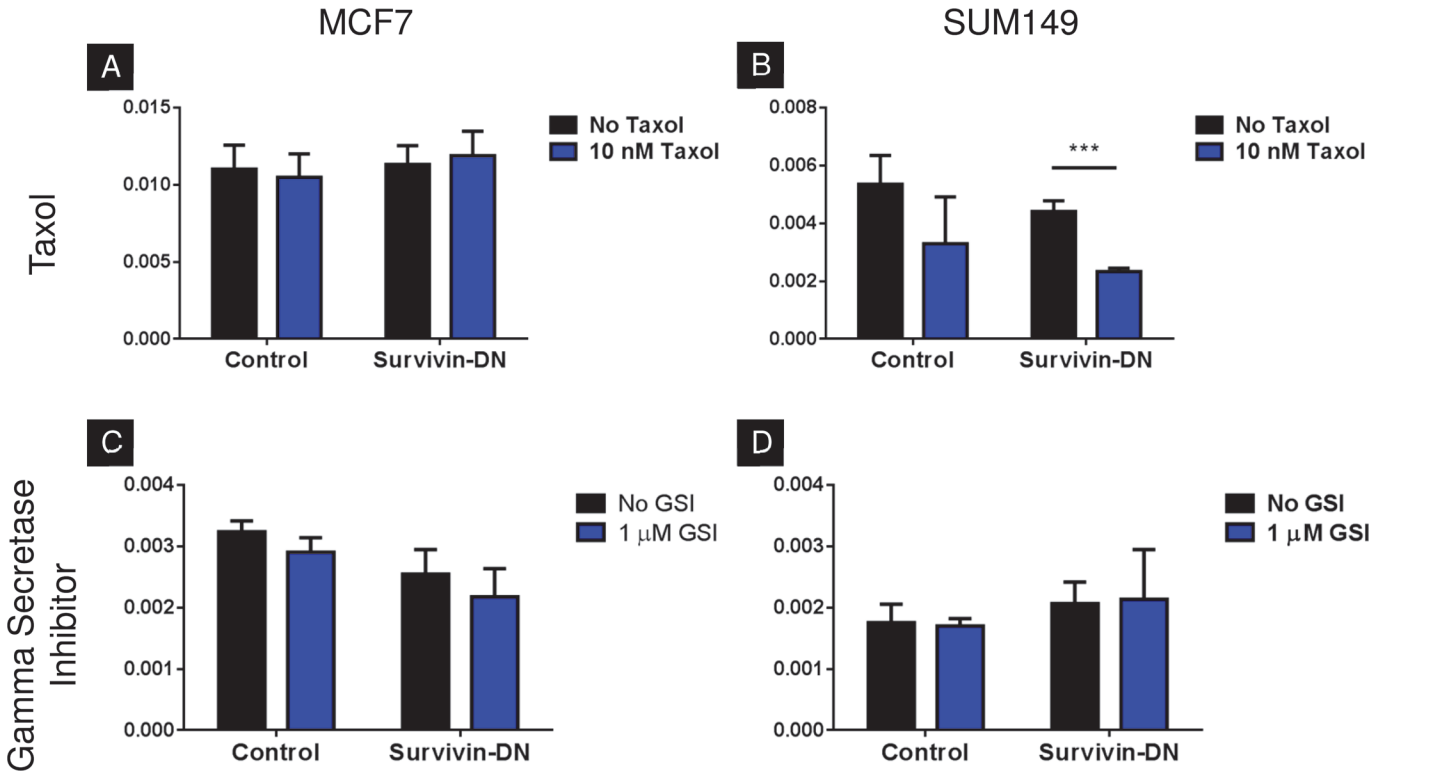

Fig 6. Mammosphere-formation efficiency in MCF7 and SUM149 when selected drugs are administered to survivin-DN cells. A,C) Neither Taxol nor gamma secretase inhibitor decrease mammosphere-formation efficiency in MCF7 control or survivin-DN cells. **B)** SUM149 survivin-DN cells are sensitized by treatment with 10 nM Taxol ($p < 0.001$). **D)** Gamma secretase inhibitor shows no effect on mammosphere formation in SUM149 control or survivin-DN cells. Error bars indicate standard deviation.

doi:10.1371/journal.pone.0120719.g006

hallmark of cancer. Changes in the activity of apoptotic pathways thus influence the response to anti-cancer treatments, and disruption of these pathways by interfering with anti-apoptotic factors is an attractive strategy to counteract therapeutic resistance. Survivin, an inhibitor of apoptosis protein that is universally overexpressed in human cancers, represents one such target.

To assess the relevance of survivin function to colony formation and radiation response in breast cancer, we employed the T34A phosphorylation-defective survivin in ER+ MCF7 and ER– SUM149 breast cancer cell lines, performing apoptosis, colony- and mammosphere-formation, and clonogenic assays. As we have reported before [30], the colony-formation and clonogenic assays performed under monolayer conditions may not fully reflect the effect of treatment on the stem and progenitor cell fraction, which is often enriched after treatment. The mammosphere assay, however, is thought to select for the self-renewing, stem cell fraction, and because of the greater relative resistance of stem cells compared to more differentiated cells to conventional treatments, we observed greater sensitivity of the monolayer cultures to irradiation compared to the mammosphere cultures as we and others have published previously [33,34,35]. Interestingly, there were greater differences in radiosensitivity between the control and phosphorylation-defective survivin populations in monolayer cultures as compared to mammosphere cultures; however, this may be due to the extreme radioresistance of the 3D cultured cells. Finally, we explored the combination of the survivin dominant-negative mutant with either Taxol or a gamma secretase inhibitor, as Notch signaling has been reported to increase survivin levels in basal-like breast cancer but not in ER+ breast cancer [36,37]. Absolute differences were detected only in the ER+ cells; however, these were modest and not significant.

Numerous attempts to target survivin in preclinical breast cancer models have been successful. One group employed the T34A phosphorylation-defective survivin to mitigate the growth and metastatic potential of a 4T1 mouse model of breast cancer [38]. In a separate study, the administration of a small-molecule survivin suppressant led to a regression of the primary and reduced spontaneous metastases in the triple-negative mouse model of breast cancer [39]. The results from these studies do not parallel our findings in the databases, in which survivin was not prognostic in estrogen receptor-negative breast cancer; further, we found that the phosphorylation-defective survivin increased colony-formation efficiency in the triple-negative SUM149. Nevertheless, all results consistently highlight the potential clinical benefit to abrogating survivin function in breast cancers.

A relationship between survivin and estrogen has been reported previously. Frasor et al. [40] observed that estradiol upregulates survivin expression in the ER+ MCF7. A mechanism was established by Sayeed and colleagues [41], who found in chromatin immunoprecipitation assays that estrogen upregulates survivin through a p53-dependent mechanism. ERα interacts with p53 bound to the promoter of survivin, inhibiting p53-mediated transcriptional repression of survivin and opposing p53-mediated apoptosis in breast cancer cells. Span et al. [42] suggested that higher survivin expression in ER– cells may be due to a difference in the cellular origin of ER– (as compared to ER+) tumors rather than due to differences in estrogen-mediated survivin expression. Chen et al. [43] observed that, among twenty endometrial hyperplasia patients that responded to progestin therapy, there was a twenty-fold decrease of nuclear survivin expression and eight-fold decrease in cytoplasmic survivin expression; conversely, there was no change in survivin expression among non-responders. These data implied that high survivin in ER+ cells is a function of unopposed estrogen in ER+ tumors, and that treatment-responsive tumors reduce survivin expression.

In conclusion, we describe the disparate effect of a dominant-negative form of survivin on the colony-forming potential and radiation response in ER+ and ER– breast cancer cell lines.

This study provides insight into the interaction between estrogen and survivin and highlights further study is warranted regarding survivin targeting to enhance therapy in ER– disease versus reduce progression in ER+ disease.

Supporting Information

S1 Fig. Survivin activity in MCF7 and SUM149 xenograft tissue.
(TIF)

S2 Fig. Staining of SUM149 primary tumor xenograft for survivin.
(TIF)

Acknowledgments

We would like to acknowledge Dr. Dario Altieri for kindly providing the T34A dominant-negative survivin construct. We would like to thank Terry Arnold for communicating the importance of our work to lay audiences.

Author Contributions

Conceived and designed the experiments: BGD DLS WAW. Performed the experiments: BGD DLS LL WX RL. Analyzed the data: BGD DLS WAW. Wrote the paper: BGD DLS WAW.

References

1. Ambrosini G, Adida C, Altieri DC (1997) A novel anti-apoptosis gene, survivin, expressed in cancer and lymphoma. Nature Medicine 3: 917–921. PMID: 9256286
2. Altieri DC (2008) Survivin, cancer networks and pathway-directed drug discovery. Nature Reviews Cancer 8: 61–70. PMID: 18075512
3. Tanaka K, Iwamoto S, Gon G, Nohara T, Iwamoto M, Tanigawa N (2000) Expression of survivin and its relationship to loss of apoptosis in breast carcinomas. Clinical Cancer Research 6: 127–134. PMID: 10656440
4. Kennedy SM, O'Driscoll L, Purcell R, Fitz-Simons N, McDermott EW, Hill AD, et al. (2003) Prognostic importance of survivin in breast cancer. British Journal of Cancer 88: 1077–1083. PMID: 12671708
5. Petrarca CR, Brunetto AT, Duval V, Brondani A, Carvalho GP, Garicochea B (2011) Survivin as a predictive biomarker of complete pathologic response to neoadjuvant chemotherapy in patients with stage II and stage III breast cancer. Clinical Breast Cancer 11: 129–134. doi: 10.1016/j.clbc.2011.03.002 PMID: 21569999
6. Mamounas EP, Tang G, Fisher B, Paik S, Shak S, Costantino JP, et al. (2010) Association between the 21-gene recurrence score assay and risk of locoregional recurrence in node-negative, estrogen receptor-positive breast cancer: Results from NSABP B-14 and NSABP B-20. Journal of Clinical Oncology 28: 1677–1683. doi: 10.1200/JCO.2009.23.7610 PMID: 20065188
7. Mamounas EP, Anderson SJ, Dignam JJ, Bear HD, Julian TB, Geyer CE, et al. (2012) Predictors of locoregional recurrence after neoadjuvant chemotherapy: Results from combined analysis of national surgical adjuvant breast and bowel project B-18 and B-27. Journal of Clinical Oncology 30: 3960–3966. doi: 10.1200/JCO.2011.40.8369 PMID: 23032615
8. Rödel F, Reichert S, Sprenger T, Gaipl US, Mirsch J, Liersch T, et al. (2011) The role of survivin for radiation oncology: Moving beyond apoptosis inhibition. Current Medicinal Chemistry 18: 191–199. PMID: 21110807
9. Capalbo G, Dittmann K, Weiss C, Reichert S, Hausmann E, Rödel C, et al. (2010) Radiation-Induced Survivin Nuclear Accumulation is Linked to DNA Damage Repair. International Journal of Radiation Oncology Biology Physics 77: 226–234. doi: 10.1016/j.ijrobp.2009.12.001 PMID: 20394854
10. Asanuma K, Moriai R, Yajima T, Yagihashi A, Yamada M, Kobayashi D, et al. (2000) Survivin as a radioresistance factor in pancreatic cancer. Japanese Journal of Cancer Research 91: 1204–1209. PMID: 11092988
11. Rödel C, Haas J, Groth A, Grabenbauer GG, Sauer R, Rödel F (2003) Spontaneous and radiation-induced apoptosis in colorectal carcinoma cells with different intrinsic radiosensitivities: Survivin as a

radioresistance factor. International Journal of Radiation Oncology Biology Physics 55: 1341–1347. PMID: 12654446

12. Pennati M, Binda M, Colella G, Folini M, Citti L, Villa R, et al. (2003) Radiosensitization of human melanoma cells by ribozyme-mediated inhibition of survivin expression. Journal of Investigative Dermatology 120: 648–654. PMID: 12648230
13. Lu B, Mu Y, Cao C, Zeng F, Schneider S, Tan J, et al. (2004) Survivin As a Therapeutic Target for Radiation Sensitization in Lung Cancer. Cancer Research 64: 2840–2845. PMID: 15087401
14. Chakravarti A, Zhai GG, Zhang M, Malhotra R, Latham DE, Delaney MA, et al. (2004) Survivin enhances radiation resistance in primary human glioblastoma cells via caspase-independent mechanisms. Oncogene 23: 7494–7506. PMID: 15326475
15. Sah NK, Munshi A, Hobbs M, Carter BZ, Andreeff M, Meyn RE (2006) Effect of downregulation of survivin expression on radiosensitivity of human epidermoid carcinoma cells. International Journal of Radiation Oncology Biology Physics 66: 852–859. PMID: 17011457
16. Cao C, Mu Y, Hallahan DE, Lu B (2004) XIAP and survivin as therapeutic target's for radiation sensitization in preclinical models of lung cancer. Oncogene 23: 7047–7052. PMID: 15258565
17. Kami K, Doi R, Koizumi M, Toyoda E, Mori T, Ito D, et al. (2005) Downregulation of survivin by siRNA diminishes radioresistance of pancreatic cancer cells. Surgery 138: 299–305. PMID: 16153440
18. Rödel F, Frey B, Leitmann W, Capalbo G, Weiss C, Rödel C (2008) Survivin Antisense Oligonucleotides Effectively Radiosensitize Colorectal Cancer Cells in Both Tissue Culture and Murine Xenograft Models. International Journal of Radiation Oncology Biology Physics 71: 247–255.
19. Iwasa T, Okamoto I, Suzuki M, Nakahara T, Yamanaka K, Hatashita E, et al. (2008) Radiosensitizing effect of YM155, a novel small-molecule survivin suppressant, in non-small cell lung cancer cell lines. Clinical Cancer Research 14: 6496–6504. doi: 10.1158/1078-0432.CCR-08-0468 PMID: 18927289
20. Woodward WA, Chen MS, Behbod F, Alfaro MP, Buchholz TA, Rosen JM (2007) WNT/β-catenin mediates radiation resistance of mouse mammary progenitor cells. Proceedings of the National Academy of Sciences of the United States of America 104: 618–623. PMID: 17202265
21. Chen MS, Woodward WA, Behbod F, Peddibhotla S, Alfaro MP, Buchholz TA, et al. (2007) Wnt/β-catenin mediates radiation resistance of Sca1+ progenitors in an immortalized mammary gland cell line. Journal of Cell Science 120: 468–477. PMID: 17227796
22. Rhodes DR, Yu J, Shanker K, Deshpande N, Varambally R, Ghosh D, et al. (2004) ONCOMINE: A Cancer Microarray Database and Integrated Data-Mining Platform. Neoplasia 6: 1–6. PMID: 15068665
23. Ringnér M, Fredlund E, Häkkinen J, Borg Å, Staaf J (2011) GOBO: Gene expression-based outcome for breast cancer online. PLoS ONE 6.
24. Curtis C, Shah SP, Chin SF, Turashvili G, Rueda OM, Dunning MJ, et al. (2012) The genomic and transcriptomic architecture of 2,000 breast tumours reveals novel subgroups. Nature 486: 346–352. doi: 10.1038/nature10983 PMID: 22522925
25. Győrffy B, Lanczky A, Eklund AC, Denkert C, Budczies J, Li Q, et al. (2010) An online survival analysis tool to rapidly assess the effect of 22,277 genes on breast cancer prognosis using microarray data of 1,809 patients. Breast Cancer Research and Treatment 123: 725–731. doi: 10.1007/s10549-009-0674-9 PMID: 20020197
26. Mesri M, Wall NR, Li J, Kim RW, Altieri DC (2001) Cancer gene therapy using survivin mutant adenovirus. Journal of Clinical Investigation 108: 981–990. PMID: 11581299
27. Lois C, Hong EJ, Pease S, Brown EJ, Baltimore D (2002) Germline transmission and tissue-specific expression of transgenes delivered by lentiviral vectors. Science 295: 868–872. PMID: 11786607
28. Debeb BG, Lacerda L, Xu W, Larson R, Solley T, Atkinson R, et al. (2012) Histone deacetylase inhibitors stimulate dedifferentiation of human breast cancer cells through WNT/β-catenin signaling. Stem Cells 30: 2366–2377. doi: 10.1002/stem.1219 PMID: 22961641
29. Dontu G, Abdallah WM, Foley JM, Jackson KW, Clarke MF, Kawamura MJ, et al. (2003) In vitro propagation and transcriptional profiling of human mammary stem/progenitor cells. Genes and Development 17: 1253–1270. PMID: 12756227
30. Debeb BG, Xu W, Mok H, Li L, Robertson F, Ueno NT, et al. (2010) Differential Radiosensitizing Effect of Valproic Acid in Differentiation Versus Self-Renewal Promoting Culture Conditions. International Journal of Radiation Oncology Biology Physics 76: 889–895. doi: 10.1016/j.ijrobp.2009.09.052 PMID: 20159363
31. O'Connor DS, Grossman D, Plescia J, Li F, Zhang H, Villa A, et al. (2000) Regulation of apoptosis at cell division by p34(cdc2) phosphorylation of survivin. Proceedings of the National Academy of Sciences of the United States of America 97: 13103–13107. PMID: 11069302

32. Jänicke RU, Sprengart ML, Wati MR, Porter AG (1998) Caspase-3 is required for DNA fragmentation and morphological changes associated with apoptosis. Journal of Biological Chemistry 273: 9357–9360. PMID: 9545256

33. Woodward WA, Bristow RG (2009) Radiosensitivity of Cancer-Initiating Cells and Normal Stem Cells (or what the Heisenberg Uncertainly Principle has to do with Biology). Seminars in Radiation Oncology 19: 87–95. doi: 10.1016/j.semradonc.2008.11.003 PMID: 19249646

34. Woodward WA, Debeb BG, Xu W, Buchholz TA (2010) Overcoming radiation resistance in inflammatory breast cancer. Cancer 116: 2840–2845. doi: 10.1002/cncr.25173 PMID: 20503417

35. Phillips TM, McBride WH, Pajonk F (2006) The response of CD24-/low/CD44+ breast cancer-initiating cells to radiation. Journal of the National Cancer Institute 98: 1777–1785. PMID: 17179479

36. Lee CW, Raskett CM, Prudovsky I, Altieri DC (2008) Molecular dependence of estrogen receptor-negative breast cancer on a notch-survivin signaling axis. Cancer Research 68: 5273–5281. doi: 10.1158/0008-5472.CAN-07-6673 PMID: 18593928

37. Lee CW, Simin K, Liu Q, Plescia J, Guha M, Khan A, et al. (2008) A functional Notch-survivin gene signature in basal breast cancer. Breast Cancer Research 10.

38. Peng XC, Yang L, Yang LP, Mao YQ, Yang HS, Liu JY, et al. (2008) Efficient inhibition of murine breast cancer growth and metastasis by gene transferred mouse survivin Thr34→Ala mutant. Journal of Experimental and Clinical Cancer Research 27.

39. Yamanaka K, Nakata M, Kaneko N, Fushiki H, Kita A, Nakahara T, et al. (2011) YM155, a selective survivin suppressant, inhibits tumor spread and prolongs survival in a spontaneous metastatic model of human triple negative breast cancer. International Journal of Oncology 39: 569–575. doi: 10.3892/ijo.2011.1077 PMID: 21674125

40. Frasor J, Danes JM, Komm B, Chang KCN, Richard Lyttle C, Katzenellenbogen BS (2003) Profiling of estrogen up- and down-regulated gene expression in human breast cancer cells: Insights into gene networks and pathways underlying estrogenic control of proliferation and cell phenotype. Endocrinology 144: 4562–4574. PMID: 12959972

41. Sayeed A, Konduri SD, Liu W, Bansal S, Li F, Das GM (2007) Estrogen receptor α inhibits p53-mediated transcriptional repression: Implications for the regulation of apoptosis. Cancer Research 67: 7746–7755. PMID: 17699779

42. Span PN, Sweep FCGJ, Wiegerinck ETG, Tjan-Heijnen VCG, Manders P, Beex LVAM, et al. (2004) Survivin is an independent prognostic marker for risk stratification of breast cancer patients. Clinical Chemistry 50: 1986–1993. PMID: 15364883

43. Chen X, Zhang Z, Feng Y, Fadare O, Wang J, Ai Z, et al. (2009) Aberrant survivin expression in endometrial hyperplasia: Another mechanism of progestin resistance. Modern Pathology 22: 699–708. doi: 10.1038/modpathol.2009.25 PMID: 19287462

APPENDIX II: PATCHED TARGETING PEPTIDES FOR IMAGING AND TREATMENT OF HEDGEHOG POSITIVE BREAST TUMORS

This appendix is based upon:

Smith DL, Kong F, Yang D, Larson R, Sims-Mourtada J, Woodward WA (2014) Patched targeting peptides for imaging and treatment of hedgehog positive breast tumors. *BioMed Research International,* vol. 2014, Article ID 525680, 9 pages, 2014. doi:10.1155/2014/525680

Hindawi Publishing Corporation
BioMed Research International
Volume 2014, Article ID 525680, 9 pages
http://dx.doi.org/10.1155/2014/525680

Research Article

Patched Targeting Peptides for Imaging and Treatment of Hedgehog Positive Breast Tumors

Daniel Smith,[1] Fanlin Kong,[2] David Yang,[2] Richard Larson,[1] Jennifer Sims-Mourtada,[3] and Wendy A. Woodward[1]

[1] *Department of Radiation Oncology, The University of Texas M.D. Anderson Cancer Center, Houston, TX 77030, USA*
[2] *Department of Cancer Systems Imaging, The University of Texas M.D. Anderson Cancer Center, Houston, TX 77030, USA*
[3] *Center for Translational Cancer Research, Helen F. Graham Cancer Center and Research Institute, Christiana Care Health System, 4701 Ogletown-Stanton Road, Newark, DE 19713, USA*

Correspondence should be addressed to Jennifer Sims-Mourtada; jsimsmourtada@christianacare.org

Received 28 May 2014; Revised 11 July 2014; Accepted 15 July 2014; Published 8 September 2014

Academic Editor: Mei-Hsiu Liao

High tumor hedgehog expression is correlated with poor prognosis in invasive ductal carcinoma. Peptides which bind the patched receptor have recently been reported to have a growth inhibitory effect in tumors with activated hedgehog signaling. We sought to examine growth inhibition with these peptides in breast cancer cells and use these peptides as molecular imaging probes to follow changes in hedgehog expression after chemotherapy. Significant growth inhibition was observed in breast cancer cell lines treated with PTCH-blocking peptides. Significant *in vitro* uptake was observed with both FITC- and ^{99m}Tc-EC-peptide conjugates. *In vivo* imaging studies displayed greater accumulation of ^{99m}Tc-labeled peptides within tumors as compared to adjacent muscle tissue. Patched receptor expression increased after treatment and this correlated with an increase in tumor radiotracer uptake. These studies suggest that peptides which bind the sonic hedgehog docking site in patched receptor correlate with patched expression and can be used to image patched *in vivo*. Further, our data suggest that radiolabeled peptides may enable us to examine the activity of the hedgehog signaling pathway and to evaluate response to anti-cancer therapies.

1. Introduction

The hedgehog (Hh) signaling pathway plays a critical role in embryonic development and wound healing, and its aberrant activity is associated with several malignancies. Recent studies implicate Hh signaling in breast cancer growth and metastasis, and high tumor sonic hedgehog (SHh) expression is correlated with poor prognosis in invasive ductal carcinoma. SHh binds to the suppressive receptor patched-1 (PTCH-1) and relieves the inhibition of the transmembrane protein smoothened (Smo) by PTCH-1, resulting in the translocation of Gli transcription factors to the nucleus and activation of Hh target genes. In tumors with activated Hh signaling, high levels of PTCH-1 have been reported, especially within the tumor stroma.

Previously, we demonstrated strong detection of tumor xenografts using an iodinated derivative of the PTCH-1 binding ligand, sonic hedgehog [1]. Although this agent was capable of delineating tumor tissue, its clinical utility is limited due to poor stability and pharmacokinetics. Imaging with radiolabeled peptides has been shown to improve pharmacokinetics and the targeting of other tumor-based receptors. Therefore, we sought to develop radiolabeled peptides which dock inside the PTCH receptor. Nakamura et al. previously reported the synthesis of several peptides targeting the PTCH-1 receptor [2]. These peptides were shown to bind to the PTCH-1 receptor on the surface of pancreatic tumors and decrease tumor growth.

Here, we selected technetium-99 m (^{99m}Tc) as the radioisotope because of its favorable physical characteristics for diagnostic imaging studies and due to the ease of using its benchtop generator-based system for clinical applications. It emits 140 keV gamma ray, with an 89% branching fraction,

which can be detected by single photon emission computed tomography (SPECT). In addition, the half-life of ^{99m}Tc is relatively long (6.02 h) compared to most nuclear imaging radioisotopes, which facilitates serial imaging that may improve the differentiation of tumor from inflammation. To label the peptide with ^{99m}Tc, the chelator N,N′-ethylene-di-*L*-cysteine (EC) is selected and used as a linker. EC is known to chelate ^{99m}Tc stably owing to the efficient binding of the oxotechnetium group to the two thiols and two amine nitrogen atoms of EC.

Here, we report the radiolabeling of these peptides to detect the PTCH receptor on breast cancer cells and breast cancer stem cell-enriched populations. These molecular imaging probes have the potential to identify Hh-induced changes in PTCH-1 expression, which is useful for the imaging of aberrant Hh signaling in malignancies.

2. Methods

2.1. Peptides. PTCH-binding peptides A—sequence FAPVL-DGAVSTLLGV— and B—sequence DNTRYSPPPPYSSHS— were commercially synthesized with or without an N-terminal FITC-Ahx modification (GenScript, Piscataway, NJ). Peptides were resuspended at a stock concentration of 200 μM in 10% DMSO in deionized water.

2.2. Synthesis and Radiolabeling of PTCH. Ethylenedicysteine (EC) was selected as a chelator for PTCH conjugation. Sodium bicarbonate (1 N, 1 mL) was added to a stirred solution of EC (5 mg, 0.019 mmol). To this colorless solution, sulfo-NHS (4 mg, 0.019 mmol) and EC (5 mg, 0.019 mmol) were added. PTCH (0.3 mg) was then added. The mixture was stirred at room temperature for 24 hours. The mixture was dialyzed for 48 hours with a cutoff at molecular weight 10,000 Da. After dialysis, the product was freeze-dried, with the product in the salt form weighing 0.5 mg.

^{99m}Tc-pertechnetate was obtained from Mallinckrodt (Houston, TX). Radiosynthesis of ^{99m}Tc-EC-PTCH was achieved by adding the required amount of ^{99m}Tc-pertechnetate into EC-PTCH (0.1 mg) and tin chloride (II) ($SnCl_2$, 100 mg). The mixture was loaded on a sephadex gel column (PD-10, G-25) (Sigma Chemical Company, St. Louis, MO) and eluted with phosphate-buffered saline (pH 7.4). One milliliter of each fraction was collected. The product was collected at fraction 3, with a 70% yield. Radiochemical purity was assessed by Radio-TLC (BioScan, Washington, DC) using saline as an eluant.

2.3. Cell Lines and Culture Conditions. The human cell lines T47-D, SKBR3, and MCF-7 were obtained from the American Type Tissue Company (ATCC) and cultured in DMEM with 10% fetal bovine serum (Atlanta Biologicals, Flowery Branch, GA) and 1% antibiotic-antimycotic (Invitrogen Life Technologies, Grand Island, NY Life Technologies, Grand Island, NY). The human cell line SUM159 was obtained from Asterand (Detroit, MI) and cultured in DMEM containing 1 μg/mL hydrocortisone (Invitrogen Life Technologies, Grand Island, NY Life Technologies, Grand Island, NY), 5 μg/mL insulin (Invitrogen Life Technologies, Grand Island, NY), and 1% antibiotic/antimycotic. The rat breast cancer cell line 13762 was derived from a tumor induced in a Fischer-344 rat by giving an oral dose of 7,12-dimethylbenz[a]anthracene [3], and the cells were cultured in RPMI-1640 medium, supplemented with 10% (vol : vol) fetal bovine serum and 1% antibiotic-antimycotic. For mammosphere assays, cells were cultured in MEM media supplemented with 1X B27 (Invitrogen Life Technologies, Grand Island, NY), 20 ng/mL epidermal growth factor (EGF; Invitrogen Life Technologies, Grand Island, NY), and 20 ng/mL basic fibroblast growth factor (bFGF; Invitrogen Life Technologies, Grand Island, NY) and seeded into ultralow attachment plates (Corning Life Sciences, Salt Lake City, UT). Cells were grown for 7–10 days and spheres were obtained. All cells were cultured at 37°C in a humidified atmosphere containing 5% carbon dioxide.

2.4. Survival Assays. Breast cancer cell lines were seeded into 96-well plates at a density of 5,000–7,000 cells per well. Cells were grown overnight and media were replaced with culture media containing unlabeled peptides A and B at the indicated concentrations. Cells were cultured for an additional 48 hours and survival was determined using the MTT-based Cell Proliferation Assay (Biotium). Data is expressed as %treated/untreated.

2.5. Fluorescence Microscopy. Breast cancer cell lines were seeded onto chamber slides (Nunc, Roskilde, Denmark) and grown overnight. For sphere assays, cells were seeded in 3D media as described above in 96-well low attachment plates at a density of 100–1000 cells per well and cultured for 7–10 days until spheres were formed. Spheres were filtered using a cell strainer and replated into low attachment plates. Cells or spheres were treated with 100 nM peptide A or B and incubated for 2 hours. Media were removed and cells or spheres were washed two times with 1X PBS. Following washes, 1 mL of 1X PBS was added to the slide or plate and cells or spheres were analyzed by fluorescence microscopy using a Zeiss motorized AxioObserver Z1 microscope. For co-localization experiments, cells were seeded at a density of 7000 cells per well in a chamber slide and cultured overnight. Cells were incubated with 100nM peptide and incubated for 2 hours. Cells were fixed in methanol at -20 degrees Celsius for 5 min, and blocked with PBS containing 10% goat serum. Cells were stained with anti-PTCH antibody (Santa Cruz Biotechnology, Dallas, TX) overnight at 4 degrees Celsius, washed 3 time in 1XPBS and incubated with an anti-rabbit Alexa-555 secondary antibody for 1 hour at RT. Slides were washed 3 times with PBS and stained with DAPI Prolong Gold (Invitrogen Life Technologies, Grand Island, NY). Slides were analyzed using a Zeiss motorized AxioObserver Z1 microscope.

2.6. Uptake Studies. To measure uptake of the FITC-tagged peptide, cells were plated at a density of 5,000–10,000 cells per well in a 24-well plate and grown overnight. For sphere assays, cells were plated as described above. Cells or spheres

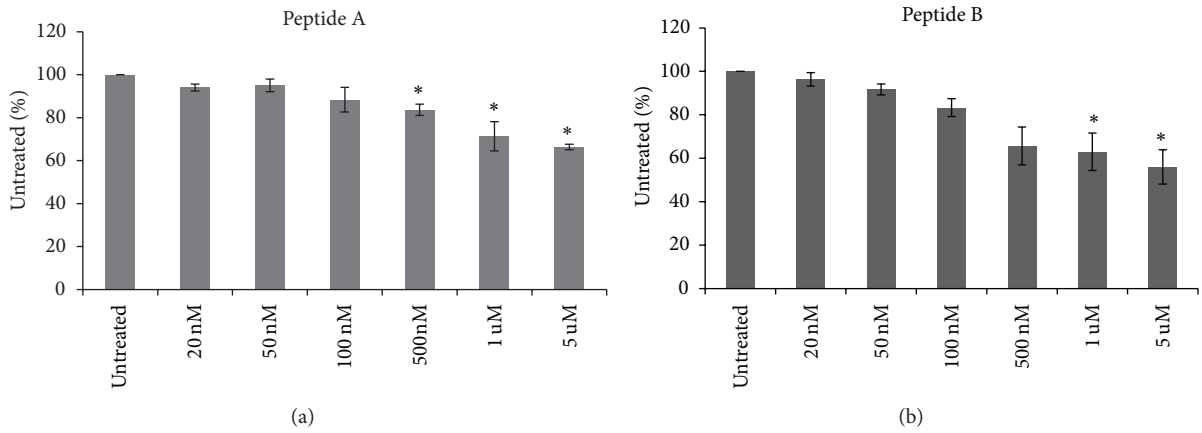

Figure 1: Patched-binding peptides decrease growth of the SKBR3 breast cancer cell line. Using the MTT assay, peptides A and B administered to SKBR3 significantly decreased growth compared to untreated cells. Error bars represent standard deviation. Significance is represented by asterisk. $^{*}P \leq 0.05$.

were treated with 100 nM peptide and incubated for 2 hours. Cells or spheres were washed 3X with PBS, trypsinized, and resuspended in 500 μL culture media. Cells were counted using a Countess automated cell counter (Invitrogen Life Technologies, Grand Island, NY Life Technologies, Grand Island, NY) after staining with trypan blue (Invitrogen Life Technologies, Grand Island, NY Life Technologies, Grand Island, NY). Next, 100 μL of cell suspension was transferred to black polystyrene 96-well plates. Fluorescence was measured at 485 nm excitation and 535 nm emission. Uptake is reported as mean fluorescence intensity per 1,000 cells.

The rat breast carcinoma cell line 13762 and the human breast cancer cell lines SUM159 and MDA-IBC3 were used for the *in vitro* radiotracer uptake. One day before the uptake experiment, 2×10^5 cells/well of each cell line were seeded in six-well plates and incubated at 37°C in 5% CO_2 under humidified conditions. The following day, 300 kBq of ^{99m}Tc-EC-peptide A or ^{99m}Tc-EC was added with 2 mL of the appropriate media to each of the wells. The cells were incubated for 30 minutes, 1 hour, 2 hours, or 4 hours, after which the media was aspirated, cells were washed twice with PBS, and then cells were suspended with trypsin. Radioactivity of collected cells was measured on a gamma counter (Packard) with an energy window of 126–154 keV for ^{99m}Tc, and percent uptake was calculated by using an appropriate standard. Percent uptake was then normalized to milligrams of protein in the sample, where the protein concentration was measured using the Bradford method (Bio-Rad Laboratories, Berkeley, CA). Each sample was run in triplicate, with error bars indicating standard deviation.

2.7. Animal Model and Chemotherapy Treatment. All animal work was carried out in the Small Animal Imaging Facility (SAIF) at the University of Texas M.D. Anderson Cancer Center under an approved Institutional Animal Care and Use Committee (IACUC) protocol. Female Fischer 344 rats (150 ± 25 g, $n = 6$) (Harlan Sprague-Dawley, Indianapolis, IN) were inoculated subcutaneously with 0.1 mL of a 13762 breast carcinoma cell suspension (10^5 cells/rat of a breast tumor cell line specific to Fischer rats) into the hind legs using 25-gauge needles. Studies were performed 12–14 days after inoculation when tumors reached approximately 1 cm in diameter. For treatment studies, rats were injected with 20 mg/kg paclitaxel and reimaged 7 days later. After the posttreatment scan, tumors were removed and formalin sections were made. Control tumors were taken from untreated mice 13 days after inoculation. Sections were stained with an anti-patched antibody (Santa Cruz) using a peroxide-based immunohistochemical detection kit (Dako) according to the manufacturer's instructions.

2.8. Planar Imaging. Planar scintigraphic images were obtained using M-CAM (Siemens Medical Solutions, Hoffman Estates, IL) equipped with a low energy high resolution (LEHR) collimator. Anesthetized breast tumor-bearing rats were injected intravenously with ^{99m}Tc-EC-peptide A (0.3 mg/rat, 300 μCi/rat; $n = 3$) before and 7 days after paclitaxel treatment. ^{99m}Tc-EC (0.15 mg/rat, 300 μCi/rat; $n = 3$) was used as a control. The images were acquired at 1 hr, 2 hr, and 4 hr after administration of radiotracers. Computer outlined regions of interest (ROIs in counts per pixel) between tumor and muscle were used to calculate tumor-to-muscle (T/M) ratios.

2.9. Statistical Analysis. Statistical analysis was performed using Graph Pad Prism 6 software (Graph Pad, La Jolla, CA) using ANOVA or unpaired t-test. For all tests, P values less than 0.05 were considered to be significant.

3. Results

3.1. Growth Inhibitory Effect of Peptides A and B in Breast Cancer Lines. Inhibition of hedgehog signaling has been shown to decrease growth and survival of breast cancer cells [2, 4]. Antibodies that disrupt the binding of sonic hedgehog to the PTCH receptor have also been reported to inhibit breast

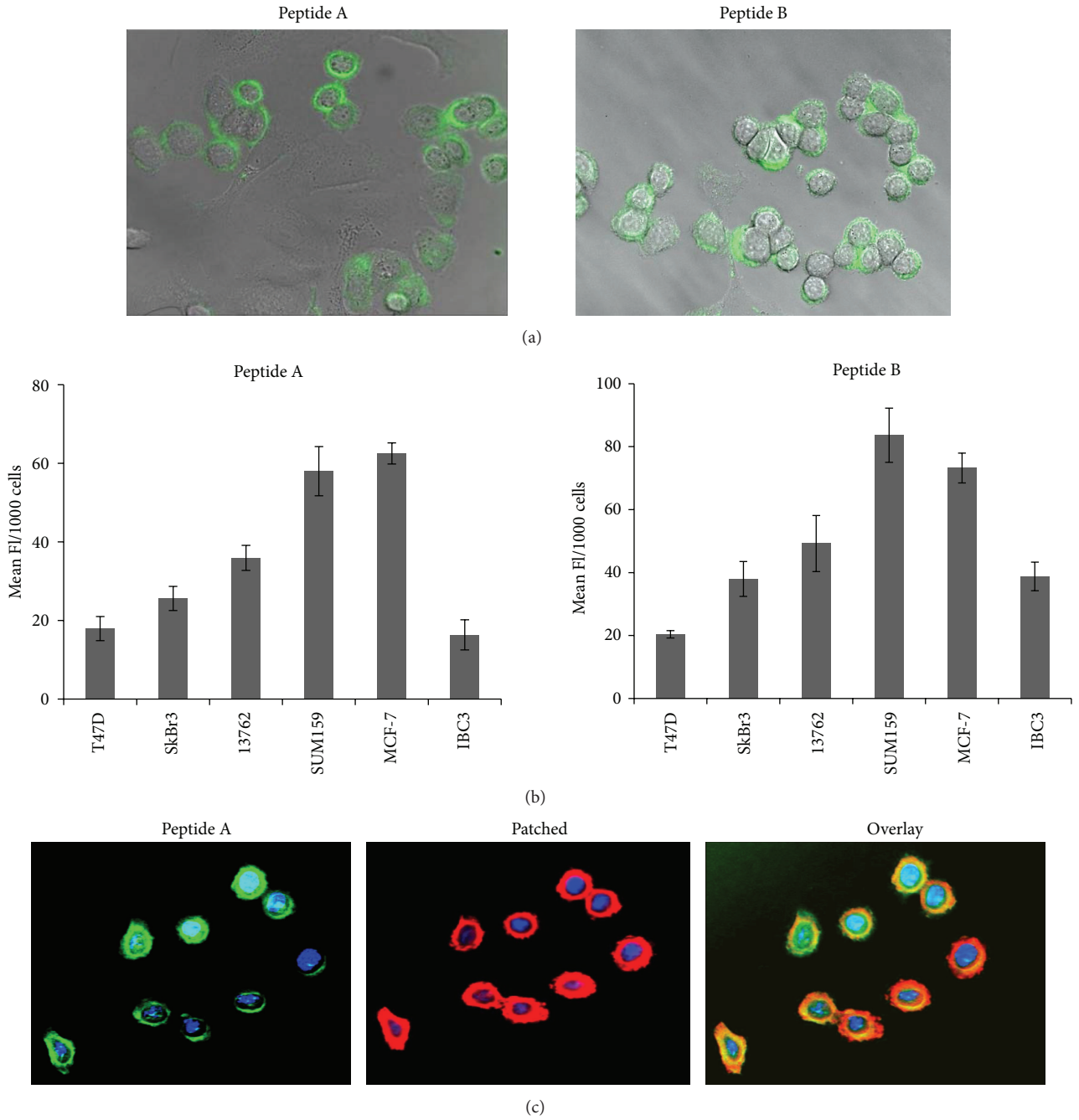

Figure 2: Patched-binding peptides have significant uptake in breast cancer cell lines. (a) Fluorescence microscopy of FITC-labeled peptides A and B in SKBR3 breast cancer cells. (b) Quantification of FITC-peptides A and B uptake in breast cancer cell lines. (c) Fluorescence microscopy of SKBR3 cells showing colocalization of peptide B (green) with the PTCH receptor (red). Colocalization appears as yellow staining in the image overlay.

cancer growth [5]. The PTCH-binding peptides, referred to, in this paper, as peptides A and B, have previously been shown to decrease hedgehog-dependent growth of pancreatic cancer cell lines. Therefore, we sought to determine their effect on breast cancer cell lines. As shown in Figure 1, treatment of SkBr3 breast cancer cell lines with peptides A and B resulted in significant growth inhibition at higher concentrations. Minimal effect was observed at lower concentrations.

3.2. Peptide Uptake in Breast Cancer Cell Lines and Mammospheres. To validate the PTCH-binding peptides A and B as ligands to detect breast cancer cells, we evaluated the cellular uptake of the peptides labeled with FITC. Fluorescence microscopy of breast cancer cell lines revealed uptake of the FITC-tagged peptides. As shown in Figure 2(a), cytosolic fluorescence was observed 24 hours after treatment of the breast cancer cell line SKBR3 with peptide A or peptide B. To

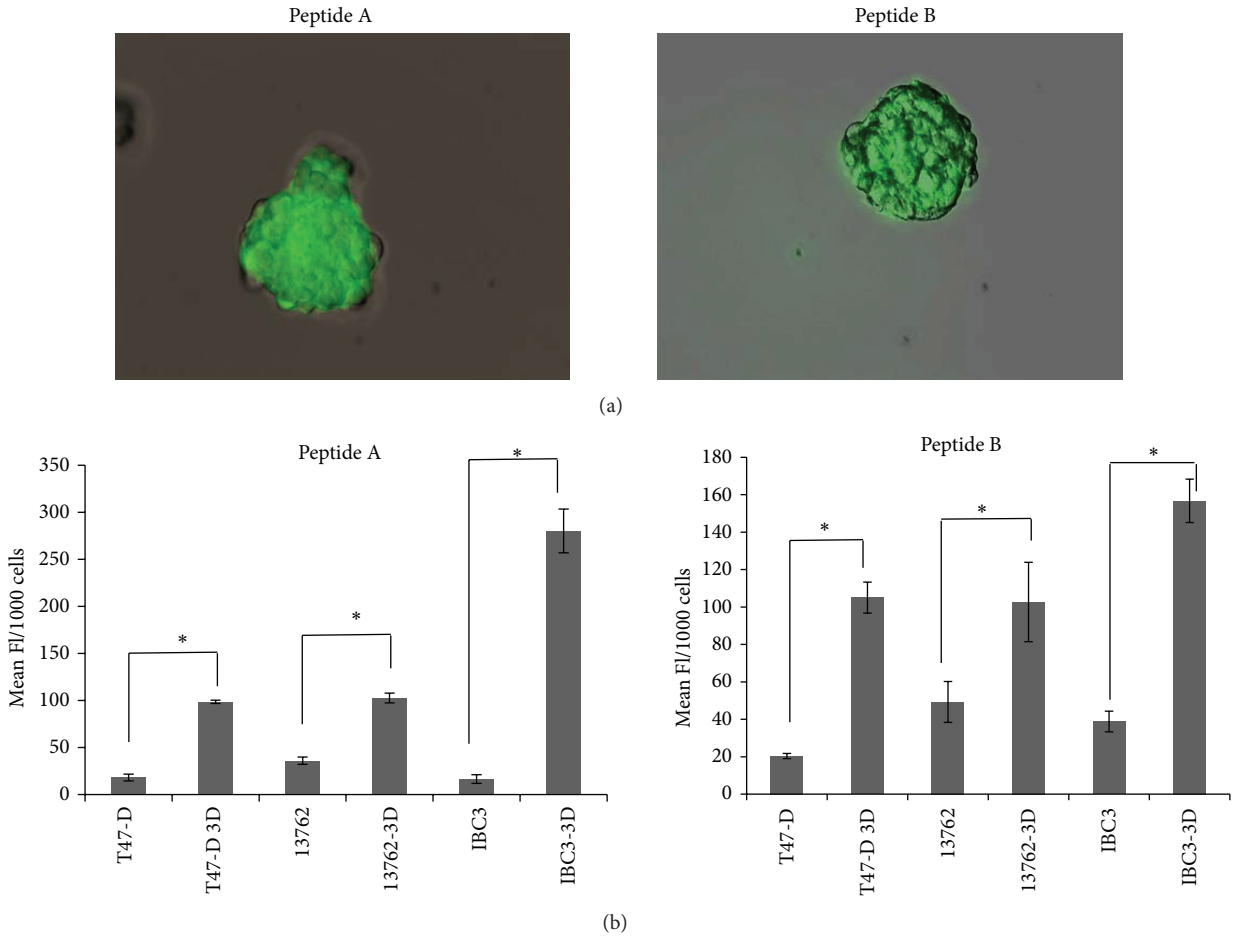

Figure 3: Uptake of patched-binding peptides is increased in mammospheres from breast cancer cell lines. (a) Fluorescence microscopy of FITC-labeled peptides A and B in mammospheres from T47-D. (b) Quantification of FITC-peptides A and B uptake in breast cancer cell lines in monolayer and mammosphere cultures. Uptake was significantly higher in cells cultured in mammosphere promoting conditions (3 dimensional cultures) than in those grown in standard monolayer conditions. Significance is represented by asterisk. $^{*}P \leq 0.01$.

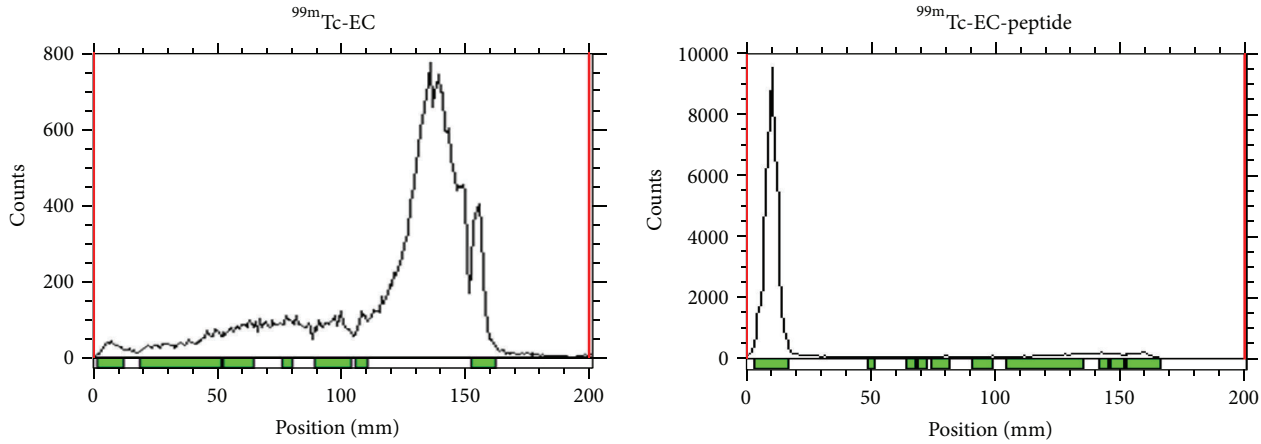

Figure 4: Radiochemical purity of ^{99m}Tc-EC and ^{99m}Tc-EC-peptide A. Radiochemical purity was determined by RadioTLC with saline as the mobile phase.

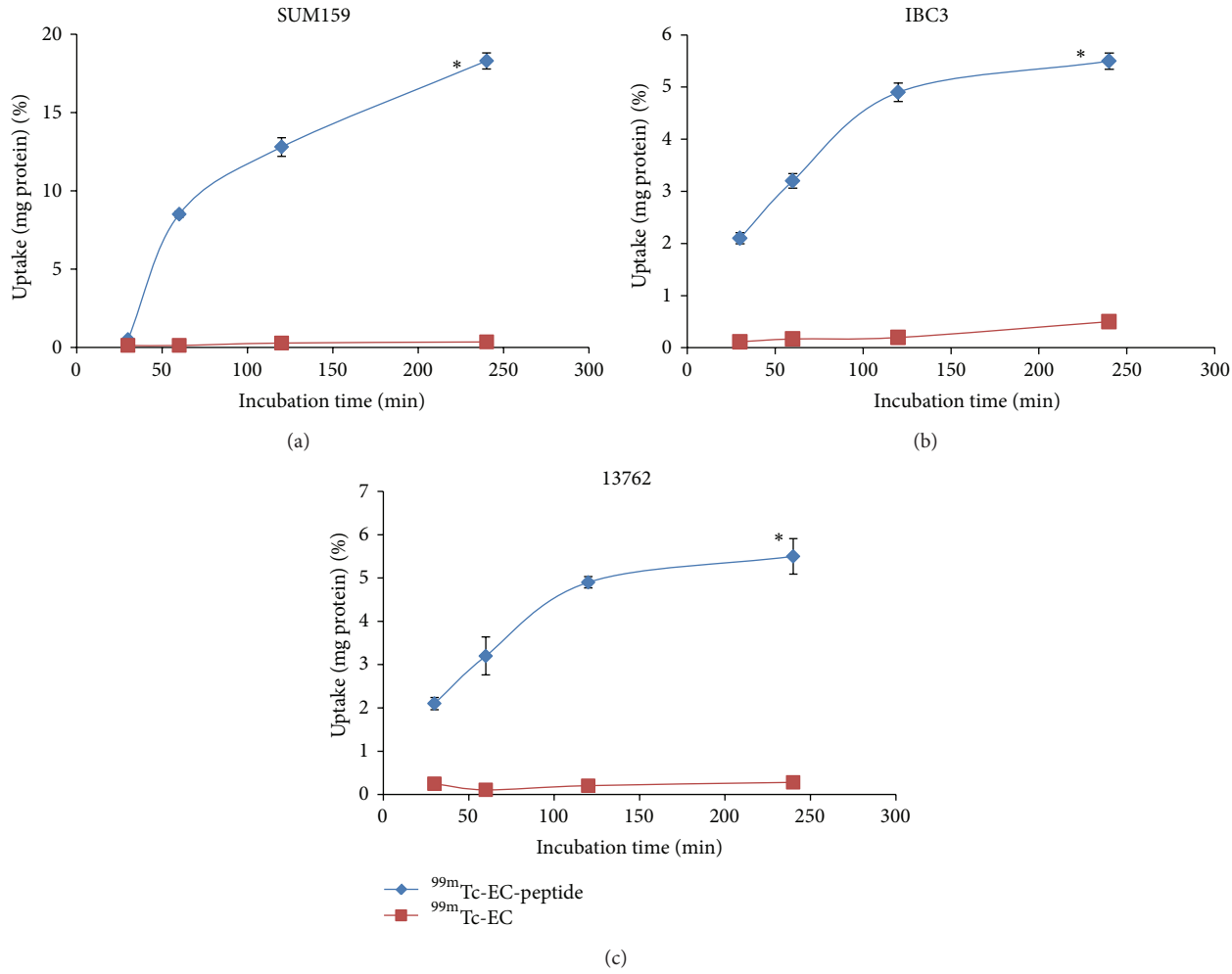

FIGURE 5: *In vitro* uptake of ^{99m}Tc-EC-peptide A. Results of *in vitro* assays showing significant uptake of peptide A compared to ^{99m}Tc-EC control in (a) SUM159, (b) MDA-IBC3, and (c) 13762 breast cancer cell lines. Data is represented as % uptake per mg/protein. Error bars represent standard deviations. Significance is represented by asterisk. $^{*}P \leq 0.001$.

quantify these findings, uptake studies were performed in a panel of breast cancer cell lines and fluorescence intensity was measured. As shown in Figure 2(b), significant uptake of the fluorescent peptides was observed. Furthermore, fluorescent intensity corresponded to PTCH expression as previously reported [1], suggesting that binding is specific to the PTCH receptor. To further confirm colocalization of PTCH-binding peptides with PTCH receptor expression, we performed fluorescence microscopy using anti-PTCH antibodies on cells treated with FITC-labeled PTCH-binding peptides. As shown in Figure 2(c), uptake of PTCH-binding peptides (green) colocalized with PTCH receptor expression (red).

Hedgehog pathway members PTCH, Gli-1, and Gli-2 have been reported to be more highly expressed in normal mammary stem cells and their malignant counterparts, breast cancer stem cells, compared to more differentiated breast cancer cells [6]. High expression of the PTCH receptor has been reported in breast cancer cells cultured in stem cell-enriching conditions (mammospheres, 3 dimensional cultures). Consistent with these findings, an increase in peptide uptake was observed in mammospheres compared to 2 dimensional monolayer cultures (Figure 3). These data indicate that PTCH-binding peptides may provide a method of targeting breast cancer stem cells.

3.3. Synthesis and Radiolabeling of EC-Peptide A. To establish the uptake of PTCH-binding peptides *in vivo*, we synthesized chelator-peptide conjugates that could be radiolabeled with ^{99m}Tc for gamma scintigraphy. A simple and efficient synthesis of ^{99m}Tc EC-PTCH was developed. EC was conjugated to the lysine residue of peptide A. ^{99m}Tc EC-PTCH was found to be radiochemically pure (100%, Figure 4).

3.4. In Vitro Uptake Studies. *In vitro* cellular uptake of the ^{99m}Tc-conjugated peptide was performed in three breast cancer cell lines: SUM159, MDA-IBC3, and 13762. As shown in Figure 5, cellular uptake of the peptide conjugate was significantly higher than that of the chelator alone in all lines. Similar to the data for the FITC-tagged peptide, the SUM159

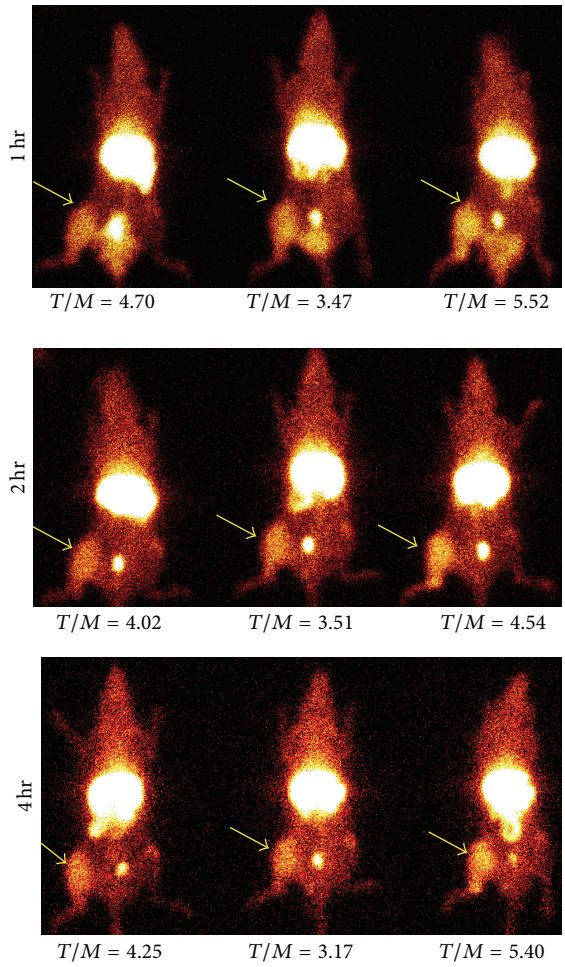

FIGURE 6: *In vivo* uptake of ^{99m}Tc-EC-peptide A in rats bearing 13762 breast carcinoma xenografts. Tumor-to-muscle (T/M) ratios are given for 3 separate rats at multiple timepoints after injection of the radiotracer. Arrows indicate tumor location.

line showed the highest radiotracer uptake with approximately 18% uptake per mg protein at 4 hours (Figure 5(a)). Significant uptake of the radiotracer was also observed in two other lines, increasing steadily in MDA-IBC3 (Figure 5(b)) and reaching saturation after 1-2 hours in 13762 (Figure 5(c)).

3.5. In Vivo Imaging. To investigate the utility of peptide imaging of the PTCH receptor in breast cancer, planar scintigraphy was performed in a rat model of breast cancer using ^{99m}Tc-EC-peptide A. Fisher rats were inoculated with the mammary carcinoma cell line 13762, and after tumors grew for two weeks, rats were injected with approximately 300 μCi of the ^{99m}Tc-labeled peptide. Planar scintigraphy was conducted at 1, 2, and 4 hours after injection of the radiolabeled peptide, and tumor-to-muscle ratios were calculated. An average tumor-to-muscle ratio of 4.5 ± 0.07 was obtained at 1 hour. Significant retention of the peptide was observed in the tumor tissue up to 4 hours after injection (Figure 6).

Several studies have reported that hedgehog signaling induces resistance to chemotherapy [4, 7, 8]. Therefore, we expect that residual cells which remain after treatment with chemotherapy would have high expression of hedgehog pathway members. We examined PTCH expression in tumor xenografts before and after treatment with paclitaxel. As shown in Figure 7(a), an increase in PTCH protein expression is observed in the residual tumor seven days after treatment. Although there was a decrease in tumor volume after treatment, planar imaging with ^{99m}Tc-EC-peptide A revealed no significant decrease in tumor accumulation of the peptide (Figure 7(b)). These findings suggest that PTCH receptor imaging may provide a useful method to assess resistant tumor tissue after chemotherapy treatment.

4. Discussion

Neoadjuvant chemotherapy is commonly prescribed for treatment of invasive or large tumors to allow for breast-conserving surgery. However, there is currently no reliable method to noninvasively follow response to chemotherapy. It is unclear whether the current standard for clinical imaging, ^{18}F-FDG PET, is predictive of treatment response due to false positive results following treatment. *In vitro* and *in vivo* studies have demonstrated high FDG uptake in inflammatory lesions [5]. Increased FDG uptake in macrophages and neutrophils caused by treatment-induced inflammation has also been reported [9, 10].

We show that *in vivo* imaging with ^{99m}Tc-PTCH peptides may offer an alternative method to follow treatment response and allow for tumor-specific imaging prior to and immediately after chemotherapy treatment. Our data suggest that peptides which bind to the ligand docking site of the hedgehog receptor, PTCH, are localized to breast cancers *in vivo*. Furthermore, we show that PTCH receptor expression is increased after paclitaxel treatment in a rat model of breast cancer. These results indicate that PTCH-positive, treatment-resistant cells may be enriched after chemotherapy. In addition to tumor uptake, significant uptake of the peptide was observed in liver and kidney tissues. This may be due to clearance of the peptide and the FITC tag. Additionally, liver uptake may be due to low level endogenous expression of the PTCH receptor by liver tissue. Although our work and that of others [2] suggest that PTCH docking peptides specifically target the PTCH receptor on cancer cells, binding to other cell surface receptors cannot be ruled out.

The cancer stem cell hypothesis states that tumors consist of a heterogeneous population of cells, including both rapidly dividing, differentiated cells that can be effectively targeted by chemotherapy and relatively resistant stem-like cells [11]. Previous studies have reported that breast cancer stem cells express high levels of the PTCH receptor and that hedgehog signaling is required for the growth of these cells [6]. Our data indicate that PTCH-binding peptides have higher uptake in cells cultured under stem cell-promoting conditions (mammospheres) and may serve as a ligand to detect and target this cell population. Additionally, our findings suggest that PTCH receptor-positive cells are resistant to chemotherapy and that ^{99m}Tc-peptide A may be a useful agent for the detection of

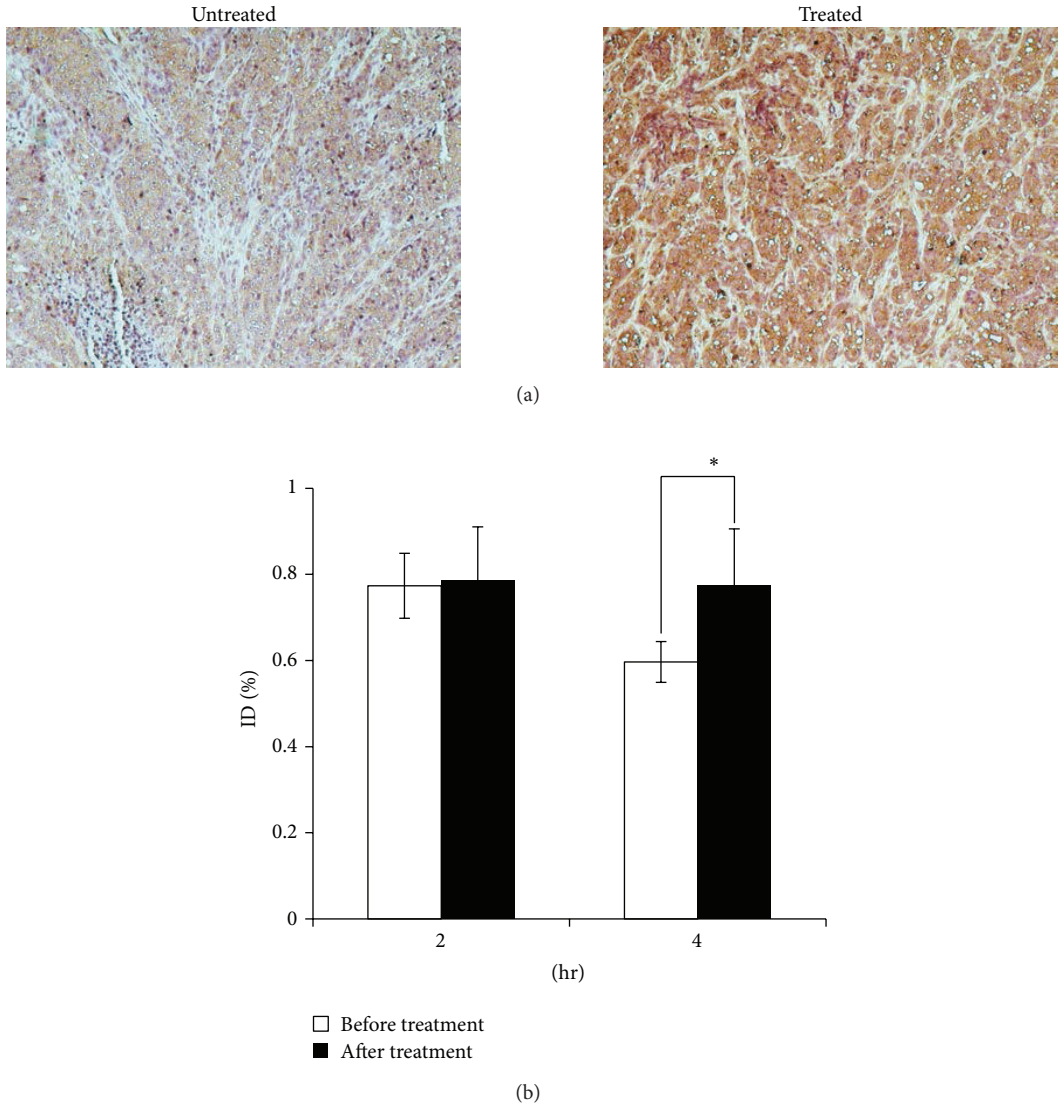

Figure 7: PTCH expression is increased in breast cancer xenografts after chemotherapy treatment. (a) Immunohistochemical detection of PTCH before and after treatment with paclitaxel. (b) Tumor uptake of ^{99m}Tc-EC-peptide A is increased after treatment with chemotherapy. Data represents % injected dose in the ROI of the tumor. Error bars represent standard deviation. Significance is represented by asterisk. $^{*}P \leq 0.05$.

treatment-resistant breast cancer cells with active hedgehog signaling.

PTCH-blocking peptides have been shown to decrease growth of pancreatic cancer cell lines [2]. Similar to previous studies, we show that treatment of breast cancer cell lines with PTCH-binding peptides decreases growth of breast cancer cell lines. While our preliminary results suggest that PTCH-binding peptides may slow growth of breast cancer, further study is needed to validate the therapeutic effect. Our data also indicate that further evaluation of the effect of PTCH-binding peptides on tumor detection, growth, and survival in orthotopic models of breast cancer is warranted. These peptides may serve as useful theranostics which may be used to both image and treat breast cancer.

Conflict of Interests

The authors declare that there is no conflict of interests regarding the publication of this paper.

Acknowledgments

This project was supported by the National Institutes of Health grant U54-GM104941, the NIH/National Cancer

Institute Grant RO1 CA138230-01 and the Delaware INBRE program, with a grant from the National Institute of General Medical Sciences—NIGMS (8 P20 GM103446-13).

References

[1] J. Sims-Mourtada, D. Yang, I. Tworowska et al., "Detection of canonical hedgehog signaling in breast cancer by 131-iodine-labeled derivatives of the sonic hedgehog protein," *Journal of Biomedicine and Biotechnology*, vol. 2012, Article ID 639562, 8 pages, 2012.

[2] M. Nakamura, H. Tanaka, Y. Nagayoshi et al., "Targeting the hedgehog signaling pathway with interacting peptides to Patched-1," *Journal of Gastroenterology*, vol. 47, no. 4, pp. 452–460, 2012.

[3] D. J. Yang, W. E. Fogler, J. L. Bryant et al., "Assessment of antiangiogenic effect using ^{99m}Tc-EC-endostatin," *Cancer Biotherapy and Radiopharmaceuticals*, vol. 17, no. 2, pp. 233–245, 2002.

[4] F. Chai, J. Zhou, C. Chen et al., "The Hedgehog inhibitor cyclopamine antagonizes chemoresistance of breast cancer cells," *OncoTargets and Therapy*, vol. 6, pp. 1643–1647, 2013.

[5] S. Law, M. Fok, S. Chow, K.-M. Chu, and J. Wong, "Preoperative chemotherapy versus surgical therapy alone for squamous cell carcinoma of the esophagus: a prospective randomized trial," *Journal of Thoracic and Cardiovascular Surgery*, vol. 114, no. 2, pp. 210–117, 1997.

[6] S. Liu, G. Dontu, I. D. Mantle et al., "Hedgehog signaling and Bmi-1 regulate self-renewal of normal and malignant human mammary stem cells," *Cancer Research*, vol. 66, no. 12, pp. 6063–6071, 2006.

[7] J. Sims-Mourtada, J. G. Izzo, J. Ajani, and K. S. C. Chao, "Sonic Hedgehog promotes multiple drug resistance by regulation of drug transport," *Oncogene*, vol. 26, no. 38, pp. 5674–5679, 2007.

[8] J. Sims-Mourtada, J. G. Izzo, S. Apisarnthanarax et al., "Hedgehog: an attribute to tumor regrowth after chemoradiotherapy and a target to improve radiation response," *Clinical Cancer Research*, vol. 12, no. 21, pp. 6565–6572, 2006.

[9] D. R. Jones, L. A. Parker Jr., F. C. Detterbeck, and T. M. Egan, "Inadequacy of computed tomography in assessing patients with esophageal carcinoma after induction chemoradiotherapy," *Cancer*, vol. 85, pp. 1026–1032, 1999.

[10] G. Zuccaro Jr., T. W. Rice, J. Goldblum et al., "Endoscopic ultrasound cannot determine suitability for esophagectomy after aggressive chemoradiotherapy for esophageal cancer," *The American Journal of Gastroenterology*, vol. 94, no. 4, pp. 906–912, 1999.

[11] G. J. Lindeman and J. E. Visvader, "Insights into the cell of origin in breast cancer and breast cancer stem cells," *Asia-Pacific Journal of Clinical Oncology*, vol. 6, no. 2, pp. 89–97, 2010.

VITA

Daniel Lee Smith was born in San Diego, California on September 15, 1987, the son of Doris and Martin Smith. He moved to Minnesota with his family in 1989, where he was raised. He received his Bachelor of Science degree with honors from the University of Notre Dame in May 2010, with a major in Physics-in-Medicine and a minor in Anthropology. Immediately after completing his undergraduate studies, he entered University of Texas Graduate School of Biomedical Sciences, pursuing a Doctor of Philosophy degree in Medical Physics. He co-authored xx publications as a graduate student, spanning the arenas of molecular imaging and radiation biology, under the supervision of Dr. Wendy Woodward in the Department of Experimental Radiation Oncology at M.D. Anderson Cancer Center. During his graduate studies, he was a Howard Hughes Medical Institute Med into Grad Fellow, received funding from the Center for Stem Cell and Developmental Biology, and won a travel award and the Scholar-in-Training Award at the 2013 AACR-SNMMI Joint Conference.

Permanent Address:
7200 Almeda Rd Apt 621
Houston, TX 77054